JOHANNES GUTENBERG UNIVERSITÄT MAINZ

Analysis and modification of biosilica-forming sponge (*Suberites domuncula*) primmorph cells and hydroxyapatite-forming human SaOS-2 cells

Dissertation

zur Erlangung des Grades

"Doktor der Naturwissenschaften"

am Fachbereich Biologie

der Johannes Gutenberg-Universität in Mainz

vorgelegt von

Julia Sofia Markl

geb. am 02. Oktober 1985 in München

Mainz, 2016

Dekan: Prof. Dr. Hans Zischler

Erster Berichterstatter: Prof. Dr. Werner E. G. Müller

Zweiter Berichterstatter: Prof Dr. Walter Stöcker

Tag der mündlichen Prüfung: 27.06.2016

D77 (Dissertation Johannes Gutenberg-Universität Mainz)

INDEX

1 SUMMARY

Biomineralization enables animals to produce hard durable composite materials by combining inorganic and organic matter. Such natural composites, used by the animal for stabilization, protection, defense or food supply, often show property combinations that are not provided by technical products. Moreover, whereas manufacturing the latter usually requires much energy and reactive chemicals, living cells produce their materials under mild physiological conditions. A prominent example is biosilica. It is produced by sponges and has silica as inorganic and proteins as organic components. Since sponges (Porifera) are among the most ancient animal phyla, they provide rich research opportunities for understanding general biomolecular processes in zoology and medicine. The marine sponge *Suberites domuncula* (Demospongiae) produces biosilica spicules ("biosilica needles") by enzymatically controlled biomineralization and is an established laboratory animal with a potential as a natural source for bioactive sponge compounds. *S. domuncula* cell culture is possible by generating three-dimensional cell aggregates termed primmorphs. Goals of this study were to improve primmorph production, to reveal phagocytic capabilities of primmorph cells and to introduce new property combinations to primmorph cells and to their biosilica spicules by using nanoparticles as a vehicle. As an initial step, a comparative transcriptome analysis was performed.

Here I describe a newly developed bioreactor for *S. domuncula* cell culture. It yields a significant improvement and upscaling of primmorph production from the cell suspension of a single *S. domuncula* individual. Per choice, it allows producing either a single primmorph of previously unmatched size, or many small primmorphs in previously unmatched numbers. Using fluorescence microscopy, transmission electron microscopy, energy-dispersive X-ray spectroscopy, magnetic attraction experiments and other analytical approaches, I surveyed the primmorph cells and their phagocytic activity in detail. I show here that most if not all primmorph cells are capable of extensive endocytosis in that they engulfed large numbers of nano-screenMAG-CMX nanoparticles and silica core-shell microparticles, respectively. By quantitative PCR, I determined that uptake of silica core-shell microparticles enhanced the expression of proteins known to be involved in spiculogenesis, notably silicatein-α and silicatein-β, while uptake of nano-screenMAG-CMX nanoparticles did not change the expression patterns of these proteins. I also found that the biosilica spicules were specifically coated by nanoparticles *in vivo*, whereas such coating of extracted spicules *in vitro* required prior chemical silanization of their surface. By using nanoparticles, I introduced magnetic and fluorescent properties to primmorph individuals, their cells, and their biosilica spicules.

Uptake of silica is also important for bone formation in humans, although in this case, calcium phosphate is the major product of biomineralization. In this context it was previously observed that the growth on biosilica scaffolds enhances the biomineralization activity of human bone-forming SaOS-2 cells, but this required their permanent activation by β-glycerophosphate, ascorbic acid and dexamethasone. I stably transfected SaOS-2 cells with the gene encoding *S. domuncula* silicatein-α, which significantly enhanced their osteogenic (bone-forming) capacity also in the absence of any activation.

The present experiments with sponge cells and human SaOS-2 cells open new possibilities in biology, material science and biomedicine in the context of research, production, modification and application of biosilica.

2 ZUSAMMENFASSUNG

Biomineralisierung gibt Tieren die Möglichkeit, durch die Kombination von anorganischen und organischen Stoffen harte, strapazierfähige Kompositmaterialien zu produzieren. Solche natürlichen Komposite, die Tieren zu Stabilisierung, Schutz, Verteidigung und Nahrungserwerb dienen, weisen oft Eigenschaften auf, die technische Produkte nicht liefern können. Zudem können lebende Zellen ihre Materialen unter milden physiologischen Bedingungen herstellen, während die technische Produktion große Energiemengen und aggressive Chemikalien erfordert. Ein herausragendes Beispiel hierfür ist Biosilikat. Es wird von Schwämmen hergestellt und hat Silikat als anorganische und Proteine als organische Komponenten. Da Schwämme (Porifera) zu den ältesten Tierstämmen zählen, bieten sie eine Fülle von Forschungsmöglichkeiten um grundlegende biomolekulare Prozesse in der Zoologie und der Medizin aufzuklären. Der marine Schwamm *Suberites domuncula* (Demospongiae) produziert Biosilikatnadeln durch enzymatisch kontrollierte Biomineralisierung und ist ein etabliertes Labortier mit Potenzial als natürliche Quelle für bioaktive Stoffe aus Schwämmen. Zellen von *S. domuncula* lassen sich als dreidimensionale Zellaggregate kultivieren, so genannte Primmorphe. Zu den Zielen dieser Arbeit gehörte, die Kultivierung von Schwammzellen zu verbessern, ihre phagozytotischen Fähigkeiten zu testen und Nanopartikel als Vehikel zu verwenden, um Schwammzellen und ihre Silikatnadeln mit neuen Eigenschaftskombinationen zu versehen. Als Einstieg wurde eine vergleichende Transkriptomanalyse durchgeführt.

Im Rahmen der Arbeit entstand ein neu entwickelter Bioreaktor, der die Zellkultur von *S. domuncula* signifikant verbessert. Er erlaubt wahlweise, aus einem individuellen Schwamm einen einzelnen Primmorphen von bisher unerreichter Größe oder viele kleine Primmorphe von bislang unerreichter Anzahl herzustellen. Vermittels Fluoreszenzmikroskopie, Transmissions-Elektronenmikroskopie, energiedispersiver Röntgenspektroskopie, magnetischer Anziehung und anderen analytischen Verfahren untersuchte ich Primmorphe und die phagozytotische Aktivität ihrer Zellen im Detail. Wie die intensive Aufnahme von Nano-screenMAG-CMX Nanopartikeln sowie Silikat core-shell-Mikropartikeln zeigte, können (fast) alle Zellen einer Suspension, die zur Bildung von Primmorphen führt, ausgiebig Phagozytose betreiben. Quantitative PCR ergab bei Aufnahme von Silikat core-shell-Mikropartikeln erhöhte Expressionsraten von Proteinen, die an der Silikatnadelbildung beteiligt sind, besonders von Silicatein-α und Silicatein-β. Die Phagozytose von Nano-screenMAG-CMX Nanopartikeln steigerte die Expressionsraten dieser Proteine nicht. Ich fand auch heraus, dass in Primmorphen befindliche Silikatnadeln spezifisch mit Nanopartikeln beschichtet wurden, wohingegen eine solche Beschichtung bei extrahierten Nadeln, also *in vitro*, eine vorhergehende chemische Silanisierung ihrer Oberfläche erforderte. Über Nanopartikel verschaffte ich Primmorphen, ihren Zellen und ihren Nadeln magnetische und fluoreszierende Eigenschaften.
Obwohl menschliche Knochen auf Calciumphosphat basieren, ist Silikataufnahme auch für die Knochenbildung wichtig. Das Wachstum menschlicher knochenbildender SaOS-2 Zellen auf Biosilikatträgern erhöht ihre Biomineralisierungsaktivität; dies erfordert jedoch die ständige Zugabe eines „Aktivierungscocktails“ von β-Glycerophosphat, Ascorbinsäure und Dexamethason. Mit für *S. domuncula* Silicatein-α codierender DNA transfizierte ich SaOS-2 Zellen stabil, wodurch sich ihre osteogene Kapazität auch ohne Biosilikatträger und Aktivierungscocktail signifikant erhöhte.

Die vorliegenden Experimente mit Schwammzellen und menschlichen SaOS-2 Zellen eröffnen neue Möglichkeiten in der Biologie, Materialwissenschaft und Biomedizin im Kontext der Erforschung, Produktion, Modifikation und Anwendung von Biosilikaten.

3 INTRODUCTION

3.1 Sponges as members of the animal kingdom

With more than 8,800 valid non-fossil species, the Porifera (sponges) are among the largest and ecologically most important animal phyla (World Porifera Database; Boxshall et al., 2015). About 220 species are limnic, whereas all other sponges live in marine habitats. Since sponges are sessile, often vividly colored by carotenoid pigments, and usually lack body symmetry, they have long been considered as plants or "plant-animals". In the 18th century, their internal water current was detected, and later, biologists could demonstrate that they develop from planktonic larvae in an animal-like manner, and that they live by digesting organic material and bacteria obtained by filter feeding. Consequently, they have subsequently been considered as animals. Sponges are among the first animals occurring in the fossil record, with some fossils dating back 580 million years (see literature cited in Wiens, 2004). Morphologically, they lack two of the four basal tissue types of animals, namely muscle tissue and nerve tissue, and moreover, their epithelioid tissue layers lack some of the cell-cell contacts that exist in "true" animal epithelia. Thus, only the fourth tissue type, connective tissue, shows animal-typical properties. Therefore, sponges might be considered as animals composed of connective tissue covered by an epithelioid cell layer. Consequently, the Porifera have been classically arranged, in phylogenetic trees, as Parazoa ("side animals") in a sister group relationship to all other animals that are usually summarized as Eumetazoa ("true animals"). Together, these groups form the animal kingdom, the taxon Metazoa (= Animalia).

More recently, extensive molecular analyses further substantiated that sponges are indeed true animals and closely related to the Eumetazoa (Müller, 1995; Cavalier-Smith et al., 1996; Borchiellini et al., 2001; Müller et al., 2006a). Ultimately, results from the *Amphimedon queenslandica* genome project (Srivastava et al., 2010) confirmed that the Metazoa are monophyletic (Fig. 1). The position of the Porifera within this clade has been modified by recent genome analyses, unraveling that the most basal branch within the Metazoa are not the sponges but the ctenophores (Moroz et al., 2014). Moreover the Placozoa, possessing the simplest morphology of all animals, in the phylogenetic tree have been inserted between Porifera and Eumetazoa (Srivastava et al., 2008). This means that the Porifera are not the sister group of the Eumetazoa, but of a newly defined taxon "Epitheliozoa" encompassing Eumetazoa and Placozoa (see Fig. 1).

Looking at the Metazoa from outside, their closest relatives are unicellular, often colonial protists termed Choanoflagellata or Choanomonada (see Fig. 1). This has been proposed by many zoologists, because the ultrastructure of a choanoflagellate perfectly fits that of a choanocyte which is the most

characteristic sponge cell type (see below). Indeed, a genome project on the choanoflagellate *Monosiga brevicollis* unequivocally confirmed this relationship (King et al., 2008).

Recent phylogenies subdivide the sponges into four taxa, but it is still not quite clear whether the Porifera are monophyletic or paraphyletic. In Fig. 1, a monophyly of the Porifera according to Philippe et al. (2009) is assumed.

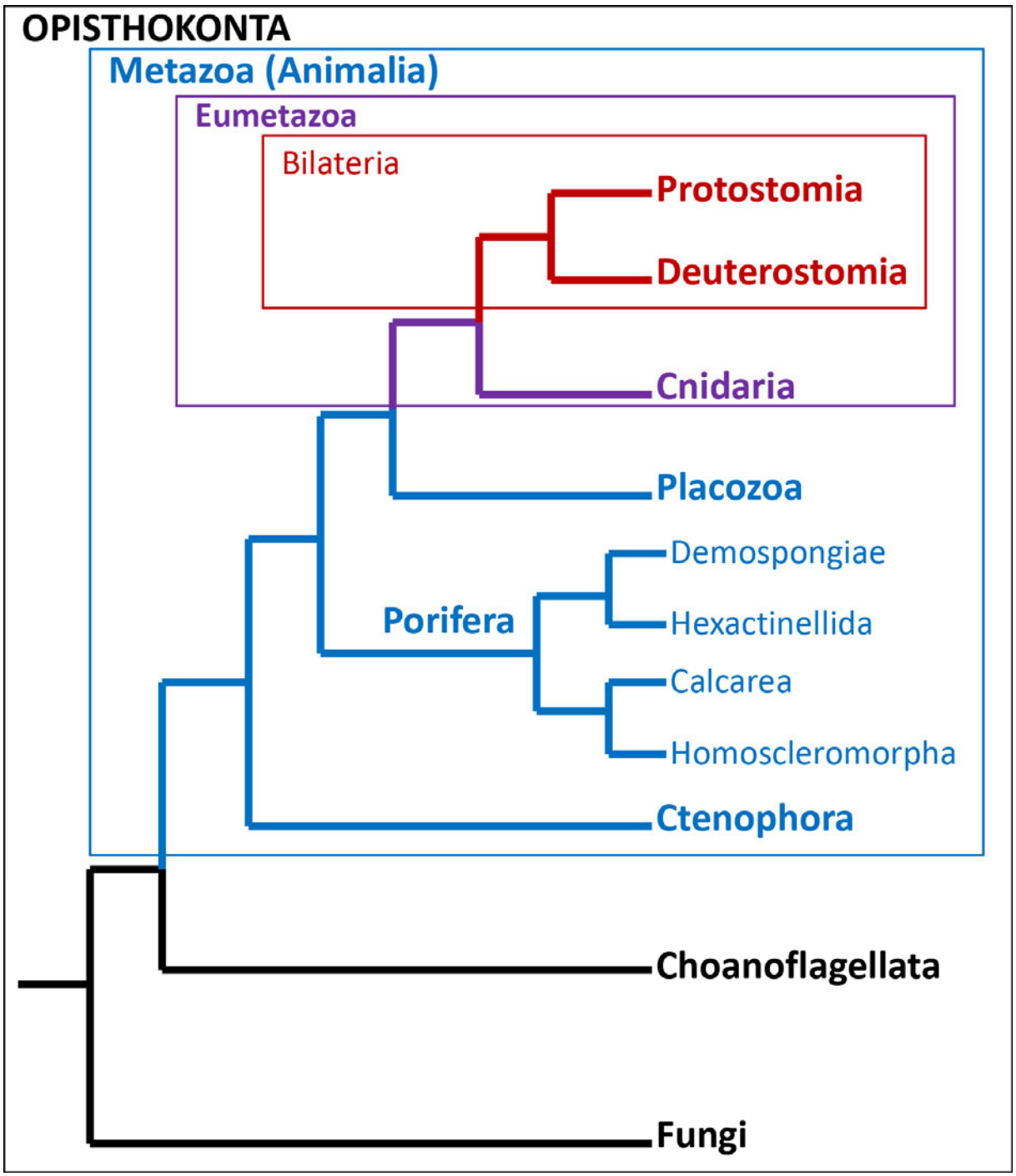

Fig. 1 Phylogenetic tree of the animals. The Metazoa (= Animalia) belong to the larger monophylum Opisthokonta that also includes the Choanoflagellata and Fungi. Whether the Porifera are monophyletic as shown here, or paraphyletic (with Calcarea and Homoscleromorpha excluded) is still debated (Adl et al., 2012). (Scheme designed in Adobe Photoshop, according to Adl et al., 2012 and Ryan et al., 2013)

Despite constant refinement of the Tree of Life (http://tolweb.org/tree/; Maddison and Schulz, 2007), in all available phylogenies the Porifera are among the first animals that occurred in nature. From such phylogenetically very old animal taxa we can learn many details about the structure, evolution and function of typical genes and proteins of the animal kingdom, and also about their functions and malfunctions in morphologically more advanced animal taxa. Therefore, analysis of sponge genes and proteins is a powerful tool in understanding biomolecular and biomedical processes even in the Mammalia, including man (Breter et al., 2003; Müller and Müller, 2003; Müller et al., 2013a).

3.2 Sponge general morphology and systematics

Sponge morphology in general consists of the outer pinacoderm, the central mesohyl and the inner choanoderm. The epithelioid pinacoderm is a sort of "skin" formed by a single layer of pinacocytes (Fig. 2). They cover the sponge and attach it to the substrate (for details, see Simpson, 1984). The epithelioid choanoderm, also a single cell layer, represents the inner surface of the sponge. It is mostly comprised of choanocytes which produce a water current with their flagellae, filter organic particles through a microvillar collar and take them up by phagocytosis (for details, see Riisgard and Larsen, 2000). Both cell layers are densely packed and polar like epithelia. However, they are often called "epithelioid" tissues, because they lack the adherens junctions and the basal lamina that are classically used to define eumetazoan epithelia (for details, see Bergquist, 2001; Richter and King, 2013). Although ultrastructural and molecular analyses revealed adherens-type junctions to be present in sponges, they appear much slighter than cell-cell junctions in eumetazoans (Leys et al., 2009). Moreover, collagenous sheets underlying sponge epithelia were detected, although it is debated whether they are distinct basal laminae (Leys et al., 2009). The prominent connective tissue between pinacoderm and choanoderm, the mesohyl, varies in thickness with the sponge species. It is comprised of a dozen or more cell types (see Fig. 2). The most prominent mesohyl cell types are: lophocytes, producing collagen (Harrison and Davis, 1982); chromocytes, responsible for carotenoid production and storage (Drumm et al., 1945); sclerocytes, building skeletal needles (spicules) through a mineralizing process (Simpson, 1984); oocytes, responsible for reproduction (Bergquist, 2001); porocytes forming the inhalant pore canals (Bergquist, 2001) and ultimately archaeocytes, pluripotent stem cells descending from totipotent cells (Simpson, 1984). Since they show pronounced motility, they are sometimes also referred to as "amoebocytes" (Simpson, 1984). One of their main features is to collect and transport nutrients from choanocytes to the other cell types (Bergquist, 2001).

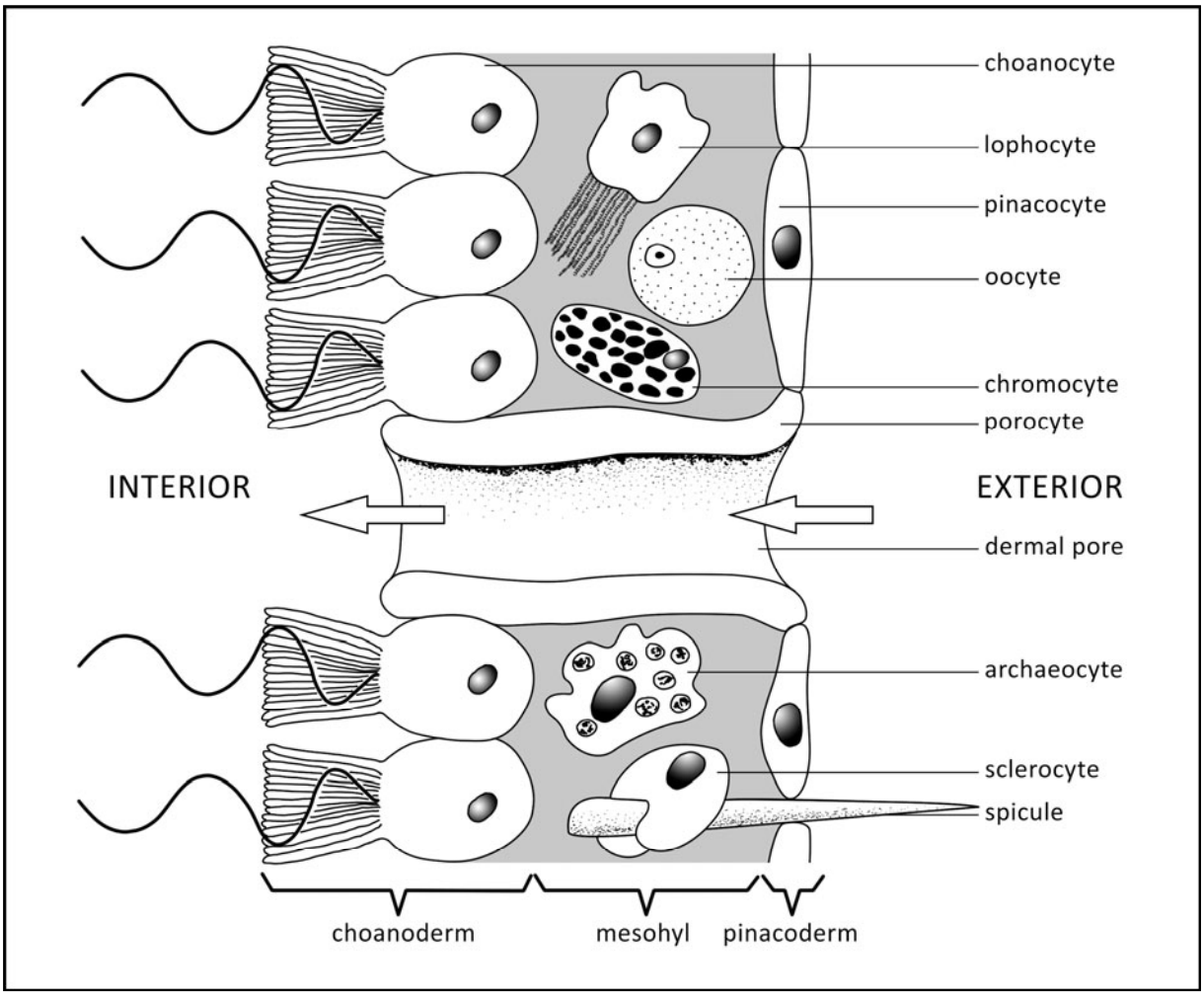

Fig. 2 Scheme of prominent sponge cell types. With their flagellum, choanocytes produce the water current through the sponge. They cover the inner surface (interior) of the sponge body. Its outer surface (exterior) is built from pinacocytes. In between, the mesohyl is comprised of many different cell types, for example spicule-producing sclerocytes, motile archaeocytes, collagen-producing lophocytes, carotenoid-producing chromocytes and oocytes for reproduction. Inner and outer surface is connected by dermal pores which in some sponges are formed by porocytes. Arrows indicate direction of water flow. (Scheme illustrated in Adobe Photoshop, adapted from Ruppert et al., 2004)

Tiny dermal pores perforate the pinacoderm. Here the water enters the sponge body due to the water current produced by the choanocytes. In case of external currents, this water flow through the sponge body is significantly enhanced by Bernoulli's principle, notably in sponges with chimney-like morphology. The filtered water is collected *via* excurrent canals in the central spongocoel and extruded through one or several larger holes termed oscula (Fig. 3). The entire sponge morphology is dedicated to a single major task: To bring as many cells as possible into direct contact with the watery environment. Independent from the phylogenetic tree, three major sponge body plans exist to fulfill this task; they are termed ascon, sycon, and leucon type, respectively, with leuconoid as the most complex condition (Fig. 3). In a leuconoid sponge such as the present research organism *Suberites*

domuncula, the choanoderm forms numerous flagellated chambers in order to enlarge its filter feeding surface.

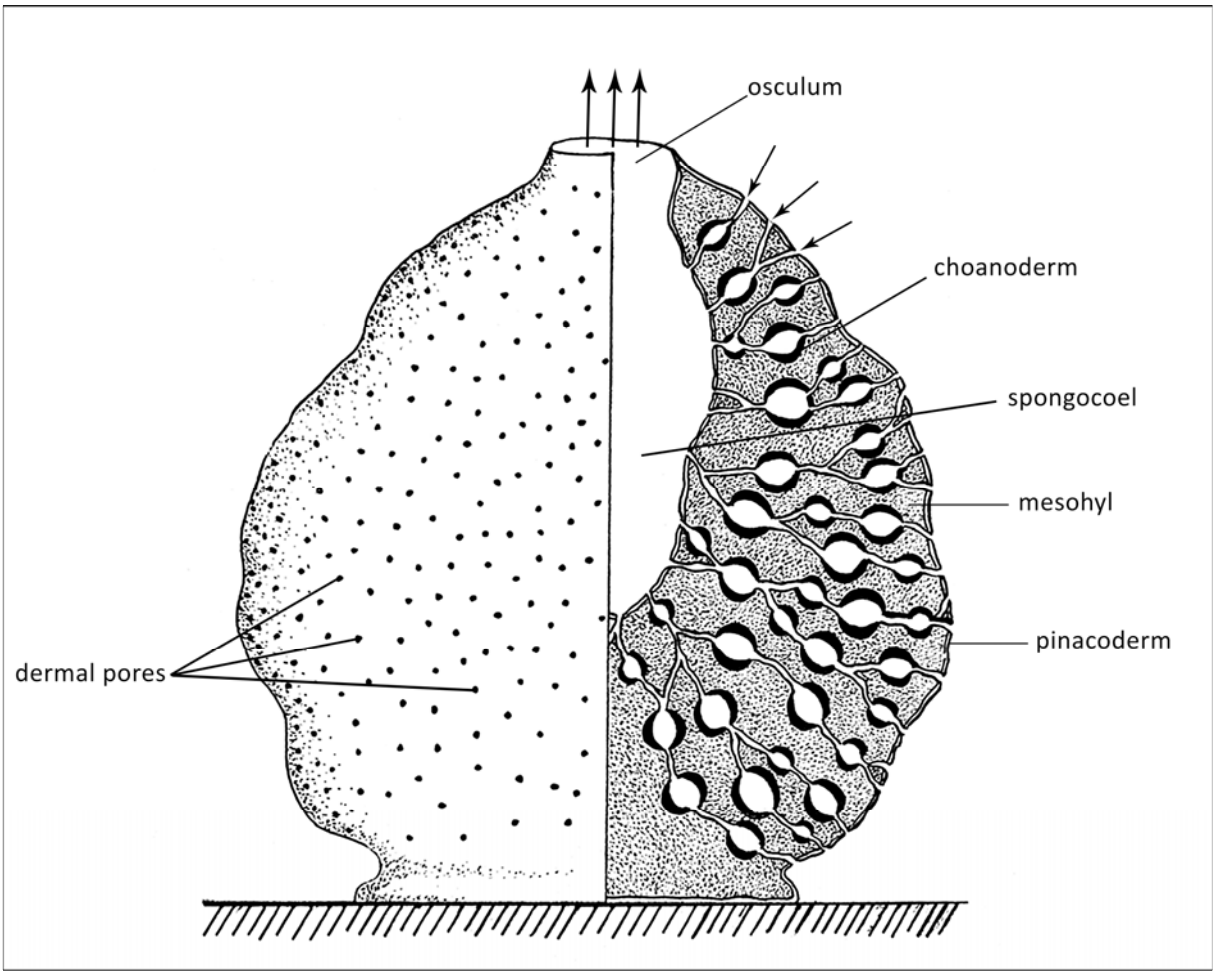

Fig. 3 Scheme of the organization of a leuconoid sponge. The leucon type is characterized by a mesohyl with many chambers lined by the choanoderm. The outer pinacoderm is perforated with dermal pores where the water enters the sponge body (arrows indicate water flow). After extraction of food particles, the water is collected in excurrent canals and extruded *via* one or several larger holes termed oscula. Among the sponge body plans, leuconoid is the most complex one (according to Lavrov and Kosevich, 2014, modified).

The Porifera are currently subdivided into four major taxa (see Fig. 1). The Demospongiae (demosponges, ca. 7,480 species) encompass 84 % of the extant sponge species (including all freshwater sponges). Also the present research organism, *S. domuncula*, and the research organism of the sponge genome project, *A. queenslandica*, belong to the Demospongiae. In this taxon, the mesohyl is stiffened by a protein (spongin) endoskeleton that in many species is additionally hardened by mineral spicules. These “needles” are composed of amorphous biosilica. Related to the Demospongiae are the fragile Hexactinellida (glass sponges, ca. 620 species). They dwell in ocean depths and polar seas and produce intricate and often most beautiful silica scaffolds. The Calcarea (calcareous sponges, ca. 715 species) are restricted to shallow marine habitats and produce calcium carbonate spicules. The

more recently defined taxon Homoscleromorpha, previously part of the Demospongiae, encompasses ca. 100 species producing biosilica spicules (Gazave et al., 2010).

3.3 Biosilica production in sponges

Sponges with spicules (needles) or scaffolds from biosilica are the only members of the animal kingdom that use silica (= silicon dioxide) instead of calcium carbonate or calcium phosphate to build their mineral skeleton (for details, see Müller et al., 2003; Arakaki et al., 2015). The silicon chemistry terms used in this thesis are defined in Table 1.

Table 1 Definition of terms related to silicon.

Term	Description	Chemistry
silicon	chemical element no 14	Si
silicate	any chemical compound containing anionic silicon	e.g. tetraethyl orthosilicate
silica	silicon dioxide, a specific silicate; (crystalline = ordered; amorphous = randomly organized)	SiO_2
silane	any compound with silicon atoms saturated by hydrogen atoms	Si_nH_{2n+2}
silicic acid	compound containing silicon bound to oxide and hydroxyl groups	$[SiO_x(OH)_{4-2x}]_n$
silanization	coating of surfaces with organofunctional alkoxysilanes	---
biosilica	biogenic composite of organic macromolecules and silica	---
biosilica spicules	needle-like skeletal elements of siliceous sponges	---
biosilica needles	synonymous for biosilica spicules	---

Technical glass production requires harsh conditions like 1700 - 1800 °C, high pressures and extreme pH values. In contrast, sponge cells are capable of producing glass at room temperature or below, under atmospheric pressure and ambient pH values. The production of glass under such mild conditions has not been achieved even rudimentarily by men. Other important organisms capable of biosilica production are the diatoms that belong to the protists (Fig. 4).

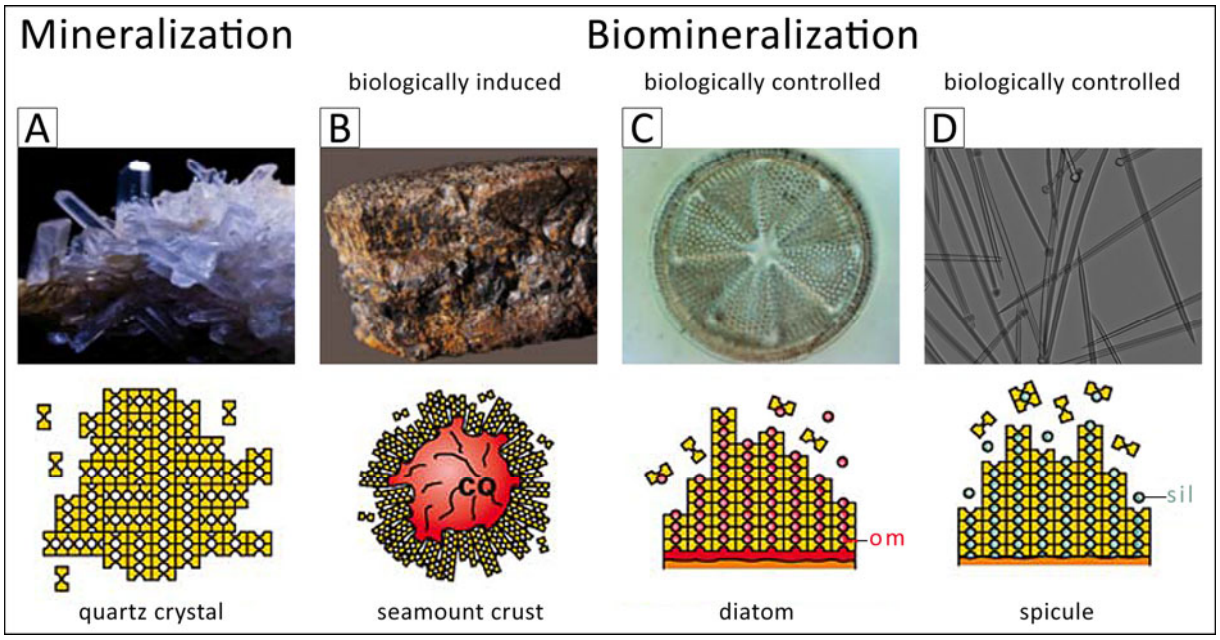

Fig. 4 Examples of mineralization and biomineralization processes occurring in nature. (A) Mineralization of quartz crystal. **(B)** Biologically induced formation of seamount crust in the deep sea. There, mineral deposition occurs around so-called coccospheres (co) of biogenic origin. **(C)** Biologically controlled initiation of silica cell wall formation in diatoms; its growth is controlled by organic macromolecules (om) which function as bioseeds and also as scaffold. **(D)** Spicule formation in the sponge *S. domuncula* as a special form of biologically controlled mineralization. In this case, soluble silicon is polycondensed by the protein silicatein (sil), assisted by several other proteins (according to Müller et al., 2009a, modified).

Sponge biosilica production is controlled by several proteins, notably silicatein-α, silicatein-β and silintaphin-1. Their sequences are known from several sponge species, including *S. domuncula* (Shimizu et al., 1998; Krasko et al., 2000; Müller et al., 2007b; Wiens et al., 2009). A three-dimensional homology model of *S. domuncula* silicatein-α is shown in Fig. 5.

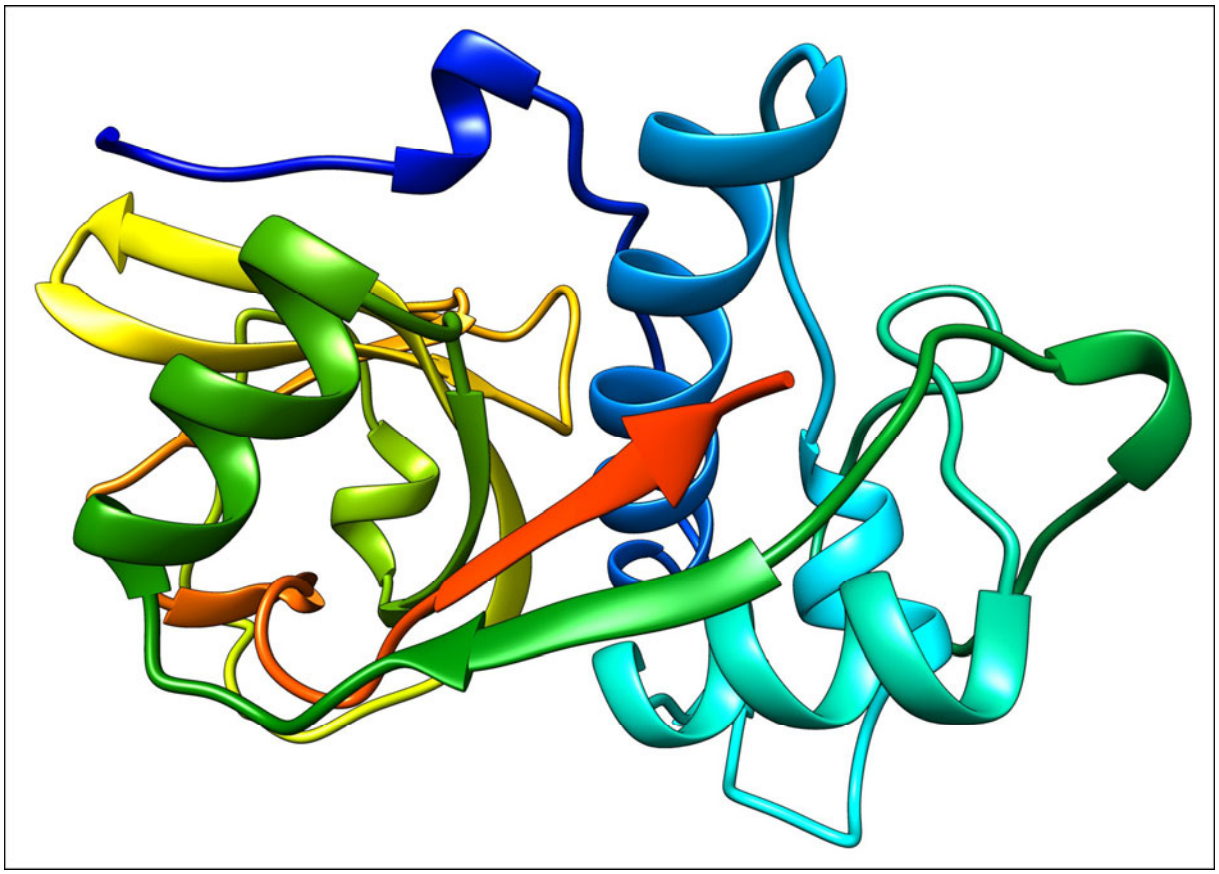

Fig. 5 Homology model of silicatein-α. As a component of the axial filament of biosilica spicules, silicatein-α is a structural protein, but additionally it catalyzes polycondensation of silicic acid (Weaver and Morse, 2003). Structure produced by homology modelling using the sequence of *S. domuncula* silicatein-α as target (GenBank accession number CAI46305) and the human cathepsin-S C25S mutant (PDB-ID 3MPF) as template. (Image visualized in UCSF Chimera)

The role of silicatein-α as a structural component of biosilica spicules, and its interaction with silicatein-β and silintaphin-1 during formation of the axial filament has been studied in the sponge *S. domuncula* and is summarized in Fig. 6. It has been proposed that four silicatein-α molecules form a tetramer, with the respective active sites pointing outward. Thereby, their serine clusters are exposed to the central hole which contains a silicatein-β molecule. The four serine clusters might bind oligosilicate which thereby functions as template for biosilica formation (Müller et al., 2007b; Wang et al., 2012a). Silica spicule formation starts within sclerocytes, in special organelles called silicasomes, by forming an axial protein filament (Schröder et al., 2007). This filament is an assembly of the proteins silicatein-α, silicatein-β and silintaphin-1 (Wiens et al., 2009; Wang et al., 2012c).

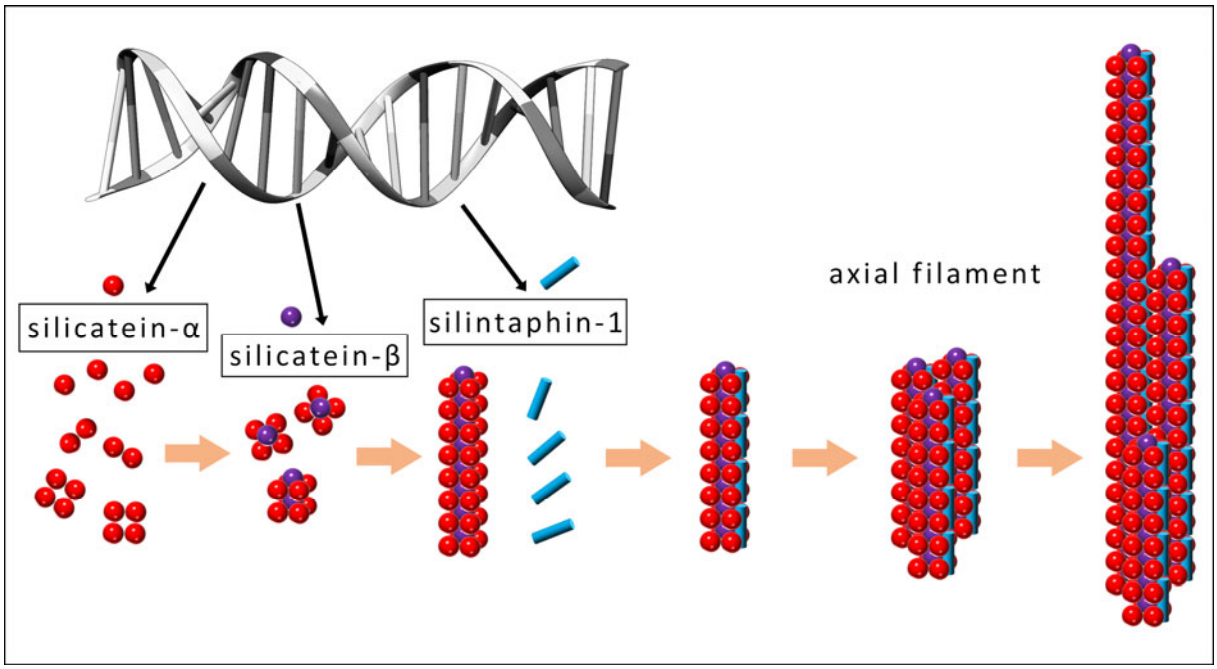

Fig. 6 Proposed formation of the axial filament. After their expression in sclerocytes, four silicatein-α molecules form a planar tetramer which in its center binds a single silicatein-β molecule. The resulting pentamers axially assemble into a "proto-filament" which is stabilized by the "silicatein interactor" silintaphin-1. Gradually, the axial filament is thickened by lateral association of proto-filaments, and elongated. (Scheme illustrated in Adobe Photoshop, adapted from Wang et al., 2012c)

Prior to axial filament formation, orthosilicate (the salt of a silicic acid) is actively taken up by the cell *via* a $Na^+/HCO_3^-[Si(OH)_4]$ cotransporter and stored in the silicasomes (Fig. 7). In the next step, silicate is deposited around the axial filament by enzymatically controlled polycondensation; the enzyme is the structural protein silicatein-α itself (Weaver and Morse, 2003; Müller et al., 2005; Wang et al., 2012a). Afterwards, cell extensions evert into the axial canal, and thereby extrude the immature spicule from the sclerocyte (Wang et al., 2011b; Fig. 7). In the extracellular space, collagen fibers surround the spicule (Müller et al., 2006b). Elongation of the axial canal and the axial filament leads to an axial growth of the spicule, while it is thickened by apposition of silica layers on its periphery (Müller et al., 2005; Schröder et al., 2006a). In both cases, silicasomes release orthosilicate and silicateins into the axial canal, respectively into the extra-spicular space. In a process called syneresis, specialized cells rich in aquaporin channels extract reaction water from the mature spicule, which hardens and ages the initially soft biosilica, thereby fusing the silica lamellae (Müller et al., 2011a; Wang et al., 2011a, Fig. 7 B, C; for possible biotechnical applications of biosilica spicules, see below).

Thus, apart from being a structural protein of the axial filament (see Fig. 6), silicatein-α has a prominent second function: It is an enzyme which controls the polycondensation of monomeric orthosilicate to amorphous silica.

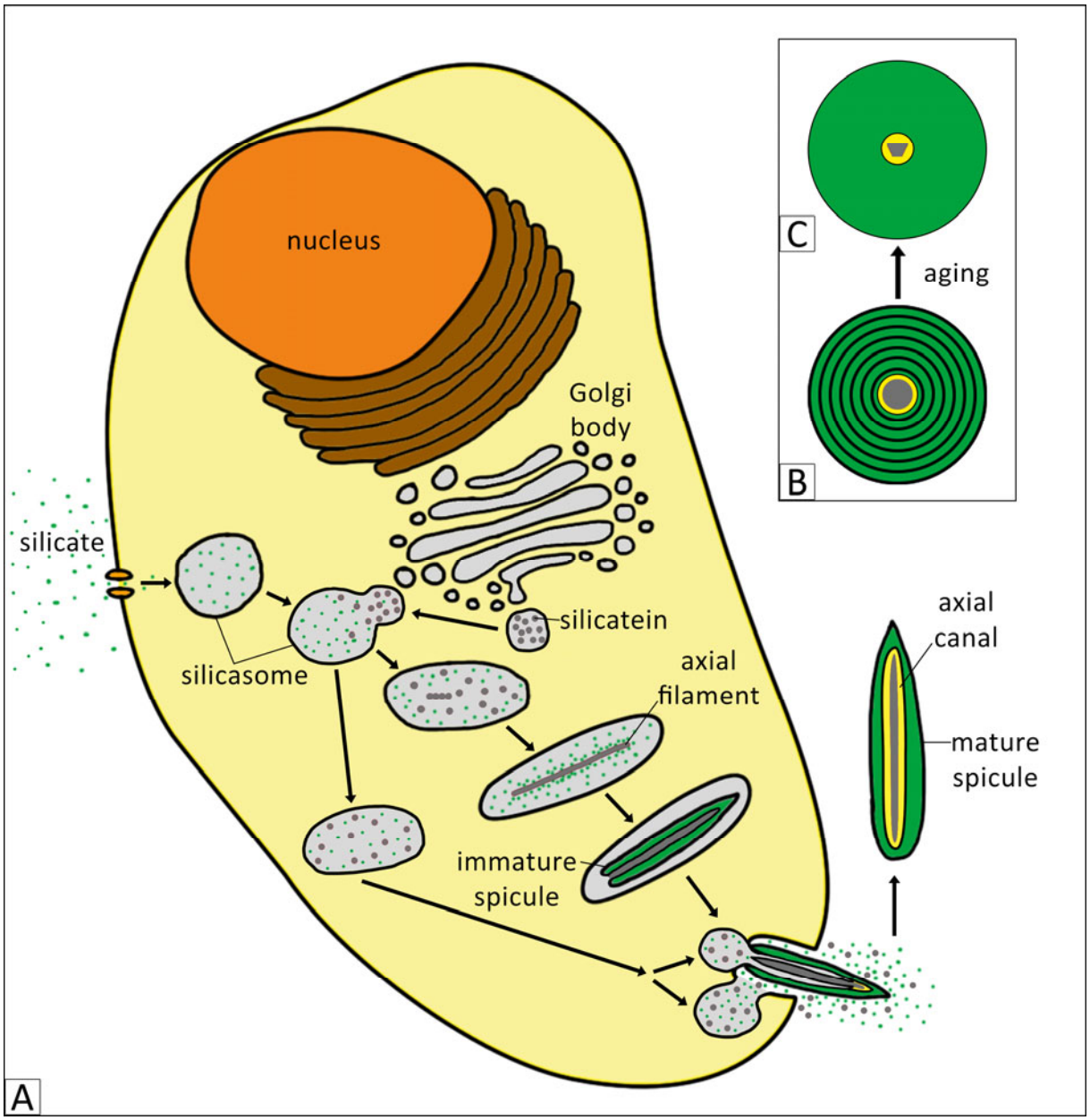

Fig. 7 Overview of spicule formation in demosponge sclerocytes. (A) Inorganic silicate is actively taken up by the cell *via* a Na^+/HCO_3^-[$Si(OH)_4$] cotransporter. It is stored in silicasomes, together with silicateins delivered from the Golgi body. Within the silicasomes, the axial filament assembles, and first layers of soft amorphous biosilica are deposited around it, thereby forming the immature spicule. Then, cell protrusions extrude into the spicule, causing its evagination. At the same time, silicasomes release silicate and silicateins into the axial canal, thereby starting axial growth of the spicule. Radial growth of the spicule occurs by secretion of silicateins and silicate into the extracellular space through silicasomes. Cross-sections of **(B)** a fresh mature and **(C)** an aged spicule give an impression of the process in which the initially soft biosilica lamellae are hardened and fused together. (Scheme illustrated in Adobe Photoshop, adapted from Wang et al., 2012c).

Silicateins belong to the cathepsin family and are most closely related to cathepsin S. The latter is a lysosomal cysteine protease, with a cysteine, an asparagin and a histidine as catalytic triade. Silicatein-α catalyzes the reverse condensation reaction, with orthosilicate as its natural substrate. Moreover, its catalytic triade contains a serine instead of the cysteine. In *S. domuncula*, its active site

contains the catalytic triade Ser26, His165 and Asn185 (Fig. 8). The putative chemical mechanisms of silicatein-α catalysis are described in detail by Schröder et al. (2012) and Wang et al. (2012a). Asn185 stabilizes the binding of the orthosilicate by a hydrogen bridge. It has been proposed that the enzyme reaction starts with a nucleophilic attack of the negatively charged oxygen atom of Ser26 at the positively charged silicon atom of the orthosilicate, followed by formation of a covalent Si—O bond and release of a water molecule. For formation of the latter, the imidazole group of His165 serves as proton donor. After two subsequent nucleophilic attacks of negatively charged oxygen atoms of the orthosilicate bound to Ser26 at the positively charged silicon atom of a second and a third orthosilicate molecule, a reactive cyclic trisiloxane is formed (Fig. 9). The trisiloxane ring is then released from the serine by hydrolysis, and oligomerizes. The produced oligotrisiloxane is probably bound to the serine cluster of silicatein-α (Fig. 8 B). Oligotrisiloxan appears to function as polymerization seed for deposition of amorphous biosilica. This polymerization might be guided by the “silicatein interactor” silintaphin-1 (Wiens et al., 2009).

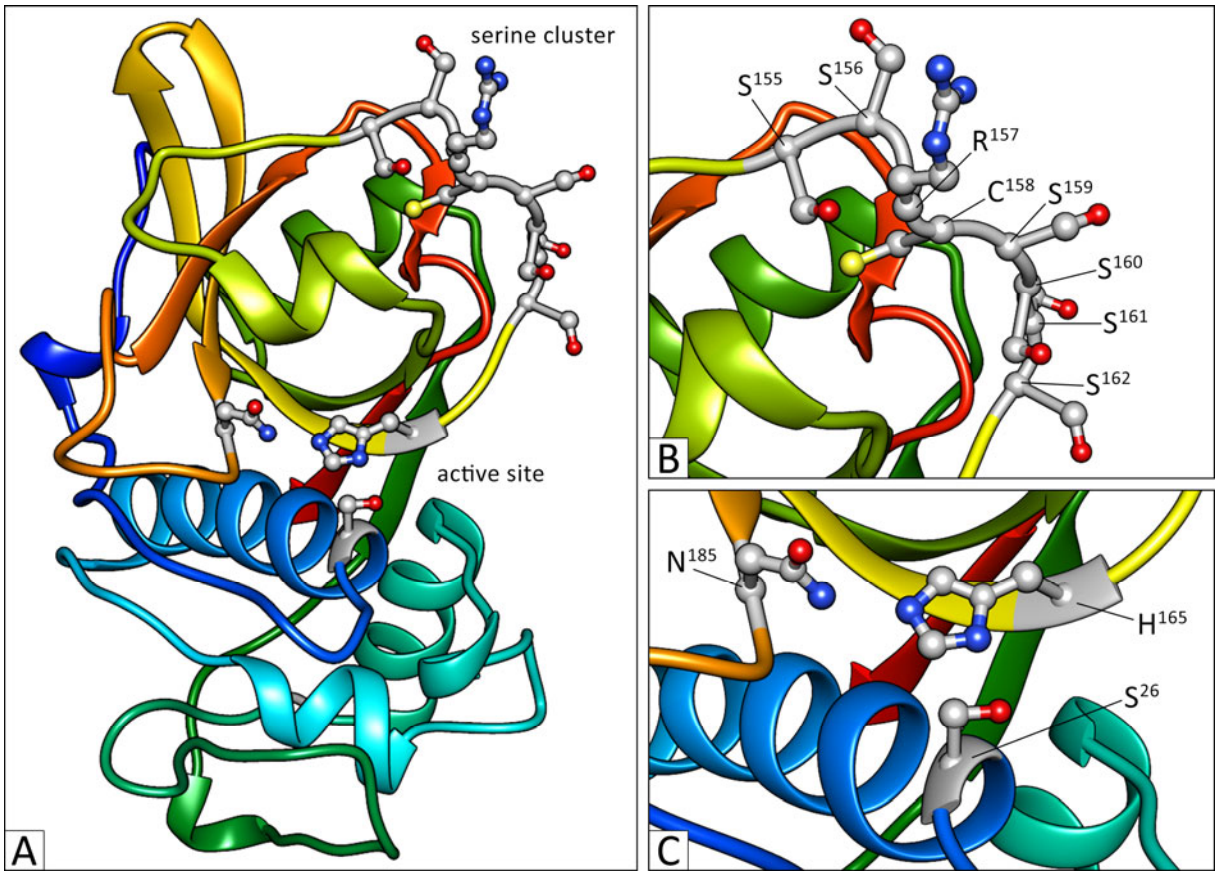

Fig. 8 Different views of the homology model of *S. domuncula* silicatein-α. (A) Overview highlighting the active site corresponding to that of the cathepsin family and the serine cluster typical for sponge silicatein-α. **(B)** Magnification of the serine cluster, comprising six serine residues in the exposed loop S155 -> S162 (C158 is part of a disulfide bridge stabilizing this loop). This cluster is proposed to interact with the produced oligotrisiloxan (Wang et al., 2012a). **(C)** Magnification of the active site, a catalytic triade. Schröder et al. (2012) proposed a reaction mechanism in which three orthosilicates yield trisiloxane by nucleophilic attacks of Ser26 supported by His165 and Asn185 (see Fig. 9) via hydrogen bonds. (Images visualized in UCSF Chimera)

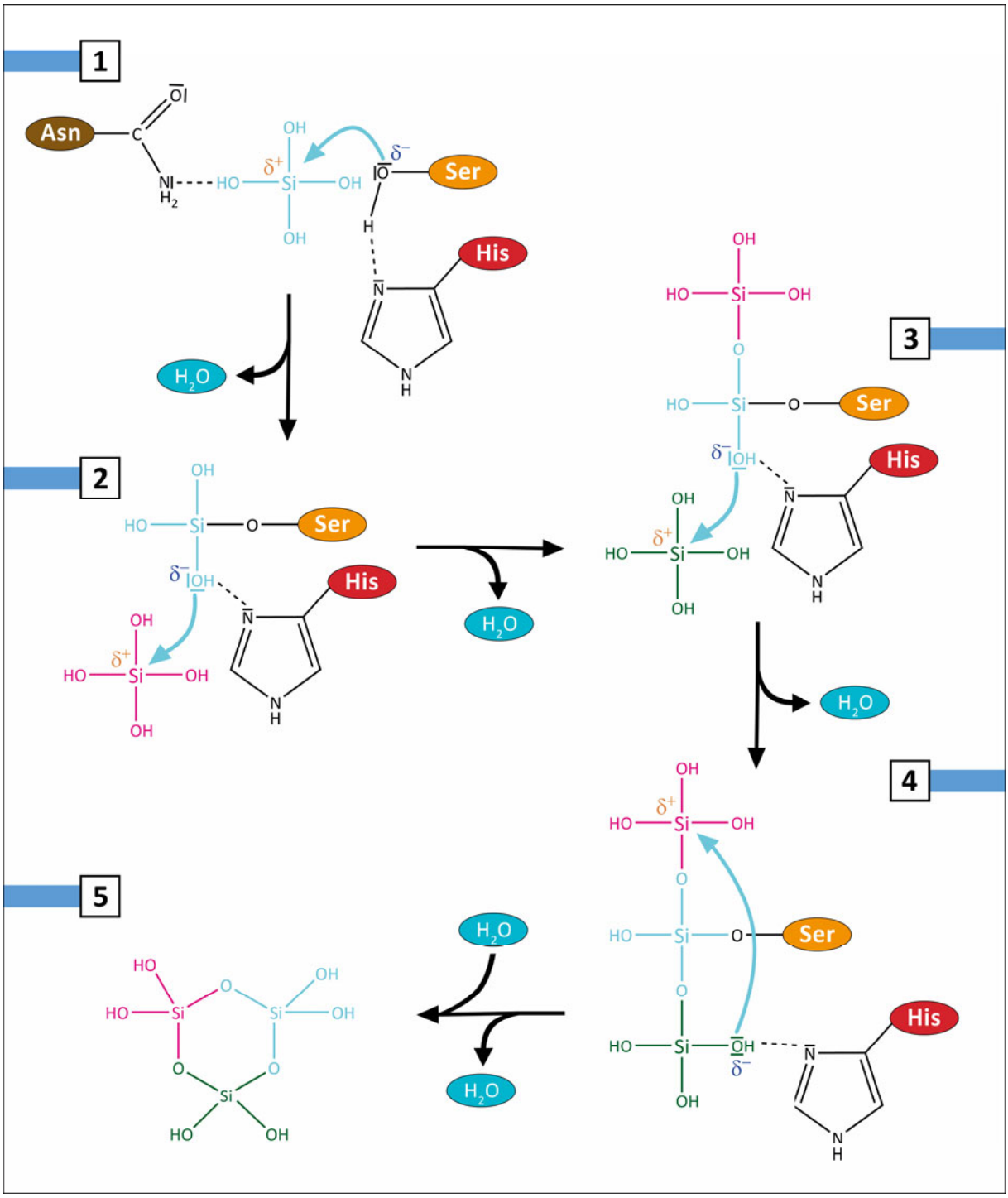

Fig. 9 Scheme of the proposed mechanism of reactive trisiloxane formation by silicatein-α. In step 1, Asn185 stabilizes the binding of the orthosilicate (respectively orthosilicic acid) by a hydrogen bridge, while a nucleophilic attack of the negatively charged oxygen atom of Ser26 at the positively charged silicon atom of the orthosilicate happens. This yields formation of a covalent Si—O bond and release of a water molecule. In steps 2 and 3, a second and a third orthosilicate molecule is attacked by oxygen atoms of the serine-bound orthosilicate, Si—O bonds are formed and a water is released. In each case, the imidazole group of His165 establishes a hydrogen bond to the attacking oxygen atom, thereby increasing its nucleophilicity. Moreover, the imidazole group serves as proton donor for H_2O formation. In step 4, a fourth condensation reaction occurs, in this case between the two peripheral orthosilicates, to form a reactive cyclic trisiloxane. In step 5, the latter is released from Ser26 by hydrolysis which regenerates the catalytic triade. (Scheme illustrated in ChemDraw and Adobe Photoshop, adapted from Wang et al., 2014b)

3.4 The sponge *Suberites domuncula* in nature and captivity

Suberites domuncula is an orange-red marine demosponge found in the Mediterranean Sea and in the Atlantic Ocean. The Mediterranean individuals grow to about 5 cm in diameter, while individuals from the Atlantics can reach 10 cm in diameter. *S. domuncula* often lives in facultative symbiosis with a hermit crab, usually *Paguristes eremita* (Fig. 10). Thereby, the sponge grows on the gastropod shell inhabited by the hermit crab. Instead of being forced to change its domicile after molting, the growing hermit crab more and more uses the simultaneously growing sponge as a live house, with the additional advantage of being protected from predators by the toxins and biosilica spicules of the sponge. The sessile sponge, on the other hand, uses the mobility of the hermit crab as a vehicle and benefits from left-over food particles. In sponge research, this symbiosis is most convenient for collecting and transporting live *S. domuncula*, since removal of the sponges from their natural substrate is not necessary. With most other sponge species, such manipulations are required and very critical for their survival. Also keeping *S. domuncula* in aquarium tanks for many days is routinely possible due to this symbiosis (Müller et al., 1999).

Fig. 10 ***Suberites domuncula* in symbiosis**. This orange-red individual covers the shell of a dead gastropod and lives, as often observed, in symbiosis with an eye-spot hermit crab (*Paguristes eremita*).

3.5 *S. domuncula* and its biosilica spicules in biological and material research

Due to these experimental advantages, *S. domuncula* has been intensively used in our laboratory and also by others as a model organism for studying sponge biology (Thakur et al., 2003; Caruso et al., 2005; Schröder et al., 2006b; Müller et al., 2009b; Garderes et al., 2015). It turned out that substances and processes revealed in this sponge have applied potential in biotechnology and medicine, and that *S. domuncula* might be used as a source for producing valuable biomolecules (Schröder et al., 2003b; Thakur et al., 2003; Müller et al., 2004; Wiens et al., 2012). In this context, biomineralization of silica by *S. domuncula* has been intensively studied (Müller et al., 2005; Müller et al., 2008; Schröder et al., 2012).

Notably, the possible application of biosilica spicules as nanoscale optical fibers is debated (Wang et al., 2009; Wang et al., 2012b). They can function as light wave guide, like industrial glass fibers (CattaneoVietti et al., 1996; Müller et al., 2006c; Kulchin et al., 2009). In contrast to the latter, spicules have a lamellar structure with protein components (see Fig. 7). Therefore, their mechanical properties are remarkable as they can resist fracture much better than the relatively stiff industrial glass fibers (Sundar et al., 2003; Aizenberg et al., 2004; Mayer, 2005).

These properties make spicules attractive for biomimetic and biotechnological approaches (Müller et al., 2009a). Notably, approaches to create hybrid materials based on biosilica spicules appear to be promising. Hybrid materials in general have a wide range of applications, because they provide new property combinations that do not exist in pure materials (Asefa et al., 1999). In many front technologies, for example the semiconductor (Laursen et al., 2012) or the renewable-energy field (Liang et al., 2011), major advances have been achieved through the invention of hybrid materials with new property combinations. Also in biology and medicine, new hybrid materials are applied, for example as cell growth supports or bioengineered tissue scaffolds (Bokhari et al., 2005; Giannitelli et al., 2014). Due to its unique inorganic/organic composition and features, the biosilica spicule is a promising candidate for developing new hybrid materials with novel property combinations.

As mentioned above, the natural substrate of silicatein-α is orthosilicate (chapter 3.3). However, whereas many enzymes exhibit high substrate specificity, silicatein-α has a relatively flexible active site and is capable to process numerous different substrates (Andre et al., 2012). Surprisingly, also a lot of non-biological metal oxides are suitable substrates for recombinantly expressed or native silicatein-α, for example zirconium dioxide (Tahir et al., 2005), tin dioxide (Andre et al., 2011) or gallium oxohydroxide (Kisailus et al., 2005). There are various approaches to use such substrates for generating biologically inspired inorganic materials (for review, see Brutchey and Morse, 2008; Andre et al., 2012).

In order to get the desired substrate in contact with silicatein-α, immobilization of the enzyme on different surfaces is favored. For coating a surface with a recombinant protein, using an amino acid tag such as the "His-tag" is often the method of choice. The His-tag contains at least six subsequent histidines. It is a standard tag for purification of recombinant proteins since the histidine residues bind with high affinity to Ni^{2+} ions, thereby allowing to isolate the tagged protein by affinity chromatography (Hochuli et al., 1988). In the context of enzyme immobilization, His-tagged silicatein-α molecules were chemically bound to different surfaces functionalized with Ni^{2+} ions, for example titanium oxide nanowires (Tahir et al., 2006), gamma-Fe_2O_3 nanocrystals (Shukoor et al., 2008) or glass slides (Andre et al., 2011). Another tag used in the context of silicatein-α immobilization is the so-called Glu-tag. It contains eight glutamic acid residues that are able to bind to the calcium portion of hydroxyapatite (Hunter and Goldberg, 1994). It has been applied for coating of bone material or calcium carbonate surfaces with silicatein-α, yielding in turn an enzymatically produced biosilica coat (Natalio et al., 2010). Rai and Perry (2010) functionalized gold-coated surfaces with amines to which they bound untagged silicatein-α by using glutardialdehyde as crosslinker. Subsequently, the silicatein-α coat generated a thin biosilica film.

Although all these new inorganic materials are not produced in nature, they are biologically inspired and used in the extremely low energy pathways and under the mild conditions of the enzymatic reactions catalyzed by silicatein-α.

3.6 The primmorph: a sponge cell accumulation in culture

Prerequisite for many biological research projects is cell culture. So far, sponge cell culture is only possible with three-dimensional cell aggregates termed primmorphs (Custodio et al., 1998). Primmorphs have been used as multicellular model systems to investigate biological processes in mature sponges, or as natural sources to produce novel bioactive compounds (Schröder et al., 2003b). The principle and procedure of sponge cell culture with primmorphs has been well elaborated (Müller et al., 1999). To prepare a primmorph (Fig. 11), sponge tissue is dissociated into single cells, filtered, and then allowed to reaggregate in an appropriate medium. Primmorphs are normally kept in petri dishes or well plates at 16 °C with shaking, and they survive this for five months and more. Dissociated sponge cells loose telomerase activity, but after reaggregation change from a telomerase-negative to a telomerase-positive state (Custodio et al., 1998). It could also be demonstrated that primmorph cells undergo DNA synthesis even when being kept without nutrients, and that sponge cells need cell-cell or cell-matrix contact to survive (Müller et al., 1999).

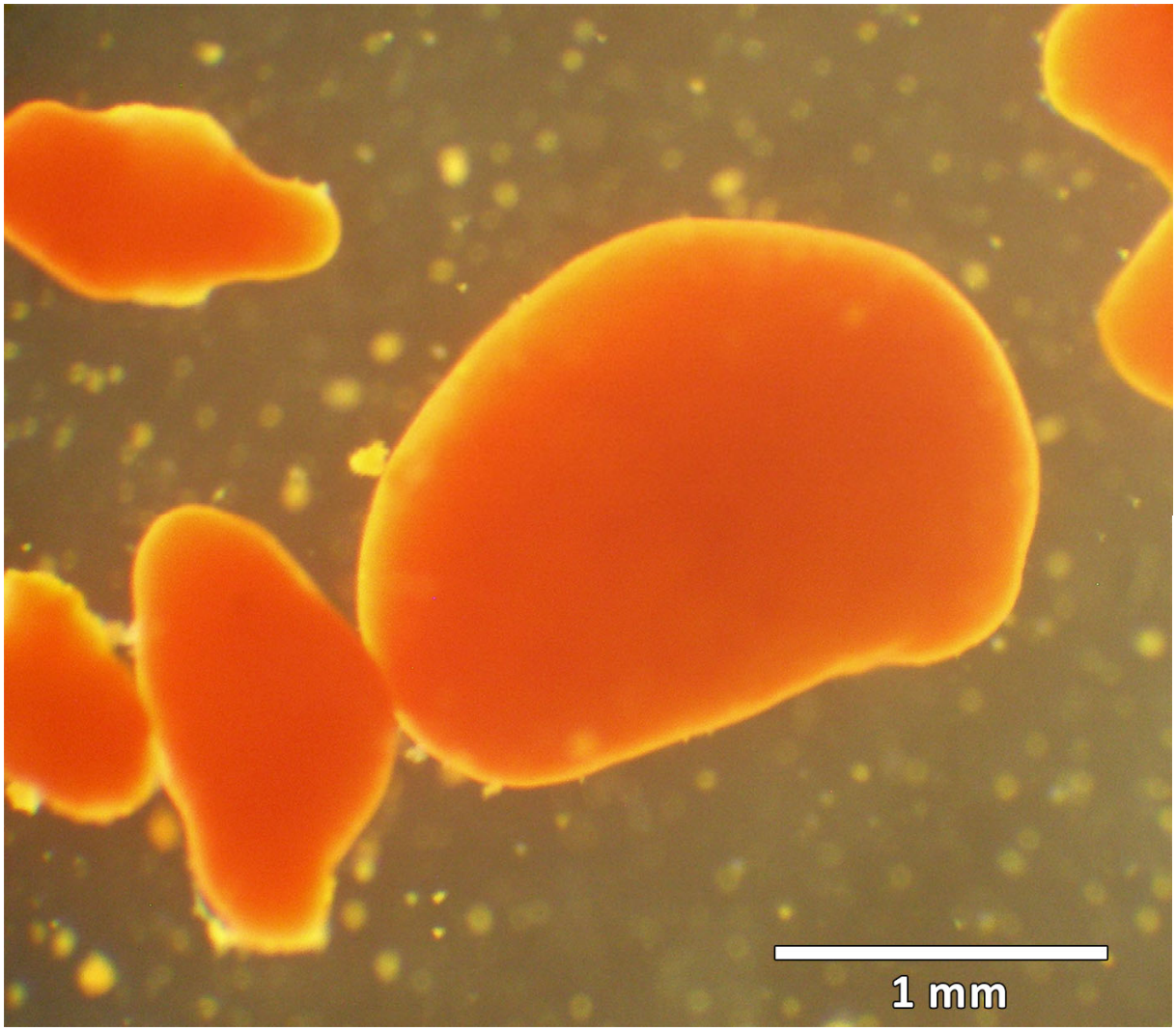

Fig. 11 Light micrograph of three days old primmorphs. They were produced according to Müller et al. (1999) in a culture dish and kept at 16 °C.

In our laboratory, primmorphs are routinely used for analyzing protein expression patterns in sponges (Müller et al., 2012; Müller et al., 2013c; Pozzolini et al., 2014). The ability of primmorphs to produce secondary metabolites was also shown (Andrade et al., 1999; Müller et al., 2000). Furthermore, it has been demonstrated that sponge cells can recognize cells from the same donor animal and undergo allograft rejection (Gaino et al., 1999; Wiens et al., 2004). Most of these findings are from demosponges, notably from *S. domuncula*, but experiments with calcareous sponges have also been done (Amano, 1990).

3.7 Phagocytosis in sponges and primmorphs, and application of nanoparticles

Sponges are filter feeders that generate a water current through their body (see Fig. 2 and Fig. 3). They filter seawater in large amounts for organic nutrients (detritus) and bacteria (for details, see Yahel et al., 2006). Thereby, they significantly clean their habitat of organic matter. Consequently, sponge cells are specialized in rapid phagocytosis of bacteria (usually 0.6 - 1 µm in diameter) and smaller detritus particles. However, little is known about the endocytic capacity of primmorph cells which, on the other hand, should be an indicator of their vitality in culture. Sponges possess a variety of cell types (see Fig. 2), and all of these cells should be capable of phagocytosis, as their exclusive mechanism for gaining nutrients.

During primmorph formation, the various cell types undergo dedifferentiation, redifferentiation and transdifferentiation (Lavrov and Kosevich, 2014). Whether all of them also maintain their phagocytic activity in the primmorph state is an open question that might be solved by applying nanoparticles as "food". Nanoparticles are widely used in biology and medicine, for example in cell labeling (Kacenka et al., 2015), reaction catalysis (Eshghi et al., 2015), drug delivery (Yilmaz et al., 2015), cancer therapy (Singh et al., 2015), as a contrast agent (Alric et al., 2008), and in many more applications. With respect to marine species, recent studies focus on the influence of nanoparticles in search for a valid bioindicator: In diatoms, uptake of nanoparticles can alter protein expression (Morelli et al., 2015), whereas in sea urchin embryos the impact of ingested nanoparticles seems to be species specific and depending on the embryonic state (Buric et al., 2015; Maisano et al., 2015).

Apart from using nanoparticles of different specifications for studying phagocytosis, they might be used as spheres to introduce new properties, or property combinations, to phagocytic cells. One might even try to use this pathway for producing new biogenic hybrid materials. However, this approach has rarely been attempted. An example is the modification of diatom shells with iron oxide nanoparticles in order to use them as carrier for chemotherapeutic agents (Javalkote et al., 2015).

3.8 Apatite formation enhanced by silicon in human bone-forming (SaOS-2) cells

Human osteosarcoma SaOS-2 cells have osteoblastic properties (Mitsui et al., 2006) and can be considered as "osteoblast-like" cells (Degasne et al., 1999), as they can differentiate and produce hydroxyapatite (Hausser and Brenner, 2005). SaOS-2 cells have been used for experiments concerning bone formation and the development of surgical implants (Saldana et al., 2007). Even though most vertebrates have a calcium-based endoskeleton, it is well established that silicon is also essential for bone formation (Carlisle, 1986; Beattie and Avenell, 1992). The influence of silicon on bone formation has been studied in animal models *in vivo* (Carlisle, 1972; Seaborn and Nielsen, 2002; Kim et al., 2009), and in clinical trials (Macdonald et al., 2012). Corresponding *in vitro* studies on cell lines were also performed (Reffitt et al., 2003; Kim et al., 2013). Additionally, the potential of silicon-based scaffolds was intensively investigated *in vitro* (Mieszawska et al., 2010; Wiens et al., 2014) and *in vivo* (Chaudhari et al., 2011). All these studies agree that silicon uptake is positively correlated with bone formation (Rodella et al., 2014).

To use these findings in biomedicine, different approaches have been considered. An early idea was to use so-called bioglass which was initially composed of a SiO_2-CaO-Na_2O-P_2O_5 complex. This first type of bioglass was considered as implant candidate because it stably binds to bone material, in contrast to metal implants (Hench et al., 1972). Since 1985, bioglass is clinically applied (for an overview, see Hench, 2013). To replace tissue, it was initially used as large solid pieces; today it is rather applied as small particles. Today, it is prepared by sol-gel processing (Sepulveda et al., 2001), and basically composed of CaO-SiO_2 (Saravanapavan et al., 2003). More recent bioglass types have the ability to activate genes that enhance bone formation (reviewed by Hench, 2006). A review covering bioglass application from its beginnings to new hybrid materials stems from Jones (2013).

In an *in vivo* study, Patel et al. (2002) found a significant increase in formation of new bone material after addition of silicate ions to hydroxyapatite implants. Even thin silicate-hydroxyapatite coatings seem to enhance bone formation (Gomes et al., 2010). The required silicate concentrations as well as the mechanisms by which silicate-hydroxyapatite grafts increase bone formation have been intensively studied (e.g. Porter et al., 2004; Kalia et al., 2016).

In contrast to the fully inorganic silicate, biosilica is a biomineral synthesized by living organisms such as sponges or diatoms, and contains proteins. Like silicate, biosilica has the potential to increase formation of new bone material in mammals (Wang et al., 2012d). Consequently, studies were performed on new hybrid materials coated with biosilica or the biosilica-producing enzyme silicatein-α (e.g. Wiens et al., 2010b; Cicco et al., 2015; Müller et al., 2015). Biosilica induces upregulation of several, but not all, known bone growth factors (Fig. 12; Wiens et al., 2010a). This leads to an

enhancement in the maturation of preosteoblasts to osteoblasts, while the differentiation of osteoclasts is blocked (Müller et al., 2011b).

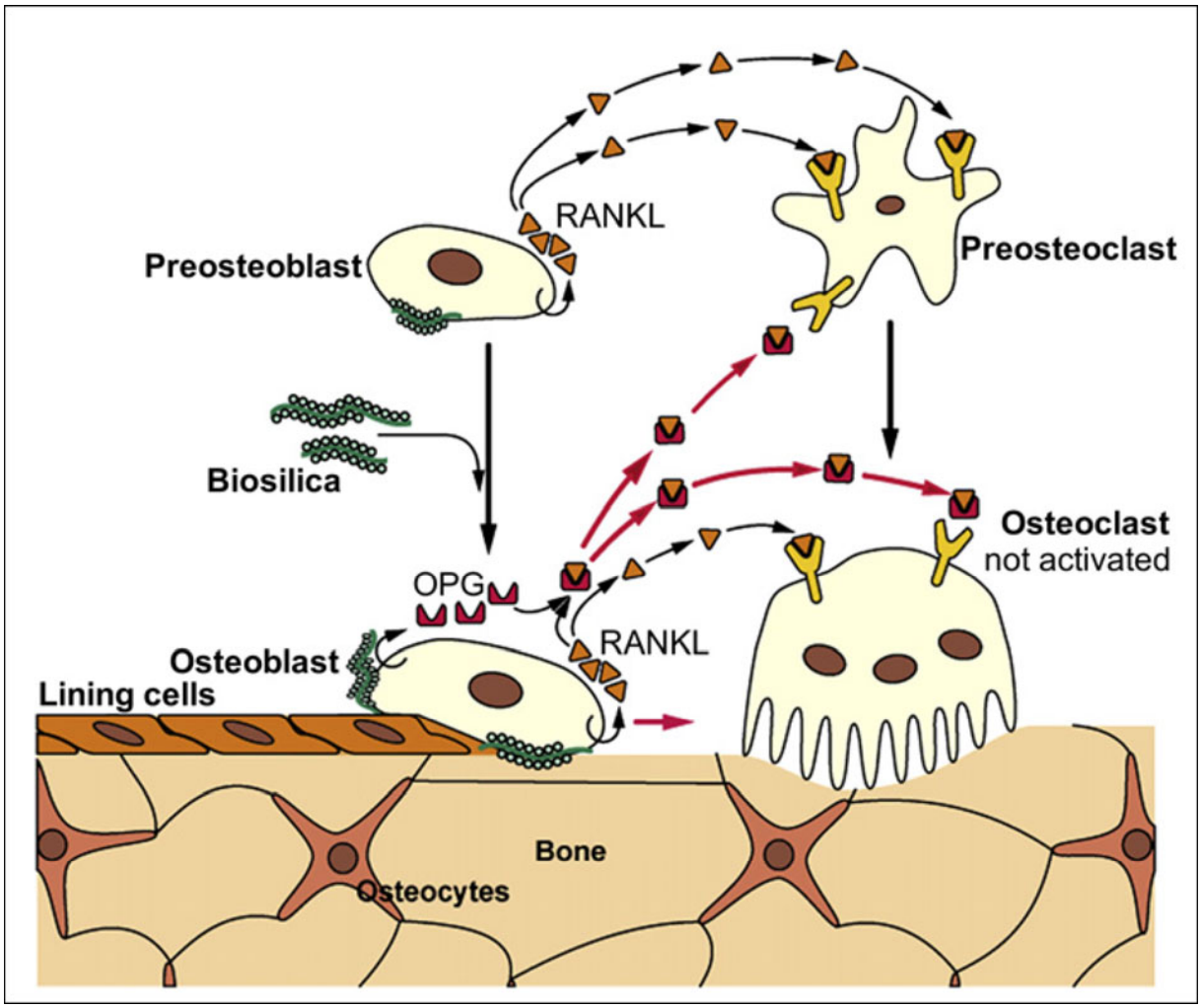

Fig. 12 Proposed effect of biosilica on mammalian osteoblasts and osteoclasts. Due to biosilica exposition, osteoprotegerin (OPG) expression in osteoblasts is upregulated, while expression of the "receptor activator of NF-kB ligand" (RANKL) is not affected. This leads to a changed OPG/RANKL ratio which enhances the osteoblast maturation and blocks the osteoclast differentiation (according to Wiens et al., 2010a, modified).

3.9 Aims of the present study

This thesis was designed to approach the following questions concerning *S. domuncula* primmorphs, their phagocytic and biomineralizing activities, and human biomineralizing SaOS-2 cells:

- Is it possible to improve primmorph cell culture in that significantly more primmorphs, respectively significantly larger primmorphs, are formed by the cells obtained from one individual sponge? Are bioreactors applicable to this task, and how could their design be modified for improvement of results? How could this be performed and evaluated?
- Is it possible to deduce the phagocytic activity of primmorphs by using nanoparticles? Which particle types and conditions are efficient and which analytical (preferentially imaging) techniques are appropriate? Are all primmorph cells capable of phagocytosis, or only a subfraction of cells? Is it possible to supply primmorph cells with magnetic, fluorescent properties by using nanoparticles? How could this be performed and monitored?
- Is it possible to confer new property combinations to primmorph biosilica spicules, by applying magnetic, fluorescent nanoscale building blocks to cells and to isolated spicules? How could this be performed and analyzed?
- Is spiculogenesis in primmorphs significantly influenced by the uptake of nanoparticles or microparticles? Are transcriptome analyses and quantitative PCR appropriate methods to study this?
- Is biomineralization in SaOS-2 cells enhanced by transfecting them with the silicatein-α gene?

4 MATERIAL AND METHODS

4.1 Material

4.1.1 Consumables

ABsolute qPCR plate seals	Thermo Scientific, Schwerte
bottle-top-filters with PES-membrane	Carl Roth, Karlsruhe
cell tissue culture flasks, CELLSTAR, filter top (25 cm^2, 75 cm^2)	Greiner bio-one, Frickenhausen
copper grids	Plano, Wetzlar
coverslips	Carl Roth, Karlsruhe
disposable scalpel No. 21	Schreiber, Fridingen
falcon tubes, CELLSTAR, conical, polypropylene (15 ml, 50 ml)	Greiner bio-one, Frickenhausen
glass slides	Carl Roth, Karlsruhe
gloves, latex or nitrile	Carl Roth, Karlsruhe
micro-filtered tips Gilson (10 µl, 20 µl, 100 µl, 200 µl, 500 µl, 1000 µl)	Greiner bio-one, Frickenhausen
Nalgene cryogenic tubes for general long-term storage	Thermo Scientific, Schwerte
nuclease-free, sterile reaction tubes for RNA isolation (1,5 ml)	Carl Roth, Karlsruhe
Nunclon cell culture dishes (Ø 100 mm)	Sigma-Aldrich, Munich
Nunc well plates (6-, 12-, 24-, 96-well)	Thermo Scientific, Schwerte
Parafilm M	Carl Roth, Karlsruhe
PCR reaction tubes (0.2 ml)	Thermo Scientific, Schwerte
plastic pipettes, sterile (2 ml, 5ml, 10 ml, 25 ml)	Greiner bio-one, Frickenhausen
Precellys ceramic-kit (1.4 mm)	Peqlab, Erlangen
reaction tubes (0.5 ml, 1.5 ml, 2 ml)	Brand, Wertheim
Roti-Store cryo-vials	Carl Roth, Karlsruhe
Scepter sensor tips (60 µm)	Merck Millipore, Darmstadt
syringe filter Filtropur S 0,2 for sterile filtration	Sarstedt, Nümbrecht
syringe filter Filtropur S 0,45 for particle removal	Sarstedt, Nümbrecht
syringe Injekt (20 ml)	B. Braun, Melsungen
universal pH indicator paper tritest	Carl Roth, Karlsruhe
white low profile 96-well plate	Thermo Scientific, Schwerte

4.1.2 Reagents

(3-aminopropyl)trimethoxysilane	Sigma-Aldrich, Munich
1-ethyl-3-(3-dimethylaminopropyl)carbodiimide	Sigma-Aldrich, Munich
1-hexadecylpyridinium chloride monohydrate	Sigma-Aldrich, Munich
2,4,6-tris(dimethylaminomethyl)phenol	Serva, Heidelberg
acetone	Carl Roth, Karlsruhe
Agarose NEEO ultra-quality	Carl Roth, Karlsruhe
alamarBlue	Bio-Rad AbD Serotec, Puchheim
alizarin red S	Sigma-Aldrich, Munich
ammonium hydroxide	Sigma-Aldrich, Munich
Araldite Hardener Hy 964	Serva, Heidelberg
ascorbic acid	Sigma-Aldrich, Munich
β-glycerophosphate disodium salt hydrate	Sigma-Aldrich, Munich
blasticidin S HCl	Life Technologies, Darmstadt
carbenicillin disodium salt	Carl Roth, Karlsruhe
chloroform	Carl Roth, Karlsruhe
clear nail polish	Beiersdorf, Hamburg
DABCO	Sigma-Aldrich, Munich
DAPI	Sigma-Aldrich, Munich
dexamethasone	Sigma-Aldrich, Munich
dimethyl sulfoxide	Sigma-Aldrich, Munich
DL-dithiothreitol solution (DTT)	Sigma-Aldrich, Munich
DNA gel loading dye, 6 x	Thermo Scientific, Schwerte
DNase I	Thermo Scientific, Schwerte
dNTP mixture (dATP, dTTP, dCTP, dGTP), 100 mM	Carl Roth, Karlsruhe
DRAQ5	New England Biolabs, Frankfurt
Dulbecco's phosphate-buffered saline (DPBS) without Ca^{2+} and Mg^{2+}	Life Technologies, Darmstadt
EDTA, 0.5 M	AppliChem, Darmstadt
ethanol, 70 %	AppliChem, Darmstadt
ethanol, absolute	AppliChem, Darmstadt
ethidium bromide	AppliChem, Darmstadt
ferric citrate	Sigma-Aldrich, Munich
fetal bovine serum	Life Technologies, Darmstadt
Fluoromount	Sigma-Aldrich, Munich

formaldehyde, 40 %	Carl Roth, Karlsruhe
formamide, deionized	Carl Roth, Karlsruhe
Formvar	Plano, Wetzlar
FuGENE HD reagent	Promega, Mannheim
GeneRuler DNA Ladder Mix	Thermo Scientific, Schwerte
gentamicin solution, 50 mg/ml	Sigma-Aldrich, Munich
GlutaMAX	Life Technologies, Darmstadt
glutaraldehyde, 25 % solution in water	Serva, Heidelberg
glycerol	Sigma-Aldrich, Munich
H_2SO_4, concentrated	Carl Roth, Karlsruhe
HCl	Carl Roth, Karlsruhe
HEPES (4-(2-hydroxyethyl)-1-piperazineethanesulfonic acid)	Carl Roth, Karlsruhe
HNO_3, concentrated	Carl Roth, Karlsruhe
isopentane	Carl Roth, Karlsruhe
isopropyl alcohol	AppliChem, Darmstadt
iTaq universal SYBR Green supermix	Bio-Rad, Munich
kanamycin sulfate	Life Technologies, Darmstadt
KCl	Carl Roth, Karlsruhe
KH_2PO_4	Carl Roth, Karlsruhe
LB broth (Luria/Miller)	Carl Roth, Karlsruhe
LB agar (Luria/Miller)	Carl Roth, Karlsruhe
lead citrate	Merck, Darmstadt
McCoy 5A mod. medium, with 2.2 g/l $NaHCO_3$, without L-glutamine	Biochrom, Berlin
methanol	Carl Roth, Karlsruhe
methyl blue	Sigma-Aldrich, Munich
$MgCl_2$	Carl Roth, Karlsruhe
Mops buffer, 10 x	Sigma-Aldrich, Munich
Mowiol	Hoechst, Frankfurt
Na_2HPO_4	Carl Roth, Karlsruhe
Na_2SO_4	Carl Roth, Karlsruhe
NaCl	Carl Roth, Karlsruhe
$NaH_2PO_4 \cdot H_2O$	Carl Roth, Karlsruhe
$NaHCO_3$	Carl Roth, Karlsruhe
nano-screenMAG-CMX nanoparticles	Chemicell, Berlin
nuclease-free water (DEPC-H_2O)	Carl Roth, Karlsruhe

Oligo(dT)$_{20}$ Primer	Life Technologies, Darmstadt
OptiMEM reduced serum medium	Life Technologies, Darmstadt
osmium tetroxide, 4 %	Carl Roth, Karlsruhe
paraformaldehyde	Sigma-Aldrich, Munich
PCR master mix, 2 x	Thermo Scientific, Schwerte
penicillin G, potassium salt	Sigma-Aldrich, Munich
propylene oxide	Serva, Heidelberg
quick start bovine serum albumin standard, 2 mg/ml	Bio-Rad, Munich
RenLam M-1	Serva, Heidelberg
rhodamine phalloidin	Cytoskeleton, Denver, USA
RNA gel loading dye, 2 x	Thermo Scientific, Schwerte
RNase-Away	Sigma-Aldrich, Munich
sea sand	Carl Roth, Karlsruhe
seawater, untreated	Sigma-Aldrich, Munich
sera marin Coraliquid	Sera, Heinsberg
Shandon Cryomatrix frozen embedding medium	Thermo Scientific, Schwerte
SIGMA*FAST* *p*-nitrophenyl phosphate tablets	Sigma-Aldrich, Munich
sodium hydroxide	Carl Roth, Karlsruhe
sodium pyruvate, 100 mM	Biochrom, Berlin
streptomycin sulfate	Sigma-Aldrich, Munich
toluol	Sigma-Aldrich, Munich
Tris	Carl Roth, Karlsruhe
Tris-borate-EDTA (TBE) buffer, 10 x	Carl Roth, Karlsruhe
Tris-HCl	Carl Roth, Karlsruhe
Triton X-100	Carl Roth, Karlsruhe
TRIzol RNA isolation reagent	Life Technologies, Darmstadt
Tropic Marin PRO-REEF	Tropic Marin, St. Niklausen, CH
Tropic Marin PRO-CORAL PHYTON	Tropic Marin, St. Niklausen, CH
trypsin/EDTA, 0.25 %	Life Technologies, Darmstadt
uranyl acetate	Sigma-Aldrich, Munich
xylol	Carl Roth, Karlsruhe

4.1.3 Buffers and solutions

1-hexadecylpyridiniumchlorid working solution	$C_{21}H_{38}ClN \cdot H_2O$	5 g
	10 mM phosphate buffer (pH 7.0)	up to 50 ml
	heated to 37 °C with shaking	
alizarin red S working solution	alizarin red S	1 g
	1 % ammonium hydroxide in H_2O	up to 100 ml
	pH 4.2	
ATB solution	penicillin G, potassium salt	0.4 M
	streptomycin sulfate	0.2 M
	NaCl	0.154 M
	in purified H_2O	
CMFSW	NaCl	460 mM
	Na_2SO_4	7 mM
	KCL	10 mM
	HEPES	10 mM
	ATB solution	1 ml/l
	in purified H_2O	
	pH 8,0	
CMFSW+EDTA	EDTA	2.5 mM
	in CMFSW	
	pH 8,0	
CMFSW+EDTA+DTT	DTT	1 mM
	in CMFSW+EDTA	
	pH 8,0	
DNA gel	agarose	1 %
	10 x TBE buffer	10 %
	in purified H_2O	
embedding medium for TEM	RenLam M-1	39 g
	Araldite hardener Hy 964	36 g
	2,4,6-tris(dimethyl-aminomethyl)phenol	1.5 g

lysis buffer (SaOS-2)	Tris	10 mM	
	$MgCl_2$	2 mM	
	Triton X-100	0.1 %	
	pH 10		
Mowiol embedding medium	glycerol	6 g	
	Mowiol	2.4 g	
	purified H_2O	6 ml	
	0.2 M Tris-HCl (pH 8.5)	12 ml	
	DABCO	0.1 %	
	DAPI	1:1000	
4 % paraformaldehyde fixation medium	paraformaldehyde	2 g	
	DPBS (heated to 60 °C)	up to 50 ml	
	NaOH	few drops to clear the solution	
10 mM phosphate buffer	Na_2HPO_4	10 mM	
	$NaH_2PO_4 \cdot H_2O$	10 mM	until pH 7.0
0.2 M phosphate buffer according to Soerensen	Na_2HPO_4	0.2 M	
	KH_2PO_4	0.2 M	until pH 7.4
RNA denaturation buffer	deionized formamide	67 %	
	40 % formaldehyde	23 %	
	10 x Mops buffer	10 %	
RNA gel	Agarose	1 %	
	10 x Mops buffer	10 %	
	40 % formaldehyde	8 %	
	in purified H_2O		
TE buffer	Tris-HCl (pH 8.0)	10 mM	
	EDTA	1 mM	

4.1.4 Kits

DNA-*free* Kit	Thermo Scientific, Schwerte
Gateway BP Clonase II Enzyme Mix	Life Technologies, Darmstadt
Gateway LR Clonase II Enzyme Mix	Life Technologies, Darmstadt
High Pure PCR Product Purification Kit	Roche, Mannheim
HighPure Plasmid Isolation Kit	Roche, Mannheim
Kaiser-Testkit	Sigma-Aldrich, Munich

OsteoImage Bone Mineralization Assay	Lonza, Cologne
peqGOLD Plasmid Miniprep Kit	Peqlab, Erlangen
Platinum *Pfx* DNA polymerase	Life Technologies, Darmstadt
QIAfilter Plasmid Midi Kit	QIAGEN, Hilden
QuantiPro BCA Assay Kit	Sigma-Aldrich, Munich
RevertAid RT Kit	Thermo Scientific, Schwerte
TC-FlAsH TC-ReAsH II In-Cell Tetracysteine tag Detection Kit	Life Technologies, Darmstadt
TC-FlAsH TC-ReAsH II In-Cell Tetracysteine tag Detection Kit with Mammalian Gateway Expression Vectors	Life Technologies, Darmstadt

4.1.5 DNA plasmids

pDONR221	Life Technologies, Darmstadt
pcDNA6.2/cTC-Tag-DEST	Life Technologies, Darmstadt

4.1.6 Culture media

LB agar medium	LB agar (Luria/Miller) in purified H_2O	40 g/l
LB liquid medium	LB broth (Luria/Miller) in purified H_2O	25 g/l
primmorph culture medium	HEPES	10 mM
	ferric citrate	10 µM
	sea sand	1 teaspoon
	GlutaMAX	1 mM
	pyruvate	0.5 mM
	ATB solution	2 ml/l
	in sterile seawater	
	pH 8,0	
SaOS-2 growth medium	fetal bovine serum	15 %
	GlutaMAX	1 %
	gentamicin	50 mg/l
	in McCoy 5A mod. medium with 2.2 g/l $NaHCO_3$ without L-glutamine	

SaOS-2 activation medium	β-glycerophosphate	10 mM
	ascorbic acid	0.2 mM
	dexamethasone	0.1 µM
	in growth medium SaOS-2	
SaOS-2 selection medium	blasticidin	5 mg/l
	in growth or activation medium SaOS-2	

4.1.7 Animals and cells

The siliceous sponge *Suberites domuncula* belongs to the phylum Porifera, class Demospongiae, subclass Heteroscleromorpha, order Suberitida. All *S. domuncula* individuals used here for the experiments lived on a gastropod shell and in a facultative symbiosis with a hermit crab (*Paguristes eremita*). They were all brightly orange in color (even though there also exist yellow or blue variants). Sponges, together with their hermit crab and gastropod shell, were collected in the Adriatic Sea near Rovinj, Croatia, by local scuba divers at a depth of 10 - 30 m. In our laboratory, the sponges were permanently kept at 16 °C, in artificial filtered seawater (prepared from "Tropic Marin PRO-REEF", Tropic Marin, St. Niklausen, Switzerland) with a salinity of 35 - 38 ‰. The water was aerated, and filtrated by a protein skimmer. Sponges were kept in a day/night rhythm of 10 hours light, 14 hours darkness. Sponges were fed two times per week with 30 µl/l phytoplankton (sera marin Coraliquid, Sera, Heinsberg and Tropic Marin PRO-CORAL PHYTON, Tropic Marin, St. Niklausen, Switzerland). The hermit crabs were fed with frozen *Artemia salina*.

Escherichia coli bacteria were purchased from Life Technologies (Darmstadt). The "One Shot TOP10 Chemically Competent" *E. coli* cells had the following genotype: F-mcrA Δ(mrr-hsdRMS-mcrBC) Φ80*lac*ZΔM15 Δ*lac*X74 recA1 araD139 Δ(ara-leu)7697 galU galK rpsL (StrR) endA1 nupG. Before using the *E. coli* cells, they were permanently kept at - 80 °C.

SaOS-2 is a human osteoblast-like cell line (ATCC HTB-85) derived from osteosarcoma, which was initially isolated and characterized by J. Fogh and G. Trempe (1975). The initial cells were taken from bones of an 11 years old Caucasian girl who suffered from osteosarcoma. SaOS-2 cells are adherently growing and when differentiated start to mineralize, thereby depositing extracellular hydroxyapatite nodules.

4.1.8 Instruments

centrifuge	cooling falcon tube centrifuge	5804 R	Eppendorf, Wesseling-Berzdorf
	Falcon tube centrifuge	ROTOFIX 32A	Hettich LAB, Tuttlingen
	table top cooling centrifuge	5415 R	Eppendorf, Wesseling-Berzdorf
hood	cell culture hood	Laminar flow hood	Slee, Mainz
	sterile flow hood	8580	Köttermann, Uetze/Hänigsen
incubator	CO_2 humidified incubator	Queue QFD300SAUA	Nunc, Wiesbaden
	incubator for bacteria	ED115	Binder, Tuttlingen
	incubator for primmorphs	TC 175 S	AQUALYTIC, Dortmund
microscope	camera epifluorescence microscope	Leica DC 500	Leica Microsystems, Wetzlar
	digital inverted fluorescence microscope	EVOS fl	AMG, Mill Creek, USA
	epifluorescence microscope	Leitz DM/RBD	Leica Microsystems, Wetzlar
	inverse light microscope	Wilovert S	Hund, Wetzlar
	laser scanning microscope	LSM 710	Zeiss, Oberkochen
	light cube for EVOS	GFP (EX 470/22, EM 525/50)	AMG, Mill Creek, USA
	light cube for EVOS	RFP (EX 531/40, EM 593/40)	AMG, Mill Creek, USA
	light cube for EVOS	CY5 (EX 628/40, EM 692/40)	AMG, Mill Creek, USA
	light microscope	Leica DM LS	Leica Microsystems, Wetzlar
	scanning electron microscope with EDX	Phenom ProX	Phenom-World B.V., Eindhoven, Netherlands

microscope	transmission electron microscope (TEM)	Tecnai12	FEI, Eindhoven, Netherlands
	TEM camera	TemCam-F416 4K x 4K CCD	TVIPS, Gauting
	transmission electron microscope with EDX	Tecnai F-30 with EDX spectrometer	FEI, Eindhoven, Netherlands EDAX, Weiterstadt
microtome	freeze microtome	HM 500 OM	Microm, Walldorf
	ultra-microtome	Reichert Ultracut E	Leica Microsystems, Wetzlar
mixer	magnetic stir bar with heating	Ret Ikamag	Ika, Staufen
	roller mixer	RM5	CAT, Staufen
	shaker bacteria	VIBRAX VXR basic	Ika, Staufen
	shaker primmorphs	Labnet Rocker 25	Carl Roth, Karlsruhe
	shaker room temperature	Polymax 1040	Heidolph, Schwabach
	vortex	Reax 2000	Heidolph, Schwabach
others	air pump	Elite 801	Hagen, Holm
	autoclave	VX-75	Systec, Linden
	cell counter	Scepter 2.0	Merck Millipore, Darmstadt
	compartment dryer	FDL 115	Binder, Tuttlingen
	diamond knife	-	DiATOME, Biel, Switzerland
	electrophoresis chamber	PerfectBlue Gelsystem Mini S and Mini M	Peqlab, Erlangen
	heat block	HB-2	Wealtec, Cambridge, UK

others	heat plate	14801	Medax, Neumuenster
	homogenizer	Precellys 24	Peqlab, Erlangen
	knife maker	-	LKB, Stockholm, Sweden
	micropipettes (0.5 - 2, 10, 20, 100, 200, 1000 µl)	PIPETMAN	Gilson, Limburg
	pH meter	FiveEasy	Mettler Toledo, Gießen
	precision scale	Adventurer Pro	Ohaus, Greifensee, Switzerland
	power supply	Power Pac 300	Bio-Rad, Munich
	sonifier	Cell Disruptor B-12	Branson Ultraschall, Dietzenbach
	UV-transilluminator	E-Box 1000	Peqlab, Erlangen
	vacuum coating system	EM MED020	Leica Microsystems, Wetzlar
	vacuum oven	VTR 5022	Heraeus, Hanau
	video thermoprinter	P 93	Mitsubishi Electrics, Ratingen
	water bath (SaOS-2)	3047	Köttermann, Uetze/Hänigsen
spectrometer	Fourier transform infrared spectrometer	Varian 660-IR	Agilent Technologies, Waldbronn
	spectral scanning multimode reader	Varioskan Flash	Thermo Scientific, Schwerte
	UV/Vis-micro-volume spectrophotometer	NanoDrop 2000c	Thermo Scientific, Schwerte
thermocycler	thermocycler	PeqSTAR 2 x Gradient	Peqlab, Erlangen
	thermocycler qPCR	C1000 Touch	Bio-Rad, Munich

4.1.9 Software

Adobe Photoshop, CS6	Adobe, San José, California, USA
CFX Manager, version 3.1	Bio-Rad, Munich
ChemDraw Professional 15.0	PerkinElmer, Waltham, Massachusetts, USA
Element identification	Phenom-World B.V., Eindhoven, Netherlands
EM-MENU 4 software package	TVIPS, Gauting
ES Vision, version 4.0.173	FEI, Eindhoven, Netherlands
ExPASy translate tool	web.expasy.org/translate/; Gasteiger et al., 2003
Geneious version 6.0.5	www.geneious.com; Kearse et al., 2012
NIH-NCBI BLAST Service	www.ncbi.nlm.nih.gov; Geer et al., 2010
Paint Shop Pro	PSP, Jasc Software, Eden Prairie, Minnesota, USA
Phenom ProSuite	Phenom-World B.V., Eindhoven, Netherlands
R-Project, version 3.2.3	www.R-project.org; R-Core-Team, 2014
UCSF Chimera, version 1.10.2	www.cgl.ucsf.edu/chimera/; Pettersen et al., 2004

4.2 General procedures

Glassware, consumables and liquids used for the experiments were either purchased sterile, or autoclaved before usage at a temperature of at least 121 °C and 1 bar overpressure for 30 min, or sterile filtrated with syringe filters or vacuum bottle-top devices. For preparation of buffers, solutions and culture media, purified water (VE water) or nuclease-free water (DEPC-H_2O) was used. Latex or nitrile gloves as well as a lab coat were worn at all times in order to protect the samples from contamination and for self-protection. When working with DNA, RNA or mammalian cells, filtered tips were used for all steps. All temperature-sensitive procedures were performed on ice. If measuring of the pH of solutions was needed, a digital pH meter (FiveEasy, Mettler Toledo, Gießen) was used for volumes larger than 10 ml. For smaller volumes pH indicator paper was used. If not mentioned otherwise, adjusting of the pH value was achieved by addition of hydrochloric acid or sodium hydroxide.

4.3 Assembly of magnetic nanoscale building blocks to sponge biosilica spicules

4.3.1 Isolation of sponge spicules

Spicules of *S. domuncula* were isolated by placing sponge tissue in a solution of four parts of concentrated sulfuric acid (H_2SO_4) and one part of concentrated nitric acid (HNO_3) (Müller et al., 2007a). The incubation was done for 1 day on ice. Subsequently, the spicules were centrifuged for 5 min at 2000 rpm and washed with VE water. Spicules were separated from VE water by sedimentation and washed again until the pH value was above 6.

4.3.2 Silanization of spicules

Spicules of *S. domuncula* consist of biosilica. In order to cover spicules with a biocompatible layer for the attachment of biomolecules, we used a common silanization method for glass slides (Han et al., 2006). The first step was to completely remove the water from isolated spicules, which was achieved by drying them for 4 hours at 150 °C. Subsequently, spicules were washed with toluol and resuspended in 10 % (3-aminopropyl)trimethoxysilane in toluol. For speeding up the silanization reaction, a reflux system was used, were the reaction could proceed at 80 °C for 24 hours. After cooling down, the spicules were washed three times with toluol, centrifuged for 5 min at 2000 rpm, and vacuum dried overnight. The silanization of spicules was controlled by Fourier transform infrared spectrometry (Griffiths and de Haseth, 2007) by using a Varian 660-IR spectrometer (Agilent Technologies, Waldbronn). The analyses were performed by averaging 36 scans with a resolution of 4 cm^{-1}. Additionally, the silanized spicules were incubated with ninhydrin (2,2-dihydroxyindane-1,3-dione; Kaiser-Testkit, Sigma-Aldrich, Munich) which reacts with primary amines, such as present in (3-aminopropyl)trimethoxysilane, to form a dark blue compound (Kaiser et al., 1970).

4.3.3 EDC-activation of nano-screenMAG-CMX nanoparticles and binding to spicules

Nano-screenMAG-CMX nanoparticles (Chemicell, Berlin; Fig. 13) were immobilized on the surface of the silanized spicules. These nanoparticles possess a magnetite core with superparamagnetic properties, covered by a lipophilic pink fluorescent dye (pink; excitation maximum at 547 nm, emission maximum at 581 nm). The dye layer is enveloped by a hydrophilic polysaccharide matrix consisting of carboxymethyl dextran (CMX), which is a weak cation exchanger (see Fig. 13). According to Chemicell (Berlin), the hydrodynamic diameter of the nanoparticles is 100 nm.

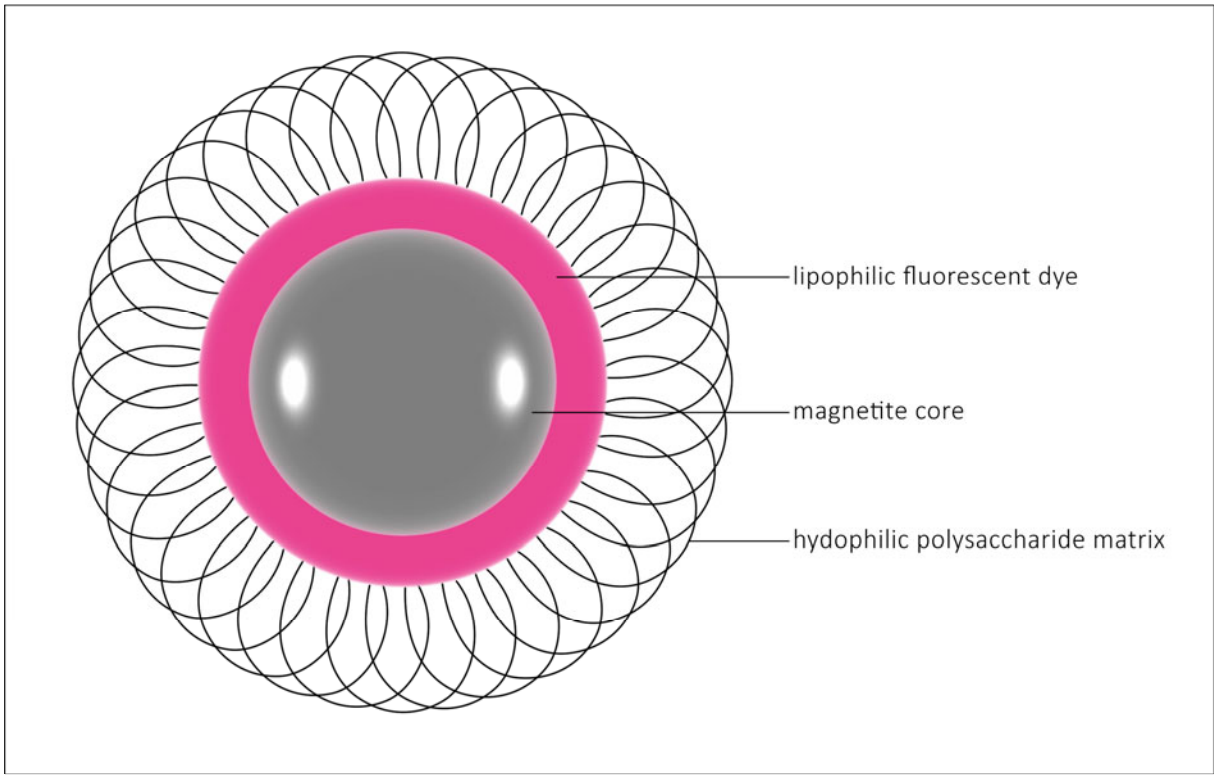

Fig. 13 Scheme of a nano-screenMAG-CMX nanoparticle (Chemicell, Berlin). The magnetite core is covered by a pink lipophilic fluorescent dye. A layer of carboxymethyl dextran (CMX), providing a hydrophilic polysaccharide matrix, envelops the nanoparticle. According to Chemicell, the hydrodynamic diameter is 100 nm. (Scheme illustrated in Adobe Photoshop, adapted from Chemicell, Berlin)

Before immobilization, the nano-screenMAG-CMX nanoparticles were activated by 1-ethyl-3-(3-dimethylaminopropyl)carbodiimide (EDC). EDC reacts with the carboxylic groups of the carboxymethyl dextran matrix to form an intermediate that can be displaced easily by the amino group of (3-aminopropyl)trimethoxysilane and thereby couple the nanoparticles to the silanized spicule surface. For the activation I followed the instructions for the two-step method protocol provided by Chemicell (Protocol 11A). According to this protocol, EDC was freshly dissolved in VE water and added to the same volume of nanoparticles. After ten minutes of incubation they were washed 2 times with VE H_2O and resuspended herein. Subsequently, silanized spicules were incubated with activated nanoparticles for 2 hours with shaking. After that, the silanized spicules with immobilized nanoparticles on the surface were washed 3 times with Dulbecco's phosphate buffered saline (DPBS, pH 7).

The resulting spicules were spaced out on slides, and their quality controlled by fluorescence microscopy (EVOS fl, AMG, Mill Creek, USA) using the RFP light cube (AMG, Mill Creek, USA) or by laser scanning microscopy (LSM 710, Zeiss, Oberkochen) using an helium/neon laser (excitation 543 nm).

4.4 A bioreactor procedure to raise exceptionally large primmorphs

4.4.1 Standard primmorph preparation

Until today, cultivation of sponge cells is only possible as a self-assembled, three-dimensional, amorphous cell aggregate termed primmorph. To prepare primmorphs from fresh sponge tissue, the latter has to be dissociated into single cells which then tend to reaggregate, in the appropriate medium, into smaller primmorphs (Custodio et al., 1998). The detailed procedure was as follows: Fresh sponge (*S. domuncula*) tissue was cut from the adult sponge with a clean scalpel directly in the aquarium under seawater, transferred into a 50 ml falcon tube filled with aquarium seawater, and immediately transported to the laboratory. The tissue was then cut into small pieces (1 mm^3) in a culture dish filled with calcium and magnesium free seawater containing EDTA (CMFSW+EDTA, for recipe see 4.1.3), in order to facilitate chemical dissociation (see Fig. 14). After cutting, the pieces were put into a fresh 50 ml tube filled with fresh CMFSW+EDTA and shaken for 30 min at room temperature. After this incubation, the supernatant was filtered through gaze into a fresh 50 ml tube. The tube with the tissue cubes was filled with fresh CMFSW+EDTA supplemented with 1 mM of dithiothreitol (DTT) and again incubated for 30 min with shaking, followed by a second filtration through gaze (Fig. 14). The single dissociated sponge cells in the filtered supernatants were each time, directly after filtration, pelleted by centrifugation at 2000 x g for 5 min. The pellets were then resuspended in 10 ml CMFSW and pooled, followed by a last centrifugation step, again at 2000 x g for 5 min. After that, the resulting pellet was resuspended in culture medium (composition described above) and transferred to the culture dish. Directly after transfer, the single sponge cells started to aggregate. Within three days they formed complete primmorphs.

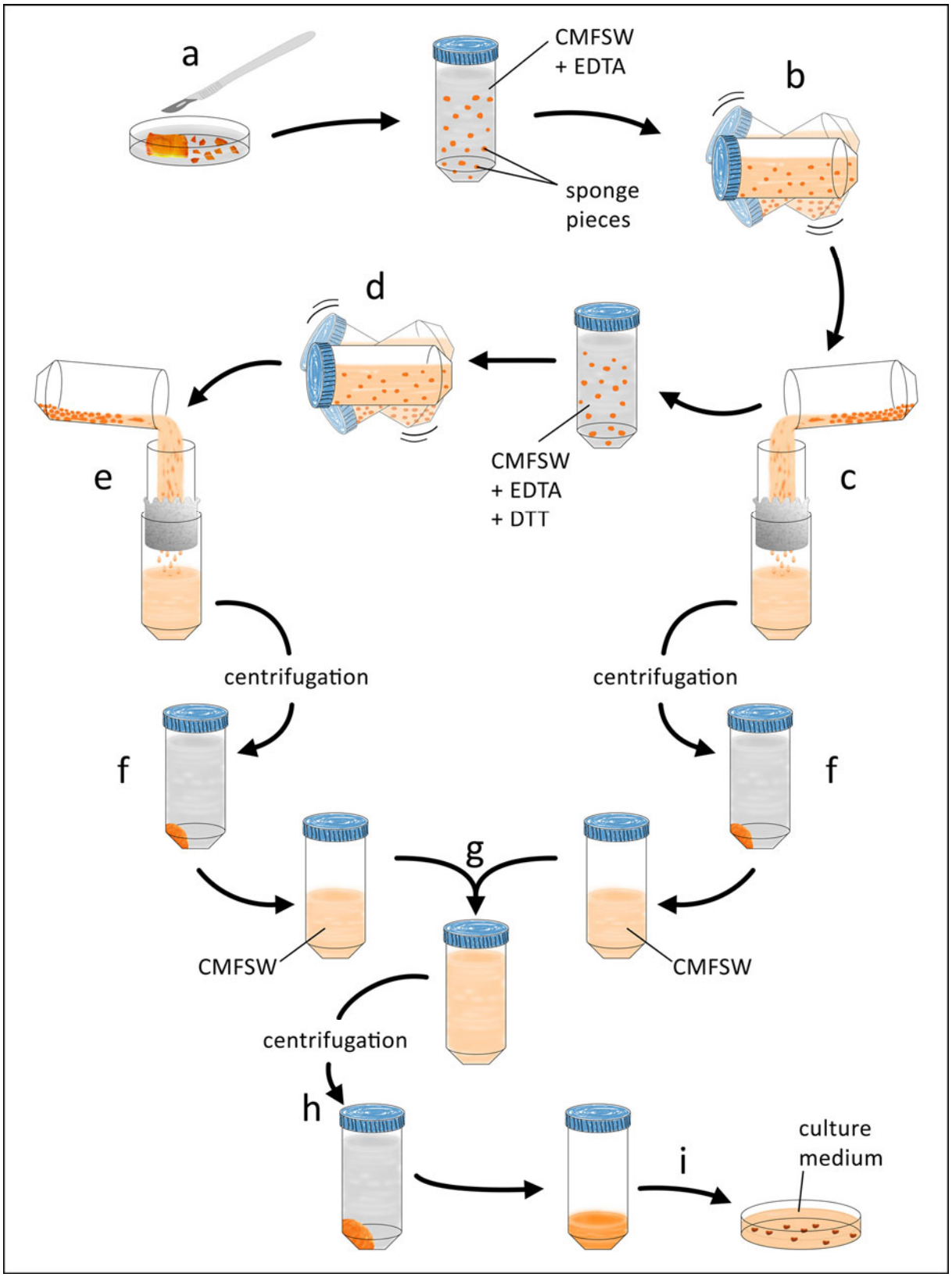

Fig. 14 Scheme of standard primmorph preparation. *S. domuncula* tissue was cut into small pieces (a) and incubated in calcium and magnesium free seawater (CMFSW) and EDTA with shaking (b). Resulting liquid with dissociated cells was filtered through gaze into a fresh tube (c). Remaining sponge tissue particles were incubated again in CMFSW, EDTA and DTT with shaking (d), followed by another filtration (e). Filtered dissociated cells were centrifuged (f), resuspended in CMFSW, and pooled (g). After a last centrifugation step (h) cells were resuspended in culture medium and transferred to a culture dish (i), where they formed complete primmorphs within 3 days. (Scheme designed in Adobe Photoshop)

4.4.2 Sponge cell culture

Sponge cells were kept as primmorphs in culture medium with the following composition: Sterile seawater was supplemented with HEPES and ferric citrate. The pH value was adjusted to 8. After addition of one table spoon of sea sand the medium was sterilized. GlutaMAX, pyruvate and antibiotics solution (penicillin/streptomycin) were added afterwards (for recipes see 4.1.6). The culture medium was stored at 4 °C.

Primmorphs were kept in culture dishes or well plates at 16 °C with constant gentle shaking, in order to promote cell-cell contact. One third of the culture medium was changed every 2 - 3 days and replaced by fresh culture medium.

4.4.3 How to use the custom made bioreactor

Our custom made bioreactor is described in the Results. It has a capacity of 3 liters. To run it, we used 2 liters of primmorph culture medium (see 4.1.6). The reactor was first filled with the complete volume of culture medium and kept at 16 °C. A supply tube added air bubbles to the medium which was moved by stirring elements. A suspension of single sponge cells from a mature sponge, dissociated in the same way as for standard primmorph preparation, was slowly added through a second supply tube. In contrast to the standard primmorph preparation in which all sponge cells come together from the start, the single cells were kept and added to the bioreactor in small portions (suspended in ca. 3 ml CMFSW), in order to prevent the tube from being blocked by aggregating cells. In this way a whole sponge individual can be dissociated in several subsequent cycles and added to the bioreactor. For cultivation of primmorphs, 1/3 of the medium was changed once per week.

4.5 Uptake of magnetic and fluorescent particles

4.5.1 Incubation of primmorphs with nano- and microparticles

For incubating primmorphs with nanoparticles, single *S. domuncula* cells were obtained the same way as described above (see 4.4.1) until the last centrifugation step. The cells were then briefly resuspended in culture medium and directly supplemented with nanoparticles in the respective concentration. For my experiments, besides 100 nm nano-screenMAG-CMX nanoparticles (see 4.3.3) I used silica core-shell microparticles with a diameter of 800 nm. They consist of a core of fluorescein isothiocyanate (FITC, green; excitation maximum at 492 nm, emission maximum at 520 nm) bound to

(3-aminopropyl)triethoxysilane (APTS), and a dense silica network as outer shell. The silica core-shell microparticles were produced and kindly provided by Dr. Tarek Elkhooly from our research group. Since nanoparticles are defined as particles up to 100 nm in size (Auffan et al., 2009), the nano-screenMAG-CMX particles (hydrodynamic diameter of 100 nm) are here referred to as "nanoparticles", whereas the silica core-shell particles (diameter of 800 nm) are addressed here as "microparticles".

Nano-screenMAG-CMX nanoparticles were used in concentrations of 0.1 or 1 mg/ml; the respective concentration is given in the text. Silica core-shell microparticles were used in a concentration of 0.5 mg/ml. After addition of nanoparticles, primmorphs were kept and treated as described in 4.4.2. Repeated addition of nanoparticles to already prepared primmorphs was avoided. Uptake success of micro- and nanoparticles was examined by fluorescence microscopy (EVOS fl, AMG, Mill Creek, USA). For nano-screenMAG-CMX nanoparticles I used the RFP light cube (AMG, Mill Creek, USA), and for silica core-shell microparticles the GFP light cube (AMG, Mill Creek, USA), respectively.

4.5.2 Frozen tissue sectioning and fluorescence microscopy

In a drop of embedding medium (Shandon Cryomatrix Frozen Embedding Medium, Thermo Scientific, Schwerte) 19 days old primmorphs incubated with silica core-shell microparticles were frozen in liquid nitrogen. In order to ensure a uniform freezing process, the primmorphs in embedding medium were transferred to small containers filled with isopentane. The containers were then put in liquid nitrogen. Frozen tissue sections (6 µm thickness) were cut with a freeze microtome (HM 500OM, Microm, Walldorf) at a permanent temperature of -25 °C. Sections were transferred to glass slides and dried overnight. After fixation with chloroform, methanol and acetone, sections were covered with Mowiol (Hoechst, Frankfurt) embedding medium (4.1.3) and coverslips. Primmorph sections were examined by fluorescence microscopy (Leitz DM/RBD, Leica, Wetzlar), and images were taken with the camera Leica DC 500 (Leica Microsystems, Wetzlar) in phase contrast or epifluorescence optics by using the software program Paint Shop Pro (PSP, Jasc Software, Eden Prairie, Minnesota, USA).

4.5.3 Chemical fixation and sectioning for electron microscopy

For electron microscopy, primmorphs were embedded 3 days, 9 days or 19 days after preparation and incubation with or without particles as described in 4.5.1. Incubation took place with nano-screenMAG-CMX nanoparticles at a concentration of 1 mg/ml cell suspension, and with silica core-shell microparticles at a concentration of 0.5 mg/ml cell suspension. All buffers used were freshly

prepared. Primmorphs of 3 - 6 mm³ in size were used. They were fixed for at least 2 h at room temperature with 2.5 % glutaraldehyde in 0.2 M phosphate buffer (pH 7.4) supplemented with 0.82 % NaCl. After washing with 0.2 M phosphate buffer supplemented with 1.75 % NaCl a post-fixation step was performed. For this step, fixed primmorphs were incubated for 1 h in a solution of 2 % osmium tetroxide, 1.25 % $NaHCO_3$ and 1 % NaCl (pH 7.4). In this case, osmium tetroxide is used for fixation as well as for staining of the tissue. After repeated washing steps and dehydration with increasing ethanol concentrations, primmorphs were embedded in araldite. For this, the araldite concentration ascended *via* the evaporation of propylene oxide. Araldite is a water-immiscible glycerol-based epoxy resin (Hayat, 2000). At the end of this procedure, primmorph tissue was completely and evenly penetrated by the embedding medium, which is a crucial step for successful sectioning. Primmorphs were transferred to embedding molds and heated for at least 48 h at 60 °C. After that, the resin was sufficiently hard and stable for ultrathin sectioning. Primmorphs embedded in such blocks were kept at room temperature.

Sectioning was done in two steps: First, semi-thin sections of ca. 1 µm thickness were cut with a glass knife. They were dried on a heat plate, stained with methyl blue and observed with a light microscope for control. Second, from the trimmed embedding block ultrathin sections (70 -100 nm) were cut on an ultra-microtome (Reichert Ultracut E, Leica Microsystems, Wetzlar) with a diamond knife. Ultra-thin sections were stretched on a water surface with xylol fume and collected on copper grids. Prior to that, the grids were covered with a Formvar film (1.2 % in chloroform). Ultra-thin sections on copper grids were stained for 10 min with uranyl acetate (2 %) in 50 % ethanol and for 2 min with lead citrate.

4.5.4 Transmission electron microscopy and energy-dispersive X-ray (EDX) spectroscopy

Transmission electron microscopy (TEM) was done with a Tecnai12 transmission electron microscope (FEI, Eindhoven, Netherlands) equipped with a BioTWIN lens. It operated at 120 kV and had a LaB_6 electron source. It was equipped with a TemCam-F416 4K x 4K charge-couples device (CCD) camera to take electron micrographs.

In order to analyze the elemental composition of deposits, that from the TEM images were assumed to represent nanoparticles, we used energy-dispersive X-ray (EDX) spectroscopy in combination with TEM. Therefore it was necessary to evaporate the ultra-thin sections on the grids with a carbon layer of 3 nm. X-rays emitted by the sample were collected for 60 sec by using a Tecnai F30 transmission electron microscope (FEI, Eindhoven, Netherlands) running in scanning TEM mode and equipped with an EDX spectrometer.

4.5.5 Scanning electron microscopy

Scanning electron microscopy (SEM) was done with a Phenom ProX table top device (Phenom-World B.V., Eindhoven, Netherlands) possessing a CeB_6 electron source and operated at 10 kV. Samples were not specially prepared for SEM analysis, because we used the primmorph tissue already available in the embedding blocks prepared for TEM. Since the ultrathin sectioning described above yielded cuts into the primmorph tissue, the surface of those embedding blocks could be directly scanned by SEM. The resolution of the EDX map scans was 128 x 90 pixels. This means that each pixel represents one EDX measurement. The elements were automatically identified by the supplemented software "Phenom ProSuite" and "Element Identification".

4.5.6 RNA preparation

RNA was isolated from tissue of five mature *S. domuncula* individuals, as well as from primmorphs prepared from the same five sponge individuals, incubated with and without nano-screenMAG-CMX nanoparticles or silica core-shell microparticles. Prior to the RNA preparation, the working space and all consumables were wiped with RNase-Away (Sigma-Aldrich, Munich). Phenol chloroform extraction of RNA as described by Chomczynski and Sacchi (1987) was applied. The isolation procedure followed the instructions of the TRIzol manual (Life Technologies, Darmstadt). In brief, the tissue was homogenized in TRIzol by using a Precellys 24 homogenizer (Peqlab, Erlangen) and the corresponding reaction tubes of the “Precellys Ceramic-Kit 1.4 mm” (Peqlab, Erlangen). An extra centrifugation step was performed, and then a phase separation with chloroform; only the RNA phase was kept. The RNA was precipitated with isopropanol. After washing with ethanol, the RNA was resuspended in 30 µl of nuclease-free water and stored at -80 °C. Before using the RNA, its concentration was measured in a NanoDrop spectrophotometer (Thermo Scientific, Schwerte), and its composition analyzed by agarose gel electrophoresis.

4.5.7 Agarose gel electrophoresis

In order to analyze RNA or DNA fragments, agarose gel electrophoresis was performed. It is a convenient method to separate nucleic acid fragments according to their size. In general, the resolution of fragments increases with increasing agarose concentration in the gel (Sambrook and Russell, 2001). For the respective analysis of DNA and RNA fragments, I applied the agarose gel protocols termed here “DNA gel” and “RNA gel” (see 4.1.3).

Agarose was melted in the appropriate buffer and then poured in a horizontal chamber, leaving pockets for the nucleic acid. For DNA gels, 10 x Tris-borate-EDTA buffer (Roth, Karlsruhe) was used as gel buffer. The gel buffer for RNA gels was identical with the "RNA denaturation buffer" (see 4.1.3). After polymerization, the gel was put into an electrophoresis chamber (PerfectBlue Mini S or Mini M Gelsystem, Peqlab, Erlangen). The running buffer was identical with the gel buffer. An electric field of 80 V was applied for ca. 1 h. Nucleic acids are negatively charged and therefore migrate from the cathode to the anode. Due to pores in the agarose gel, smaller fragments migrate faster in the electric field than larger fragments. Prior to loading, the sample was mixed with loading dye. For DNA gels, 6 x DNA gel loading dye (Fermentas, St. Leon-Rot) was used, for RNA gels 2 x RNA gel loading dye (Thermo Scientific, Schwerte) was applied. To determine the size of DNA fragments, a DNA standard was used, encompassing various DNA fragments of defined size (GeneRuler DNA Ladder Mix, Thermo Scientific, Schwerte). After electrophoresis, the gel was stained in an ethidium bromide bath. The fluorescent stain ethidium bromide intercalates between the nucleotide bases of the nucleic acid and thereby makes the DNA or RNA visible under UV illumination.

4.5.8 cDNA preparation from RNA

For cDNA preparation, the total RNA extracted from five sponge individuals and their primmorphs was used. Prior RNA preparation primmorphs were incubated with and without nano- or microparticles. 1 µg RNA from each individual was taken, and the five samples were pooled. The resulting 5 µg of RNA were incubated for 20 min at room temperature with 4 µl 5 x reaction buffer from the "RevertAid RT Kit" (Thermo Scientific, Schwerte) and 1 µl DNase I (Thermo Scientific, Schwerte) in order to eliminate contaminating DNA. The mixture was replenished to 25 µl with nuclease-free H_2O. After incubation, 3 µl DNase inactivation reagent (DNA-*free* Kit, Thermo Scientific, Schwerte) were added for 2 min. This reagent binds DNase I plus cations and can simply be sedimented by centrifugation. 20 µl of the supernatant were transferred to a fresh 1.5 ml reaction tube, incubated for 5 min at 80 °C and then put 10 min on ice. For preparation of the reverse transcriptase mixture, components of the "RevertAid RT Kit" (Thermo Scientific, Schwerte) and Oligo$(dT)_{20}$ primer (Life Technologies, Darmstadt) were used. In the end, the mixture contained 1 x concentrated reaction buffer, 0.5 mM deoxynucleotides, 3.7 µM random hexamer primer and 1.8 µM oligodeoxythymidine primer as well as 220 U reverse transcriptase enzyme. The whole mixture was incubated for 10 min at room temperature, 30 min at 37 °C, 10 min at 56 °C and finally 5 min at 80 °C. In the end, the mixture was diluted 1:10 with nuclease-free water, in order to dilute the initial components. Reverse transcriptases are RNA-dependent DNA polymerases which create single-stranded cDNA from a RNA template (Sambrook and Russell, 2001). As starting point for the polymerase, the oligodeoxythymidine primer, in this case consisting of 20

deoxythymidines, was hybridized to the poly(A) tail of the mRNA. Random primers make sure that all RNA molecules are transcribed to cDNA. In contrast to a standard polymerase chain reaction (PCR), this reaction has only one cycle, because the resulting cDNA should not be amplified. To check the quality of the cDNA, a preliminary quantitative PCR was carried out.

4.5.9 Quantitative PCR (qPCR)

Quantitative PCR is a technique to analyze gene expression through the abundance of RNA transcripts converted to cDNA. Sequence-specific primers of the gene of interest are used to amplify, by PCR, DNA sequences of ca. 100 bp. As soon as double-stranded DNA is produced, a fluorescent dye (here SYBR Green) intercalates into the DNA double helix and is thereby converted to a fluorescent state. Double-stranded DNA is abundant after each PCR cycle, prior to the next denaturation step. At this point, the fluorescence intensity is measured automatically by the real-time PCR instrument. This means, the earlier the fluorescence signal is detectable, the more initial cDNA representing the gene of interest is available. This correlates signal occurrence time with initial number of RNA copies of the respective gene. In other words, this technique provides information about the expression rate of a gene of interest. For example, the expression rates of a gene under different physiological conditions of the animal can be compared. Reference genes with constant expression rates under the chosen physiological conditions are necessary to normalize the expression rate of the gene of interest.

For this thesis, the influence of nano-screenMAG-CMX nanoparticles or silica core-shell microparticles on the expression rates of four different genes in *S. domuncula* primmorphs were surveyed, namely silicatein-α (GenBank AJ877017), silicatein-β (GenBank AJ784227), silintaphin-1 (GenBank AM902264) and slowpoke-binding protein (sequence kindly provided by Dr. Matthias Wiens). As reference genes, β-tubulin (GenBank AJ550806) and glycerol 3-phosphate dehydrogenase = GAPDH (GenBank AM902265) were used. To analyze the expression rates, I applied the “iTaq universal SYBR Green supermix” (Bio-Rad, Munich), which is 2 x concentrated. It contains antibody-mediated hot-start iTaq DNA polymerase, deoxynucleotides (dNTPs, a mixture of dATP, dTTP, dCTP, dGTP), $MgCl_2$, SYBR Green I dye and additionally enhancers and stabilizers. This master mix was used in 1 x concentration, with the respective primers added. Primers for the genes of interest or for reference genes were used in the reaction mixture in 0.3 µM final concentrations. The reaction mixture was filled up to 27 µl with nuclease-free water if needed. For gene expression analysis, the respective cDNA was diluted 1:10 with nuclease-free water; 3 µl were used per reaction. Each reaction was carried out in triplets on a white, low profile 96-well plate (Thermo Scientific, Schwerte), the plates were sealed with “ABsolute qPCR Plate Seals” (Thermo Scientific, Schwerte). The thermocycler used for quantitative PCR was “ C1000

Touch" (Bio-Rad, Munich). Before analyzing gene expression, the primer efficiency was tested by using cDNA in 1:10, 1:100 and 1:1000 dilutions for the qPCR. The primer efficiency was then automatically calculated by the "CFX Manager" software, version 3.1 (Bio-Rad, Munich). Only primers with efficiencies above 90 % were used. The qPCR conditions are shown in Table 2, sequences of the used primers are given in Table 3. Expression rates were calculated automatically by the CFX Manager software.

Table 2 Conditions used for qPCR

initial denaturation	95 °C	30 sec	
denaturation	95 °C	10 sec	40 x
annealing	58 °C	20 sec	
elongation	72 °C	30 sec	
measuring fluorescence			
denaturation	95 °C	10 sec	

Table 3 Sequences of the primers used for qPCR

Gene	Forward primer sequences (5' to 3')	Nucleotide position	Reverse primer sequences (5' to 3')	Nucleotide position
silicatein-α	AGCGTGATCCTCTAC AGGACTACCC	320 - 344	GCATTAGCACCCTCCAAA GCACCC	432 - 455
silicatein-β	TCCTCTAGCACGCTG AGTCATGCC	970 - 993	GCCCTTGTTTCTTGCCAA CTTCCC	1084 - 1107
silintaphin-1	CACAACACTGAAGGC CGTAAGC	589 - 610	TGACAGTCTTGTCCAGGT CAGC	670 - 691
slowpoke-binding protein	AAGACACCATTTACA GGGCCACAC	614 - 637	AAATCCCTTGCTGTCCAG GAACAC	733 - 756
β-tubulin	CAGCCGTGGATCTCA GCAATAC	822 - 843	GCCACGGAACATAGCAGC AAC	937 - 957
GAPDH	TCCAAACCAGCCAAG TACGATG	745 - 766	AGTGAGTGTCTCCCCTGA AGTC	853 - 874

4.6 Apatite formation of SaOS-2 cells transfected with sponge silicatein-α

4.6.1 Gateway cloning of silicatein-α in pcDNA6.2 cTC

Gateway cloning was performed according to the user guide for "Gateway Technology" (Life Technologies, Darmstadt). An overview of the basic reaction steps applied for gateway cloning is shown in Fig. 15.

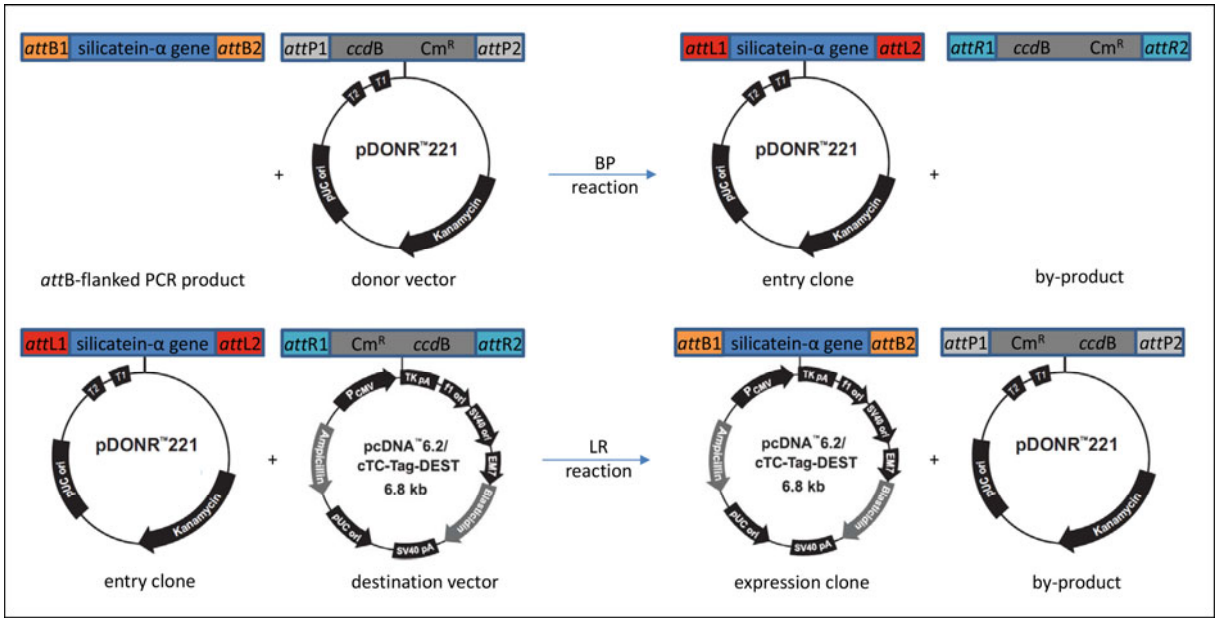

Fig. 15 Overview of the performed cDNA cloning steps by using the Gateway Technology (Life Technologies, Darmstadt). The first step after preparing the attB-flanked PCR product was to integrate the cDNA of interest (here encoding silicatein-α) into the donor vector (here pDONR221) *via* the "BP" reaction. The resulting "entry clone" was amplified in *E. coli*, and purified. Then, the "LR" reaction was performed in which the amplified entry clone was combined with the destination vector (here pcDNA6.2/cTC-Tag-DEST), yielding the expression clone (here termed pcDNAcTC-sili). (Scheme according to Life Technologies, Darmstadt, substantially modified)

The first step was to produce the attB-flanked cDNA sequence coding for mature silicatein-α (without signal sequence). This was achieved by PCR (for components and conditions, see Table 4 and Table 5). The PCR template (pQE30 Siliα) was produced and kindly provided by Dr. Thorben Link from our research group. The used polymerase, amplification buffer and $MgSO_4$ were taken from the Platinum *Pfx* DNA Polymerase kit (Life Technologies, Darmstadt). If not mentioned otherwise, all PCR reactions were performed in a PeqSTAR 2 x gradient thermocycler (Peqlab, Erlangen). The primer sequences are shown in Table 8. The resulting PCR product was identified by electrophoresis in a 1 % agarose gel and subsequent staining with ethidium bromide (for description see 4.5.7). The respective cDNA bands were excised and then extracted from the gel by using the "High Pure PCR Product Purification Kit" (Roche, Mannheim) following the user guide. This kit is based on a column system with integrated silica filters, to which the PCR product is reversibly bound through destruction of its hydration shell, while

contaminants are washed away. Subsequently, the cDNA is eluted by low salt concentrations. After the entire purification procedure, the concentration of PCR products or plasmid DNA was measured in a NanoDrop spectrophotometer (Thermo Fisher Scientific, Waltham, USA).

Table 4 Components of the initial PCR for producing the attB-flanked cDNA sequence coding for silicatein-α

Component	Final concentration or volume
10 x *Pfx* amplification buffer	2 x
dNTP mixture (dATP, dTTP, dCTP, dGTP)	0.3 mM each
$MgSO_4$	1 mM
forward primer (attB1 SP/Silicatein 6.2c)	0.2 µM
reverse primer (attB2 ASP/Silicatein 161)	0.2 µM
template (pQE30 Siliα)	75 ng
Platinum *Pfx* DNA Polymerase	2.5 U
nuclease-free H_2O	to 50 µl

Table 5 Conditions of the initial PCR producing the *att*B-flanked cDNA sequence coding for silicatein-α

initial denaturation	94 °C	5 min	
denaturation	94 °C	15 sec	32 x
annealing	55 °C	30 sec	
elongation	68 °C	1 min	
storage	4 °C	∞	

In order to create an entry clone, the so-called BP reaction was performed according to the user guide for the "Gateway BP Clonase II Enzyme Mix" (Life Technologies, Darmstadt). In brief: 85 ng of the purified *att*B-flanked PCR product encoding the sequence of silicatein-α were combined with 150 ng of the donor vector (pDONR 221, Life Technologies, Darmstadt; Fig. 16).

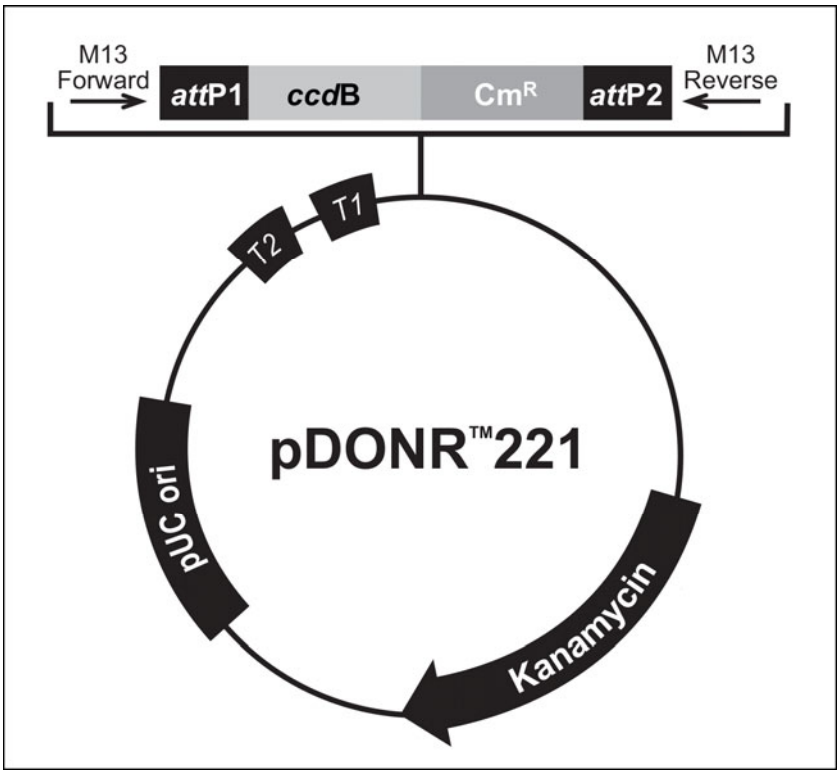

Fig. 16 Map of the used donor vector (pDONR221) for Gateway cloning (purchased from Life Technologies, Darmstadt). Among other components it comes with the Gateway cloning site and a resistance gene for kanamycin. (Scheme taken from Life Technologies, Darmstadt)

"One Shot TOP10 Chemically Competent" *E. coli* cells (Life Technologies, Darmstadt) were transformed with the resulting entry clone according to "Transforming Competent Cells" in the user guide for "Gateway Technology" (Life Technologies, Darmstadt) and grown over night on lysogeny broth (LB) agar plates (see 4.1.6) containing 50 µg/ml kanamycin at 37 °C. The next day, grown cultures were picked with 10 µl pipette tips, and a so-called "checking PCR" was performed (Table 6 and Table 7).

Table 6 Components of the "checking PCR"

Component	**Final concentration or volume**
picked *E. coli* colony	resuspended in 6 µl nuclease-free H_2O per colony
PCR master mix, 2 x	1 x
forward primer	0.5 µM
reverse primer	0.5 µM
nuclease-free H_2O	up to 15 µl per colony

Table 7 Conditions of the "checking PCR"

initial denaturation	95 °C	5 min	
denaturation	95 °C	15 sec	35 x
annealing	56 °C	30 sec	
elongation	72 °C	1 min	
final elongation	72 °C	10 min	
storage	4 °C	∞	

A "checking PCR" was always performed when it was necessary to analyze the transformation success of bacteria colonies. In this case, the gene-specific forward primer was "SiliαF" and the vector-specific reverse primer was "M13Rev" (Table 8). Pipette tips used for *E. coli* colony picking were kept in 500 µl liquid LB medium (see 4.1.6) containing 50 µg/ml kanamycin at 37 °C with shaking until the results of the checking PCR were evaluated. Successfully transformed *E. coli* colonies were added to 6 ml liquid LB medium (see 4.1.6) containing 50 µg/ml kanamycin and grown over night at 37 °C with shaking. The next day, plasmid isolation was performed. For all mini plasmid isolations, the "HighPure Plasmid Isolation Kit" (Roche, Mannheim) or the "peqGOLD Plasmid Miniprep Kit" (Peqlab, Erlangen) were used according to the manufacturer's instructions; all optional steps were performed. Like the previously described kit for purifying PCR products, these plasmid isolation kits are based on a column system with integrated silica filters to which the plasmid DNA is reversibly bound, while all other cell components are washed away. The plasmid DNA was subsequently eluted with 70 °C preheated nuclease-free water, yielding a final volume of 50 µl.

Table 8 Primer sequences used for different PCRs

Primer name	Primer sequences (5' to 3')	Producer
T7	AAT ACG ACT CAC TAT AGG	Eurofins MWG, Ebersberg
M13Rev	CAG GAA ACA GCT ATG AC	Eurofins MWG, Ebersberg
SiliαF (binding to Nt_{343}-Nt_{365} of the sequence encoding silicatein-α)	CCT GAA GCT GTA GAC TGG AGA AC	Eurofins MWG, Ebersberg
SiliαRev (binding to Nt_{967}-Nt_{990} of the sequence encoding silicatein-α)	TAG GGT GGG ATA AGA TGC ATC GGT	Eurofins MWG, Ebersberg
attB1 SP/Silicatein 6.2c	GGG GAC AAG TTT GTA CAA AAA AGC AGG CTT AAC CAT GGA CTA CCC TGA AGC TGT AG	Life Technologies, Darmstadt
attB2 ASP/Silicatein 161	GGG GAC CAC TTT GTA CAA GAA AGC TGG GTA TAG GGT GGG ATA AGA TGC	Life Technologies, Darmstadt

The isolated entry clone (pDONR221, containing the sequence encoding silicatein-α) was then combined, by the LR reaction, with the destination vector pcDNA6.2/cTC-Tag-DEST (Fig. 17) purchased from Life Technologies (Darmstadt). A prominent feature of this destination vector is the integrated C-terminal sequence for a tetracysteine (TC) tag. Later in the cell, this TC tag is expressed as part of the protein of interest, thereby allowing detecting the latter in living cells (chapter 4.6.3.3).

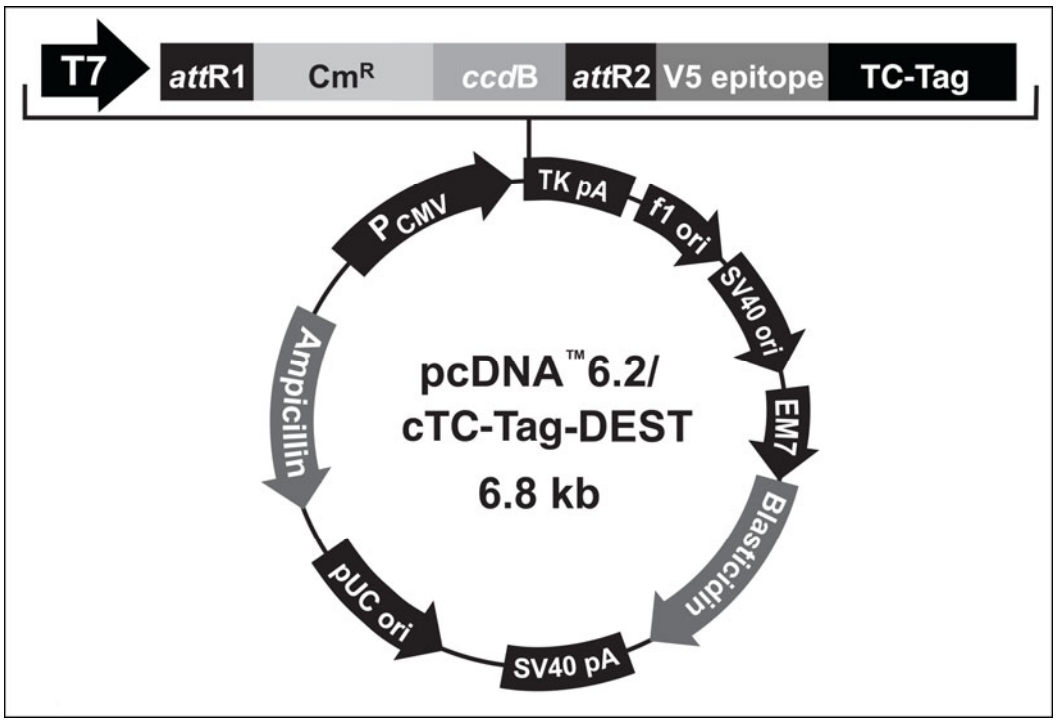

Fig. 17 Map of destination vector "pcDNA6.2/cTC-Tag-DEST" for Gateway cloning (purchased from Life Technologies, Darmstadt). Among other components it comes with the Gateway cloning site, resistance genes for ampicillin (to select transformed bacteria colonies, carbenicillin can be used alternatively) and blasticidin (to select transfected mammalian cells), the sequence encoding the recognition site of the V5 antibody, as well as the sequence encoding the TC tag. (Scheme taken from Life Technologies, Darmstadt)

For the so-called LR reaction, the "Gateway LR Clonase II Enzyme Mix" (Life Technologies, Darmstadt) was used. The reaction was performed according to the user guide. For the reaction, 150 ng of the entry clone were mixed with 150 ng of the destination vector. "One Shot TOP10 Chemically Competent" *E. coli* cells (Life Technologies, Darmstadt) were transformed with the resulting expression clone according to "Transforming Competent Cells" in the user guide for "Gateway Technology" (Life Technologies, Darmstadt). The cells were grown overnight on LB plates containing 50 µg/ml carbenicillin at 37 °C. Carbenicillin can be used instead of ampicillin; it has the advantage, that it is more thermostable than ampicillin (Sambrook and Russell, 2001). The next day, a checking PCR with subsequent agarose gel electrophoresis was performed as described above (4.5.7). The checking PCR was performed with the gene-specific reverse primer "SiliαRev" and the vector-specific forward primer "T7" (see Table 8). Pipette tips used for *E. coli* colony picking were kept in 500 µl liquid LB medium (see 4.1.6) containing 50 µg/ml carbenicillin at 37 °C with shaking until checking PCR results were evaluated. Successfully transformed *E. coli* colonies were added to 6 ml liquid LB medium containing 50 µg/ml carbenicillin and grown overnight at 37 °C with shaking, followed by plasmid isolation. The isolated expression clone was called "pcDNAcTC-sili". For controlling the sequence, the purified clone pcDNAcTC-sili was sent to a commercial sequencing service (StarSEQ, Mainz). For this, 600 ng of plasmid DNA were mixed with T7 primer (final concentration of 14.3 µM). Nuclease-free water was added to 7 µl. The obtained nucleotide sequence was compared, by pairwise sequence alignment, to the authentic nucleotide sequence encoding silicatein-α (GenBank AJ877017). For this, the software Geneious version 6.0.5 (Kearse et al., 2012) was applied. Only if the sequences matched 100 % from start codon to stop codon (with the exception of the additional TC tag present in the clone), the respective original bacteria culture was later used for amplification of the pcDNAcTC-sili plasmid. For cryopreservation of the respective bacteria colonies "Roti-Store cryo-vials" (Roth, Karlsruhe) were used according to the instructions and kept at -80 °C.

4.6.2 Amplification and purification of plasmids from *E. coli* for transfection

For successful transfection, ultrapure plasmid DNA is necessary. In order to reach the required purity, I used the "QIAfilter Plasmid Midi Kit" (QIAGEN, Hilden). This system is based on alkaline lysis of the bacteria cells followed by binding the plasmid DNA to a special resin. The cell lysate is pushed by a syringe plunger through the resin. After washing and thereby removing contaminants, the plasmid DNA is eluted in high salt buffer and concentrated by isopropanol precipitation. 25 ml of fresh liquid LB medium supplemented with 50 µg/ml carbenicillin were inoculated with an *E. coli* colony bearing the pcDNA6.2cTC-sili plasmid. The *E. coli* colony was taken from cryopreservation or 100 µl fresh

bacteria culture. The mixture was kept at 37 °C overnight with shaking. The next day, it was used for midi plasmid preparation according to the QIAfilter Plasmid Purification Handbook, with the exception that the centrifugation steps for bacteria cell collection and collection of the precipitated plasmid DNA were performed at 5000 x g and doubled time. For elution of the plasmid DNA, 50 µl of TE buffer were used (for prescription of TE, see 4.1.3). After measuring the concentration, if required the DNA was diluted with TE buffer to a concentration of 1 µg/µl.

4.6.3 SaOS-2 cell culture

4.6.3.1 Daily culturing of SaOS-2 cells

All procedures regarding SaOS-2 cells were performed under common sterile conditions with sterile equipment and consumables in a vertical laminar flow hood (BioNova, Roma, Italy) equipped with high efficiency particulate air filters of 0.2 µm.

SaOS-2 cells are a human osteoblast-like cell line derived from osteosarcoma cells (Fogh et al., 1977). They were kept in McCoy 5A mod. medium (Biochrom, Berlin), supplemented with fetal bovine serum, GlutaMAX (Life Technologies, Darmstadt) and gentamicin (see 4.1.6). SaOS-2 cells are adherent cells. They were grown in monolayers (until 90 % confluence) in sterile 25 cm^2 flasks with 10 ml, or 75 cm^2 flasks with 20 ml of culture medium. Flasks were kept in darkness in a humidified incubator at 37 °C, with 5 % CO_2 (Müller et al., 2007a; Wiens et al., 2010b). Every two to three days, subcultures were seeded in fresh flasks. For this, medium was removed, the cell layer was once washed with 10 ml 37 °C Dulbecco's phosphate-buffered saline (DPBS) and detached with 1 ml (25 cm^2) or 3 ml (75 cm^2) 0.25 % trypsin/EDTA (containing 2.5 mg/ml trypsin and 0.38 mg/ml EDTA). To mediate the detaching, the cells were incubated for 3 - 5 min at 37 °C. One third of the cell suspension was then transferred into a fresh flask with culture medium preheated to 37 °C.

When needed, cell density was determined by counting a 1:10 dilution of SaOS-2 cells in suspension after detaching them with trypsin/EDTA. A scepter 2.0 cell counter (Merck Millipore, Darmstadt) was applied, according to the manufactures manual, using 60 µm sensor tips.

For long-term preservation, SaOS-2 cells were stored in stocks of 1 ml in sterile cryopreservation vials in liquid nitrogen. To prepare cells for cryogenic preservation, they were washed and detached as described above. After detaching, cells from a confluent 25 cm^2 flask were suspended in 1 ml of culture medium and centrifuged at 600 rpm for 5 min, in order to remove trypsin/EDTA. The cell pellet was then resuspended in culture medium with additional 5 % fetal bovine serum (meaning 20 % in total)

and 10 % dimethyl sulfoxide (which prohibits water crystallization during freezing). Cryopreservation vials were initially frozen to -80 °C in a polystyrene container (Nalgene Mr. Frosty freezing container, Thermo Scientific, Schwerte) filled with isopropyl alcohol which mediates a controlled cooling process of 1 °C per minute. After one day, frozen cells were transferred to liquid nitrogen. In order to start new cultures from a cryopreservation stock, cryopreservation vials were removed from the liquid nitrogen, carefully dipped in a water bath (37 °C) until the medium was liquid, and the cells transferred to a 25 cm^2 flask with preheated culture medium. Medium was changed after 24 h.

4.6.3.2 Activation of SaOS-2 cells

SaOS-2 cells have the ability to mineralize and thereby precipitate nodules composed of inorganic hydroxyapatite and organic compounds in the extracellular matrix, after incubating them in activation medium (Shioi et al., 1995; Orimo and Shimada, 2006; Wiens et al., 2010b). In addition to the normal culture medium, the activation medium was supplemented with a mineralization cocktail containing β-glycerophosphate, ascorbic acid and dexamethasone (4.1.6). Activation medium was added after the cells reached a density of 80 %. Thereafter, the cells were permanently kept in activation medium, which leads to hydroxyapatite deposition and a strong reduction in cell proliferation.

4.6.3.3 Transfection and selection of SaOS-2 cells

SaOS-2 cells were transfected with the construct pcDNAcTC-sili mediated by FuGENE HD (Promega, Mannheim). At the day prior to transfection, the cells were seeded in 500 µl of culture medium on 24-well plates (5 x 10^4 cells/well). At the day of transfection, per well 0.5 µg of highly pure plasmid DNA from the midi plasmid preparation (4.6.2) were added to OptiMEM medium (a reduced serum medium from Life Technologies, Darmstadt) at a concentration of 0.02 µg/µl. After addition of 1.7 µl FuGENE HD reagent (Promega, Mannheim), the solution was mixed by vortexing and incubated for 10 min at room temperature. In this step, FuGENE (a non-liposomal transfection agent) envelops the plasmid DNA. After incubation, the plasmid DNA/FuGENE complex was added to the cells. Transfection batches were up-scaled according to the desired number of wells.

One of the main features of the expression construct was the C-terminal TC tag (Griffin et al., 1998; Griffin et al., 2000; Adams et al., 2002). It is expressed only together with silicatein-α and encodes the amino acid sequence NH_2-Cys-Cys-Pro-Gly-Cys-Cys-COOH. The non-fluorescent, non-toxic biarsenical labeling reagent FlAsH-EDT_2 (Life Technologies, Darmstadt) is able to diffuse through membranes of

living cells. It forms disulfide bridges with the four thiol groups of the TC tag and is thereby converted to a highly fluorescent state (Fig. 18).

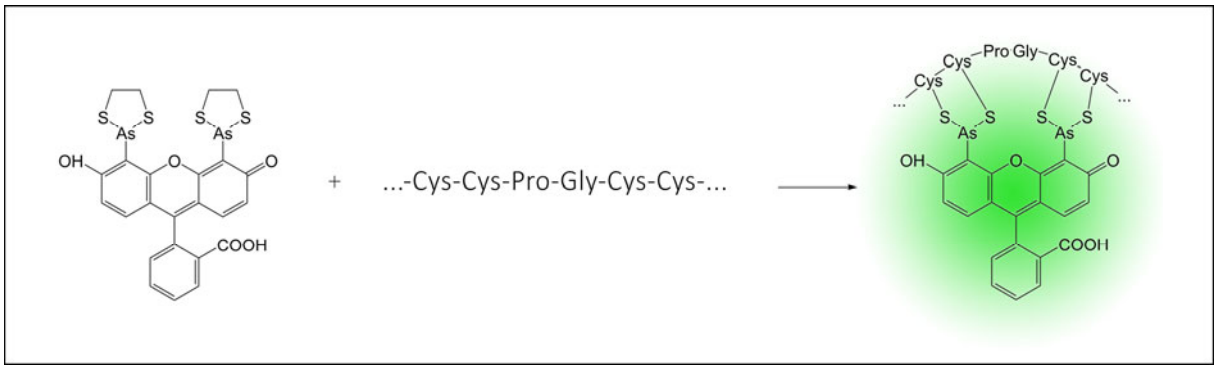

Fig. 18 Scheme of the non-fluorescent biarsenical labeling reagent FlAsH (= fluorescein arsenical helix binder) forms disulfide bridges with the thiol groups of the four cysteines and is thereby converted to a highly fluorescent state. (Scheme illustrated in ChemDraw and Adobe Photoshop, adapted from Adams et al., 2002)

Transfection success was evaluated by adding the FlAsH-EDT_2 to transfected and selected cells, using the "TC-FlAsH TC-ReAsH II In-Cell Tetracysteine tag Detection Kit" (Life Technologies, Darmstadt), following the instructions of the manufacturer. In brief, cells to be evaluated were washed with OptiMEM, and labeling solution consisting of FlAsH-EDT_2 diluted in OptiMEM was added. After 30 min of incubation in the cell incubator, cells were washed with BAL washing buffer provided with the kit and diluted in OptiMEM. Until examination, cells were kept in OptiMEM. Cells were examined by fluorescence microscopy (EVOS fl, AMG, Mill Creek, USA) using the GFP light cube (AMG, Mill Creek, USA).

Stably transfected cells were subsequently selected by permanent addition of 5 µg/ml blasticidin to the culture medium.

4.6.3.4 Cell fixation

For many tests it is necessary to fix the cells on the surface were they grow, in order to prevent them from detaching during the following incubation and washing steps. Paraformaldehyde is a standard crosslinking fixative which links proteins covalently and binds adherent cells to the surface. For fixation, cells were always washed two times with DPBS, incubated for 10 min at 37 °C with 4 % paraformaldehyde fixation medium (see 4.1.3), and then washed again two times with DPBS. The applied amounts of liquid depend on the size of the culture dish, making sure that the cells were always completely covered with liquid.

4.6.3.5 Alizarin red assay

The components yielding hydroxyapatite deposits are calcium ions (Ca^{2+}) and phosphate (Somogyi et al., 2004). The alizarin red assay is a convenient method to stain Ca^{2+} depositions, with 1 mol alizarin red S binding to 2 mol Ca^{2+} (Wang et al., 2006). Therefore, the alizarin red assay can also function as a marker for mineralization in SaOS-2 cells. For this assay, SaOS-2 cells to be evaluated (transfected and non-transfected cells, for 10 days in activation medium or standard growth medium) were fixed with 4 % paraformaldehyde fixation medium as described above. Afterwards, they were completely covered with filtered alizarin red S working solution (see 4.1.3) and incubated for 60 min under gentle agitation at room temperature. Then cells were washed extensively with distilled water until all unbound stain was removed. Afterwards, all deposited calcium is visible as a red color. The precipitate was subsequently dissolved in 1-hexadecylpyridinium chloride working solution (see 4.1.3) during 2 hours with gentle agitation. The absorbance of the colored supernatant was measured at 595 nm with a spectral scanning multimode reader (Varioskan Flash, Thermo Scientific, Schwerte), and the resulting calcium concentration was calculated.

4.6.3.6 AlamarBlue assay

With the reagent alamarBlue (Bio-Rad AbD Serotec, Puchheim), for different cell types the cytotoxicity of treatments can be analyzed. It functions as viability indicator, because only living cells are capable to reduce it from blue resazurin to bright pink resorufin. The resulting amount of resorufin is proportional to the number of living cells. For the alamarBlue assay, $1/10^{th}$ volume of alamarBlue reagent was directly added to the culture medium of SaOS-2 cells (transfected and non-transfected, for 10 days in activation medium or standard growth medium). Cells were incubated for 4 h in the cell incubator (37 °C, 5 % CO_2, darkness). The absorbance of the supernatant was directly measured at 570 nm and normalized to 600 nm with a spectral scanning multimode reader (Varioskan Flash, Thermo Scientific, Schwerte).

4.6.3.7 Alkaline phosphatase activity assay and protein concentration assay

Alkaline phosphatase hydrolyzes pyrophosphate and thereby makes inorganic phosphate available for hydroxyapatite deposition (Orimo, 2010). Its expression is known to be increased in mineralizing cells (Golub and Boesze-Battaglia, 2007) and thus it is used as a marker for hydroxyapatite deposition. For a comparison of the absolute alkaline phosphatase activity in differently treated cells, the total protein concentrations were used for normalization.

For measuring the cellular alkaline phosphatase activity as well as the protein concentration, the first step was to lyse SaOS-2 cells (transfected and non-transfected, for 10 days in activation medium or standard growth medium) with ice-cold lysis buffer (see 4.1.3). After an incubation of 10 min, the cells were sonicated, and the proteins separated from cell debris by centrifugation. The supernatant was transferred to fresh reaction tubes and used for measuring the alkaline phosphatase activity and the protein concentration.

As soluble substrate of alkaline phosphatase, *p*-nitrophenyl phosphate (SIGMA*FAST* *p*-nitrophenyl phosphate tablets, Sigma-Aldrich, Munich) was used. For analysis, 1 tablet of *p*-nitrophenyl phosphate and 1 tablet of Tris buffer components were dissolved together in 5 ml VE water. Per reaction, 200 µl substrate solution was mixed with 20 µl cell extract (diluted 1 to 20 with lysis buffer), and incubated for 30 min at room temperature in darkness. During this step, available alkaline phosphatase hydrolyzes *p*-nitrophenyl phosphate to the yellow *p*-nitrophenol. The absorbance of this product was measured at 405 nm with a spectral scanning multimode reader (Varioskan Flash, Thermo Scientific, Schwerte). The absorbance is proportional to the alkaline phosphatase activity and was normalized to the respective protein amount.

To measure the protein concentration of different samples, I used the "QuantiPro BCA Assay Kit" (Sigma-Aldrich, Munich) which is especially sensitive for lower protein concentrations (linear response from 0.5 - 30 µg/ml). Like other protein assays it is based on the reduction of Cu^{2+} to Cu^{1+} by different amino acids (Wiechelman et al., 1988), followed by the building of a purple-blue complex of Cu^{1+} with bicinchoninic acid in an alkaline environment (Smith et al., 1985). The reaction was performed on 96-well plates. Per reaction, 100 µl of the cell lysis supernatant were mixed with 100 µl of "QuantiPro Working Reagent", prepared as recommended by the manufacturer (Sigma-Aldrich, Munich). The plate was sealed and kept overnight at room temperature in darkness. The same was done for seven known protein concentrations (from 0 - 50 µg/ml) to obtain a standard curve. The absorbance of the assay was measured at 562 nm with a spectral scanning multimode reader (Varioskan Flash, Thermo Scientific, Schwerte). The concentrations of the unknown samples were determined by using the standard curve. From the protein concentration, the total amount of protein in each sample was calculated, and these values were used to normalize the alkaline phosphatase activity.

4.6.3.8 Staining of hydroxyapatite

As mentioned before, activated SaOS-2 cells mineralize by depositing hydroxyapatite. To make this hydroxyapatite visible by fluorescence microscopy, it can be stained by the fluorescent OsteoImage Staining Reagent (Lonza, Cologne). This dye specifically binds to hydroxyapatite (Langenbach et al.,

2011). The “OsteoImage Bone Mineralization Assay” was applied according to the user guide (Lonza, Cologne). Briefly, the cells were fixed as described above (4.6.3.4), followed by washing with 1 x OsteoImage washing buffer, incubation for 30 min in diluted staining reagent and an additional washing step with washing buffer. OsteoImage has an excitation maximum at 492 nm and an emission maximum at 520 nm. Hydroxyapatite depositions were examined by fluorescence microscopy (EVOS fl, AMG, Mill Creek, USA) using the GFP light cube (AMG, Mill Creek, USA).

4.6.3.9 Staining of cell nuclei

DRAQ5 is a fluorescent dye which can easily pass through the lipid bilayer of cell membranes. It selectively and efficiently intercalates with double-stranded DNA (Smith et al., 2000). Therefore I used DRAQ5 for counterstaining of SaOS-2 cell nuclei. After fixation with paraformaldehyde as described above (4.6.3.4), cells were incubated for 10 min at 37 °C in 5 µM DRAQ5 (in DPBS) followed by washing steps to reduce background fluorescence. DRAQ5 has an excitation maximum at 650 nm and an emission maximum at 680 nm. Cell nuclei were examined by fluorescence microscopy (EVOS fl, AMG, Mill Creek, USA) using the Cy5 light cube (AMG, Mill Creek, USA).

4.6.3.10 Staining of the actin cytoskeleton

Phalloidin is a toxin which interacts with actin and enhances its polymerization (Estes et al., 1981). It can be labeled with tetramethylrhodamine B isothiocyanate, a fluorescent dye which has an excitation maximum at 540 nm and an emission maximum at 565 nm. Due to its characteristics it is widely used to specifically stain the actin cytoskeleton. Rhodamine phalloidin (Cytoskeleton, Denver, USA) was used as counterstaining for subsequent fluorescence microscopy according to the manufacturer’s instructions. Briefly, fixed cells were permeabilized with Triton X-100, washed with DPBS and incubated with 100 nM rhodamine phalloidin in DPBS for 30 min at room temperature in darkness. After another washing step with DPBS the cytoskeleton was examined by fluorescence microscopy (EVOS fl, AMG, Mill Creek, USA) using the RFP light cube (AMG, Mill Creek, USA).

4.6.3.11 Complete staining procedure

For fluorescence microscopy, cells were seeded and grown on coverslips put into 24-well plates. The staining procedure started with fixing the SaOS-2 cells (transfected and non-transfected, for 10 days in activation medium or standard growth medium) with 4 % paraformaldehyde as described above

(4.6.3.4). Then the actin cytoskeleton was stained with rhodamine phalloidin as described above (4.6.3.10). In the next step, hydroxyapatite depositions were stained by OsteoImage as described above (4.6.3.8). In the final step, DRAQ5 was used to stain cell nuclei as described above (4.6.3.9). After all staining steps, the coverslips were removed from the well plates, rinsed with water and allowed to drip dry. They were inverted with a drop of antifade (Fluoromount, Sigma-Aldrich, Munich) on a glass slide and sealed after drying with clear nail polish. Staining was examined by fluorescence microscopy (EVOS fl, AMG, Mill Creek, USA).

4.6.3.12 Statistical Analysis

Statistical analyses were conducted in R-Project software (version 3.2.3, R-Core-Team, 2014). The differences among cell treatments were analyzed with one-way analysis of variance (ANOVA). If this resulted in a significant difference between treatments, subsequent Tukey's honest significance test was performed as post-hoc test. Statistically significant differences are indicated in the respective figures in the results (significance codes are *** $p < 0.001$, ** $p < 0.01$, * $p < 0.05$, • $p < 0.1$).

4.7 Transcriptome analysis of sponge tissues adapted to daylight and night

4.7.1 Incubation of sponges

A mature *S. domuncula* individual was transferred to a separated aquarium 30 x 20 x 20 cm in size, filled with sea water taken from the sponge's original aquarium. The sponge individual was kept in permanent light for 5 days by using an attachable light for mini-aquaria. The compact fluorescent lamp had a light color of 6000 K and a mirror-finish reflector (Nano Light 11 W, Dennerle, Vinningen). After 5 days a tissue sample was collected and incubated directly in TRIzol (Life Technologies, Darmstadt). The sample was homogenized and kept until RNA preparation in -80 °C. Subsequently, the aquarium with the *S. domuncula* individual was transferred to complete darkness (black covered box) for another 5 days, followed by tissue sample collection as described above. During the whole experiment, the aquarium with the sponge was kept in our standard aquarium room under the usual standard conditions and parameters except of light (e.g. temperature, feeding, salinity, aeration). RNA preparation with TRIzol was performed according to the description in 4.5.6.

4.7.2 Transcriptome analysis

Isolated RNA of *S. domuncula* was given to a commercial service (GENterprise Genomics, Mainz), where the RNA was converted to cDNA and sequenced by the Illumina technique (Illumina HiSeq 2000). The resulting transcriptome data were processed and analyzed with the software Geneious, version 6.0.5 (www.geneious.com; Kearse et al., 2012). For details, see results (5.1). In brief, transcriptome data were either used to analyze the proportional expression level of genes already known in *S. domuncula* by using the "map to reference" function, or *in silico* sequence analysis of proteins so far unknown in *S. domuncula* was performed by using the "*de novo* assembly" function of Geneious.

5 RESULTS

5.1 Transcriptome and quantitative PCR analyses on mature sponges

In the framework of my thesis I performed most of the experiments with sponge cell suspensions and primmorphs. However, some initial transcriptome and quantitative PCR (qPCR) analyses were done on mature sponge (*S. domuncula*) individuals. The results are summarized in this chapter. These analyses have not been further pursued here, but they have the potential to yield a wealth of interesting data if followed-up in the future. For the present thesis, initial comparative transcriptome analyses served to test this method for its validity to monitor changes in gene expression levels of *Suberites domuncula* proteins that are involved in spiculogenesis. As a second method for this purpose, quantitative PCR was tested.

For comparative transcriptome analysis, I changed a single environmental parameter in that I adapted a sponge individual consecutively to light and darkness, and monitored the expression levels of proteins related to spiculogenesis in both stages. A sponge individual was kept in permanent light for five days, then tissue was taken for RNA isolation. This was followed by keeping the same individual in darkness for additional five days and subsequent sampling of tissue for RNA isolation. Both RNA samples were given to GENterprise Genomics (Mainz) where two transcriptome datasets were prepared. They contained 2 x 57 million reads of 101 bp length, statistically representing all cDNA sequences in the respective sample.

These transcriptome datasets allow, among others, analyzing the proportional expression level of genes. To do so, the complete sequence of the protein of interest is needed. Every single 101 bp read is compared by the program with the "map to reference" function to this reference gene. I used the lowest sensitivity setting in Geneious (www.geneious.com; Kearse et al., 2012) to make sure that only most similar reads are aligned, and chose the seven proteins shown in Table 9. After this procedure, the program showed all aligned sequences and the number of assembled reads (for the latter see Table 9). A high number of reads should be correlated with a high proportional expression level.

As a second method, gene expression levels were monitored by quantitative PCR. This analysis method is based on the occurrence time (measured in cycle number) of the fluorescence signal in the quantitative PCR. As described in the Methods section, the more initial cDNA representing the gene of interest is available, the earlier the fluorescence signal is detectable. Consequently, the signal occurrence time is correlated with the initial number of RNA copies of the respective gene. In other words: the higher the cycle number is, the lower is the proportional expression level of the protein.

The results of qPCR experiments on a sponge adapted to the standard day/night rhythm are shown in Table 9.

Table 9 Proportional expression levels of different proteins from *S. domuncula* involved in biosilica formation and housekeeping. Analyses were done by qPCR, where a high cycle number indicates a low expression rate, and by transcriptome analysis, where a high number of assembled reads indicates a high expression rate. Note that both methods yield corresponding results.

Protein \ Expression	Transcriptome (light) number of reads assembled	Transcriptome (dark) number of reads assembled	qPCR detection in cycle
silicatein-α	32	48	24.7
silicatein-β	731	831	22.5
HPRT	2599	3780	21.6
slowpoke-binding protein	6115	7383	20.8
silintaphin-1	15127	22291	18.2
GAPDH	28178	39262	18.6
β-tubulin	180916	172049	14.9

Although the results from the transcriptome analyses were promising, for practical reasons I decided to monitor, in course of the present thesis, protein expression levels by quantitative PCR (see, for example, 5.3.4).

Apart from yielding information on protein expression levels, transcriptome data enable *in silico* sequence analysis of proteins. Consequently, I tested the present transcriptome datasets for their potential in this regard. First, sequences were *de novo* assembled. Then, the obtained sequences were compared in a batch search to the NCBI database (www.ncbi.nlm.nih.gov; Geer et al., 2010). Finally, several “map to reference” iterations were done until the protein sequence was completed. In between, sequences were manually translated using ExPASy (www.expasy.org; Gasteiger et al., 2003), in order to check for open reading frames, and analyzed in NCBI. In this way I obtained the sequence of a "calcium-activated potassium channel subunit alpha-1" (Fig. 19) which might be connected to the slowpoke-binding protein, due to the fact that slowpoke is a calcium-activated potassium channel (Ma et al., 2011). I also obtained several other protein sequences from *S. domuncula*, and discovered that these transcriptome data have the potential to deliver many more sequences. However, they were not further analyzed in the framework of this thesis.

>Protein sequence for calcium-activated potassium channel subunit alpha-1 from *S. domuncula*
MDNNTVTDCPASGQEKWWVYIVTFVVIHLVCLGLSCISYGIYYLVKKLKGPRQS
MVKVEDRRQFSYKKFHEFIRQLISGDTIPSKILIFITFVCNLIYMILAVYRAYFPAE
VEHCYSLSESPERIVELIIVIELLLFAFIRFLAANNVALYWLNVYTIIDMITLPHIFV
SIGLGVDWLGLRSARFIWLTQLVTVLRFIPFIHSQDTIDVISLIVYFVVLLFLGTGI
VHLLEYSGDPWLNFTNSVDNDFFTYAYYIIVTITTVGYGDISPATAFGRIFMVVY
IVVGLAFFAALLPVIVEVASNFNKKRQFSKFDRTRVPRHVIVCGHITAFSAQEFL
KDFLHPDRGDDRTHILFLHPERPNNELKNVLRSYYTRVQYIIGSVLNGTDLEKCK
IFDTSAVFILANKYTNIPLEEDNGNLLRLVSIKNTTTEVAVIVQLLLSTSKKQVRN
IEGWNSGQDIAICLNELKLGLLAQSCVCPGFSTLIANLFYTSDFPALTKFEGRDA
WKEGYITGASNEIYSTHFSSSFEGKTFQRTARICYEKLGLILLAFETPEGDFRKLY
VNPSSKSRPDIVIKSGEYGTKGYFIGQDLDHVSIVNSYCDICDRDVKIDPQDMD
RAVQKLVRRVTKRKCQCGDDLEDVSTSAFSGTELVDLNGGSPKRKGSTDPRKSS
VPLVMTLSWDDDDEGLENLNEQFSIYLSEPVRLDDAVLNTDIYFSERATSPKPA
LQDHIVLCVFADDKSPLLGLHNFLYPLRNKNIRKELMKPVVIVSNRTFLKREWSF
IRKIPEVYVVDGSPLRLKNLEEACVSSCSVCIVLTMLSASNENEPAINDKEVVLCS
LSLQKLLKKNAQRQVQIITDLRQESNVQFLDFGDEDEPDERIYKAQPFACGEAF
SVSMMDSVTSSAFHSPGTLYLIEDLIQSSGTKTSCQIVAMPLDSEEYANTTFRDL
YKQQLDENNLVLGLYRKLPSEDDDVVVNGNQTSLSAIATVNVSKHYVVTAPNP
QTALEPTDIAFVLVNSCDSPEETCLTAI

Fig. 19 Example of a protein sequence extracted from the transcriptome data of *S. domuncula*. This "calcium-activated potassium channel subunit alpha-1" is probably connected to the slowpoke-binding protein. More protein sequences were extracted, and many more are potentially available in this data set, but their analysis was beyond the scope of the present thesis.

5.2 A bioreactor-based procedure to improve sponge primmorph cell culture

The main focus of the present thesis was placed on experiments involving sponge primmorphs. As a first step, I had to solve the problem that the conventional sponge cell culture methods produced generally only very small primmorphs (1-2 mm in diameter), and only from different sponge individuals. They were all done at small scale, mostly in petri dishes or well plates, with culture volumes between 500 µl and 10 ml. Therefore, the first goal of this thesis was a substantial up-scaling by using bioreactors. We finally succeeded in cultivating primmorphs for several weeks in vessels of 5 liter volume (upscaling factor 1:500). We started our experiments with a disposable bioreactor from Eppendorf that is usually applied to bacterial cultures (CelliGen BLU Bioreactor with single-use vessel, Wesseling-Berzdorf). A whole *S. domuncula* individual, approximately 3 cm in size, was used. The single sponge cells were extracted in several subsequent primmorph production circles (see 4.4.1). We used 2 l of standard sponge culture medium, because stirring more liquid turned out to be problematic. The sponge cells obtained in each circle were kept suspended in 3 ml aliquots of Ca^{2+} and Mg^{2+} free seawater at 16 °C (see 4.4.3), until the sponge was completely dissociated into single cells. Then the cells were added with a pipette directly to the culture medium residing in the bioreactor which was kept at 16 °C (Fig. 20). Previously, routinely prepared primmorphs were about 0.2 cm in size (see Fig.

21 A, B). Using the bioreactor, after 2 days we obtained a primmorph 1.9 cm in size (Fig. 21 C), which was the largest *S. domuncula* primmorph hitherto reported.

Fig. 20 Commercial bioreactor initially used for primmorph production. Single-use bioreactor from Eppendorf (Wesseling-Berzdorf). The picture shows the addition of a *S. domuncula* cell suspension to primmorph standard culture medium. This bioreactor allowed to scale up the culture volume to 2 l and to use a whole sponge individual for each primmorph preparation.

In the next step, the precision mechanic of our research group constructed a reusable bioreactor of 3 l capacity, according to our specifications. It was stepwise improved in the course of our growing experimental experience with this device. With this custom-made reusable bioreactor, primmorphs of the size of that shown in Fig. 21 C can now be raised routinely from the cell suspension of a single *S. domuncula* individual. It is also possible to further enlarge the primmorphs over several days by repeated addition of more cells from the same sponge individual. Due to the unidirectional flow of culture medium caused by the stirring elements, we found that for the formation of primmorphs it is crucial to add barriers on the bottom of the bioreactor by precision milling. They allow the cells to

contact each other, thereby forming aggregates. In our first disposable bioreactor the barrier was a piece of plastic, broken by chance from the top of the reactor. Later we added helical hollows to the bottom of the reactor in order to get more cells in contact to each other, thereby yielding larger primmorphs. With a routine partial medium change of 1/3 every 3 - 5 days, the primmorphs survived for several weeks.

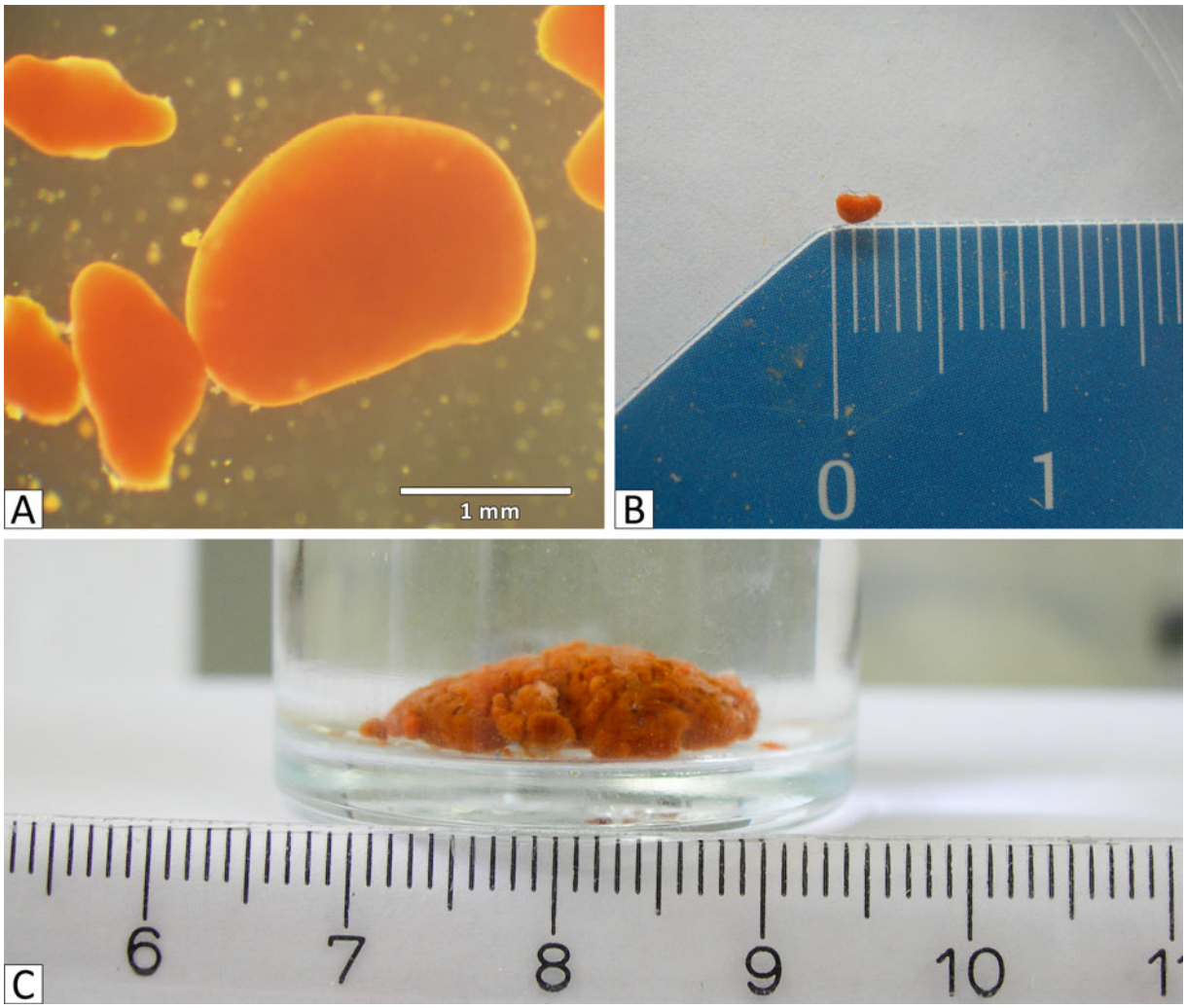

Fig. 21 ***S. domuncula*** **primmorphs. (A)** Light micrograph and **(B)** direct inspection of primmorphs conventionally produced in a culture dish. They show their typical kidney-like shape. **(C)** A bioreactor-grown primmorph. Even though its shape was round and more flat, its structure remained perfectly stable over several weeks. In contrast to the previous primmorph size of 1 to 2 mm obtained from culture dishes (A, B), primmorphs of almost 2 cm in diameter developed in the bioreactor (C). Thus, primmorph length was successfully up-scaled by the factor 1:10, and primmorph volume by the factor 1:500.

Our custom-made reusable bioreactor (Fig. 22) has a stirring element in the center to slowly move the culture medium. *Via* a small tube, air is added to the medium to provide enough oxygen. A supply tube allows adding the sponge cells directly to the culture medium without unsealing the bioreactor. We also produced different bottom types, depending on the application. For example, there is a bottom

type with circular hollows and an additional cone in the center; this device prevents primmorphs from aggregating into one big specimen, in cases in which numerous normal-sized primmorphs are desired. For culturing a single big primmorph we used a bottom with helical hollows that give the cells the opportunity to come in contact with each other and at the same time guide them to the center of the bottom ("the eye of cyclone"), were they can aggregate into one big primmorph. The biggest advantage of our custom-made bioreactor over the commercial device is reusability. It can be opened and closed at will, which allows to withdraw some primmorphs for experiments, while the remaining primmorphs stay in culture for later use. The different bottom types allow us “programming” the final primmorph size according to our needs.

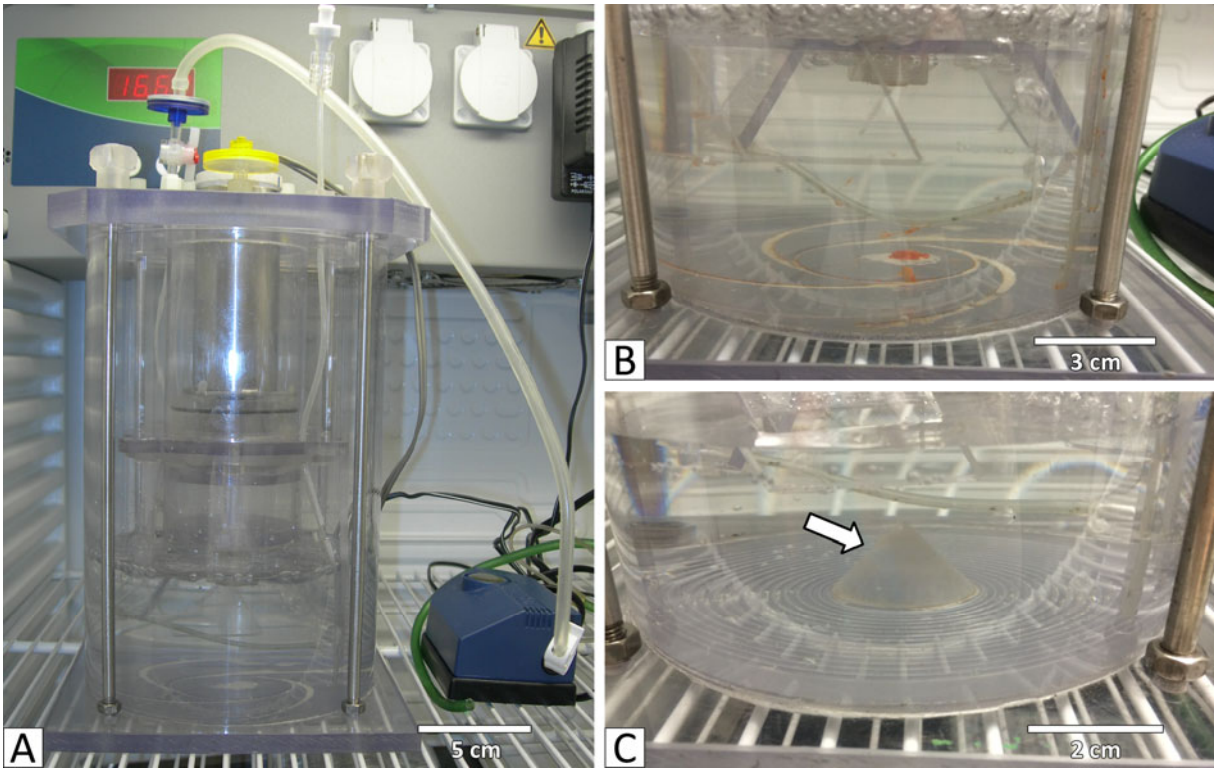

Fig. 22 Our custom-made reusable bioreactor for primmorph production. (A) Reusable bioreactor manufactured in our research group by the precision mechanic Willi Reichert, with different bottom types for preparing either large primmorphs **(B),** or large amounts of normal-sized primmorphs **(C)**. The cone in the center of the bottom (white arrow) in (C) prevents the cells from accumulating into one big primmorph. Preparing and keeping primmorphs at large scales has been greatly facilitated by this bioreactor.

5.3 Uptake of fluorescent and magnetic nanoparticles by primmorph cells

5.3.1 Experimental setting, and comparative tests with different types of nanoparticles

To this stage we could easily produce, from a single sponge individual, either one exceptionally large or numerous rather small primmorphs. One aim of this thesis was to generate new property combinations in *S. domuncula* cells and their spicules. Therefore we used nanoparticles to introduce new properties to primmorphs. We took advantage of the fact that sponges are filter feeders with extensive phagocytosis activity. The food particles are directly taken up by the cells in an amoeboid manner and digested in food vacuoles. Consequently, all sponge cell types are capable of extensive phagocytosis. We used this sponge cell ability to convey new property combinations to the biosilica spicules of living sponge cells, and thereby to whole primmorphs. To our knowledge, we were the first to attempt this.

We started the procedure prior to primmorph formation, *i.e.* with the sponge cells suspended in primmorph cultivation medium. Aliquots of freely suspended *S. domuncula* cells were incubated with six different types of nanoparticles (Table 10). The latter were all magnetic and fluorescent, but differed in the polymer matrix of their outer shell (see Fig. 13). Their cellular uptake was evaluated semi-quantitatively by fluorescence microscopy (see below). The subjectively best results were obtained with nano-screenMAG-CMX nanoparticles (from Chemicell, Berlin; for their properties, see 4.3.3). They were therefore selected for the subsequent detailed study on nanoparticle phagocytosis and the creation of a novel primmorph variant with fluorescent and magnetic properties.

Table 10 Different types of tested nanoparticles produced by Chemicell, Berlin. All nanoparticles have a magnetite core surrounded by a fluorescent dye. With respect to the polymer matrix constituting their outer shell they are all different.

Nanoparticle	Polymer matrix	Hydrodynamic diameter	Fluorescence color
nano-screenMAG-Chitosan	chitosan	100 nm	pink
nano-screenMAG-CMX	carboxymethyl dextran	100 nm	pink
nano-screenMAG-DEAE	DEAE-starch	100 nm	pink
nano-screenMAG-DXS	dextran-sulfate	100 nm	pink
nano-screenMAG-PAA	polyaspartic acid	100 nm	pink
screenMAG-Silanol	silanol	500 nm	red

With primmorph cells and nano-screenMAG-CMX nanoparticles, cellular uptake, long-term cellular storage and coating of spicules were analyzed by magnetic distraction, fluorescence microscopy, transmission electron microscopy, scanning electron microscopy and energy-dispersive X-ray spectroscopy. Moreover, by quantitative PCR the influence of the uptake on protein expression was studied.

5.3.2 Demonstration of nanoparticle uptake by fluorescence microscopy and magnets

Nano-screenMAG-CMX nanoparticles were added to the primmorph culture medium, in the last step of primmorph preparation (with the sponge cells still suspended; see 4.4.1), at concentrations of 0.1 mg/ml and 1 mg/ml (mg nanoparticles per ml culture medium). Fluorescence microscopy of wells with primmorphs formed under these conditions showed that the nanoparticles where quantitatively ingested. We could detect strong speckled fluorescence signals from the primmorphs composed of cells treated with nanoparticles, while the bottom of the well showed no fluorescence signals (see Fig. 23 A). This indicates the absence of free nanoparticles, which due to their fluorescence signal are clearly visible in culture medium lacking primmorph cells. Likewise, the control was negative (Fig. 23 B). One day after nanoparticle exposure of the cell suspension, a freshly formed primmorph was dissociated again by CMFSW+EDTA (see 4.1.3), and the cells analyzed in the fluorescence microscope (Fig. 24). The fluorescence signal could be detected inside the individual sponge cells. Within the cells, the nanoparticles were not evenly distributed, but seemed to form clusters in the cytoplasm. This indicates that they might be enclosed in food vacuoles.

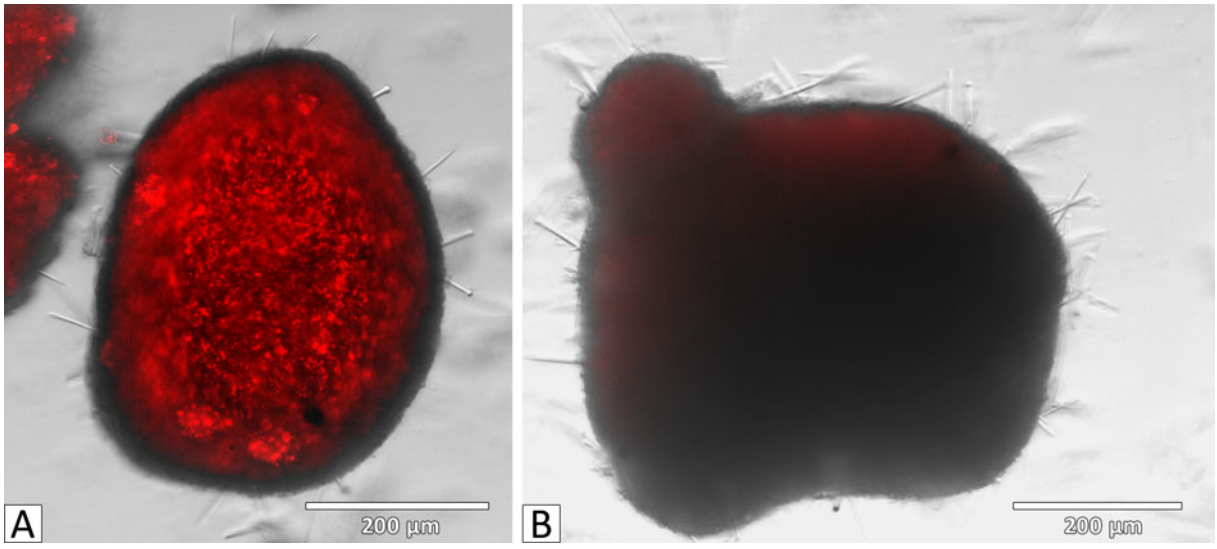

Fig. 23 Fluorescence micrographs of a primmorph formed after incubation of the cells with nano-screenMAG-CMX nanoparticles. (A) Incubated with 0.1 mg/ml nanoparticles (excitation 531 nm, emission 593 nm). Note the speckled appearance indicating that the incorporated nanoparticles are present in clusters throughout the primmorph. **(B)** Control primmorph. This experiment shows that the cells forming primmorphs take up nanoparticles from the medium and store them in large amounts.

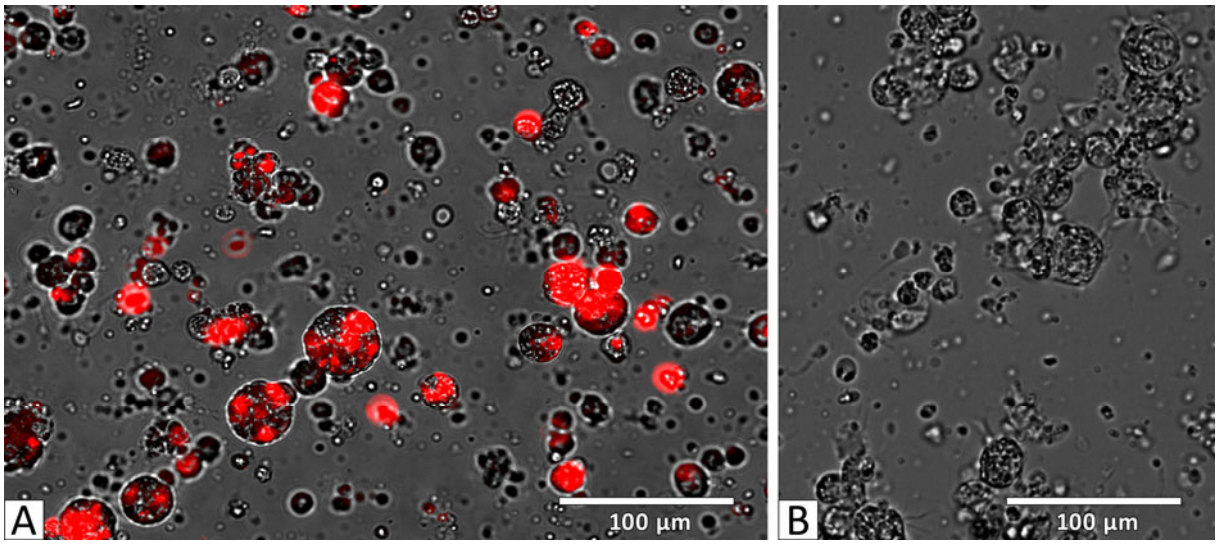

Fig. 24 Fluorescence micrographs of primmorph cells incubated with nanoparticles. (A) One day after incubation with 0.1 mg/ml nano-screenMAG-CMX nanoparticles and subsequent primmorph formation, followed by dissociation of the primmorph. The distribution of the fluorescence signal inside the cells seems to be heterogeneous. **(B)** Cells from a control primmorph

Uptake of the nanoparticles was very fast: Already after 1 min, the sponge cells were strongly attracted by a neodymium magnet. Nano-screenMAG-CMX nanoparticles show a light-brownish color, whereas primmorph cells are brightly orange. Therefore, primmorphs aggregated from cells with ingested nanoparticles show a mixed color (Fig. 25).

By resting the well plates during cell aggregation on the magnet, it was possible to pre-determine the shape of the growing primmorph. In these experiments, magnetic foil or a neodymium magnet was attached underneath the culture plates. The magnetic attraction was strong enough to influence the sponge cells through the plastic bottom of the culture plate: Instead of developing, within three days, their normal kidney/round shape, the primmorphs grew during this period in the shape of the magnet (Fig. 25 A). Primmorphs grew directly next to the magnet, thereby following its shape. In the spaces between, no primmorphs were found. In contrast, in the absence of nanoparticles, primmorph aggregation was not influenced by a magnet; they were randomly distributed in the culture plate (Fig. 25 B).

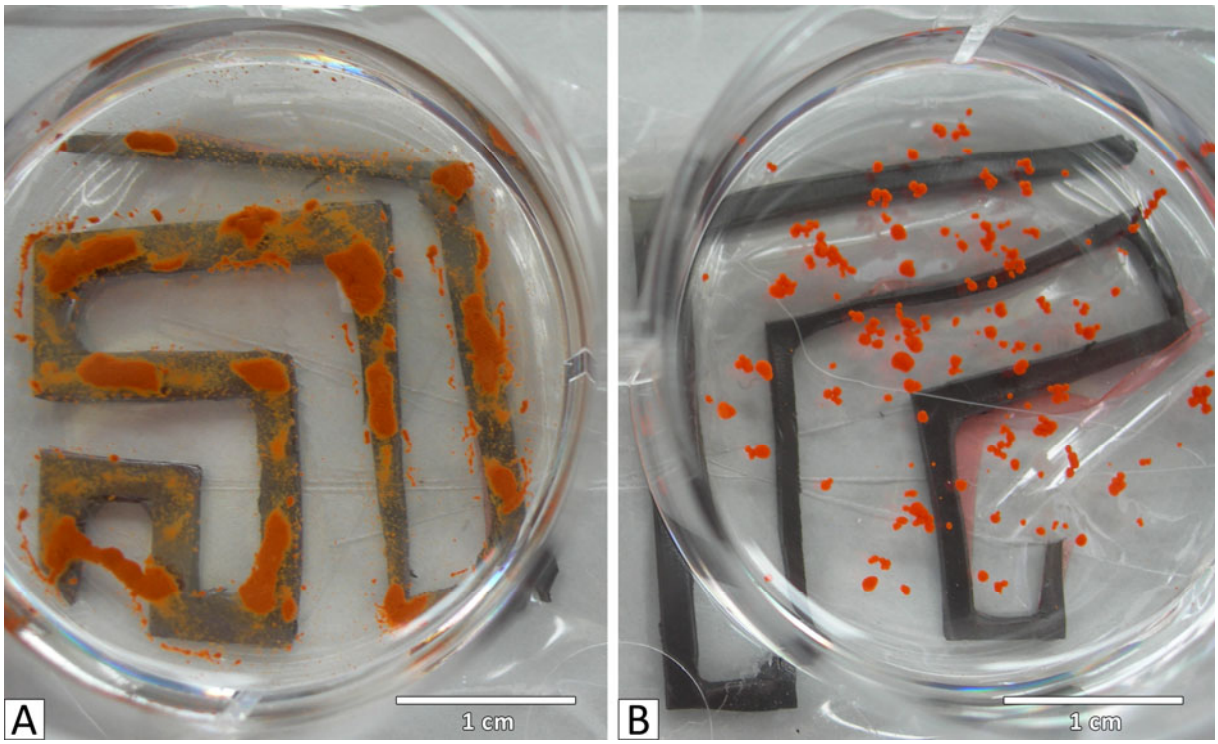

Fig. 25 Primmorph formation on magnets after incubation with nanoparticles. (A) Primmorphs incubated with 1 mg/ml nano-screenMAG-CMX nanoparticles and **(B)** control primmorphs without nanoparticles, after three days of aggregation on top of magnetic foil. Without nanoparticles the primmorphs kept the natural kidney/round shape, and they grew in random distribution (B). After the uptake of magnetic nanoparticles, the area where the primmorphs grew was determined by the magnet shape. Additionally, their color was a mixture of the nanoparticle color and the natural orange of *S. domuncula* cells (A).

In the experiments described so far, single cells with ingested nanoparticles migrated to the spots of primmorph formation. To test whether fully aggregated nanoparticle-containing primmorphs also react to the magnetic field, such primmorphs and untreated controls were placed in glass cuvettes in front of a neodymium magnet (Fig. 26). The nanoparticle-containing primmorphs showed a very strong physical attraction to the magnet in that the whole primmorphs were attracted and translocated immediately by the magnet, even against gravity. Only very few cells remained on the bottom of the cuvette. In contrast, untreated primmorphs did not show attraction to magnets.

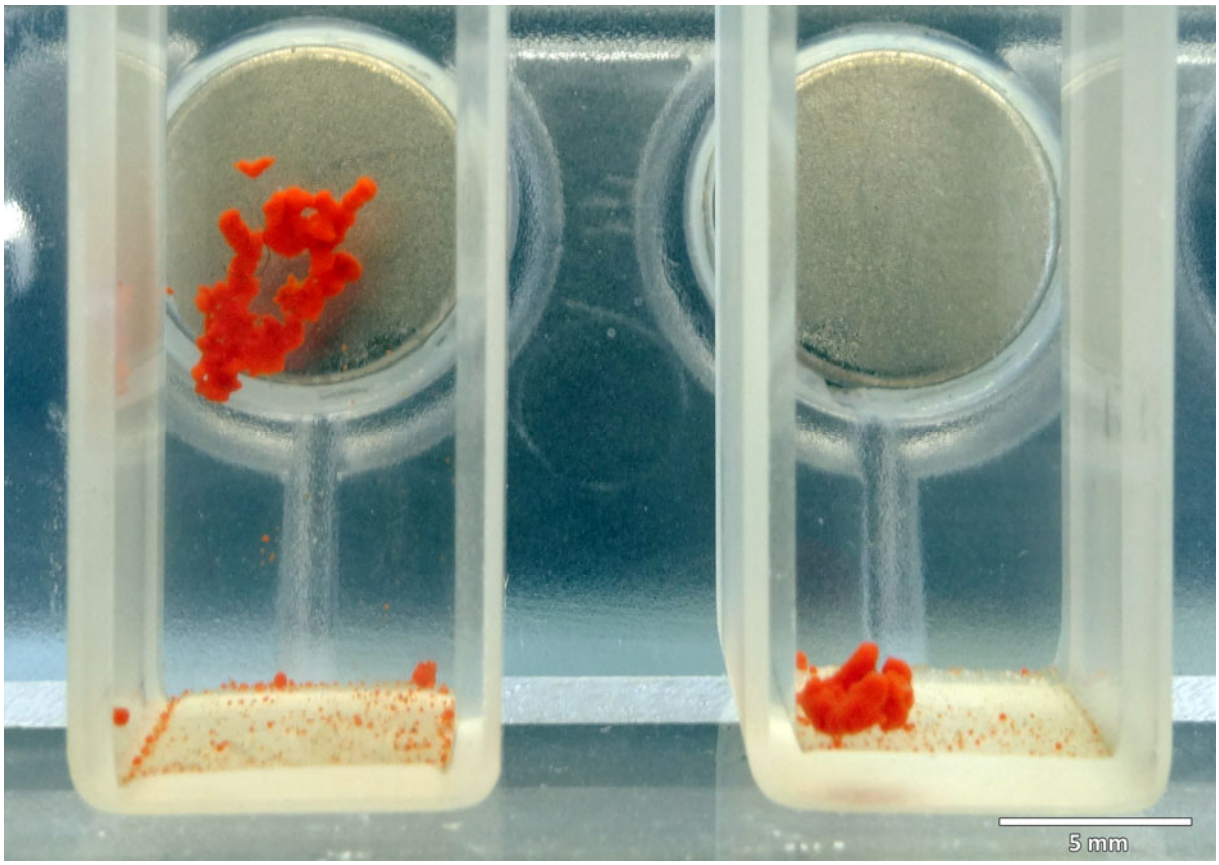

Fig. 26 Whole primmorphs containing nanoparticles: attraction by magnet. Primmorphs composed of cells incubated with 0.1 mg/ml nano-screenMAG-CMX nanoparticles (left cuvette), and control primmorphs prepared from the same sponge individual (right cuvette). Cuvettes were filled with primmorph culture medium. After exposure to magnets, entire nanoparticle-treated primmorphs were immediately drawn towards the magnets. This magnetic attraction worked even against gravity. Only few treated cells were not attracted, indicating that they did not perform phagocytosis. Untreated primmorphs did not show any attraction to magnets.

5.3.3 Verification of nanoparticle uptake by TEM, TEM-EDX and SEM-EDX

Transmission electron microscopy (TEM) was done to get more detailed information about the location of the incorporated nano-screenMAG-CMX nanoparticles within the primmorph cells. In general, in electron micrographs, primmorph cells were found to be closely associated and densely filled with smaller vesicles, larger vacuoles (formed by fusion of multiple vesicles) and electron-dense granules (Fig. 27). The latter occur either in the cytosol or in vesicles and vacuoles (Fig. 28).

Nanoparticle-containing primmorphs were embedded for TEM 3, 9 and 19 days after treatment of the cell suspension (in concentrations of 0.5 mg/ml and 1 mg/ml nanoparticles per culture medium). Intracellular flocculate material that was absent in primmorphs formed from untreated cells (see Fig. 28) was readily seen (Fig. 29), and was later identified as nanoparticle material (see below). It was mostly located in vacuoles, and after 9 and 19 days additionally found to be bound to the surface of mature biosilica spicules (Fig. 29 C).

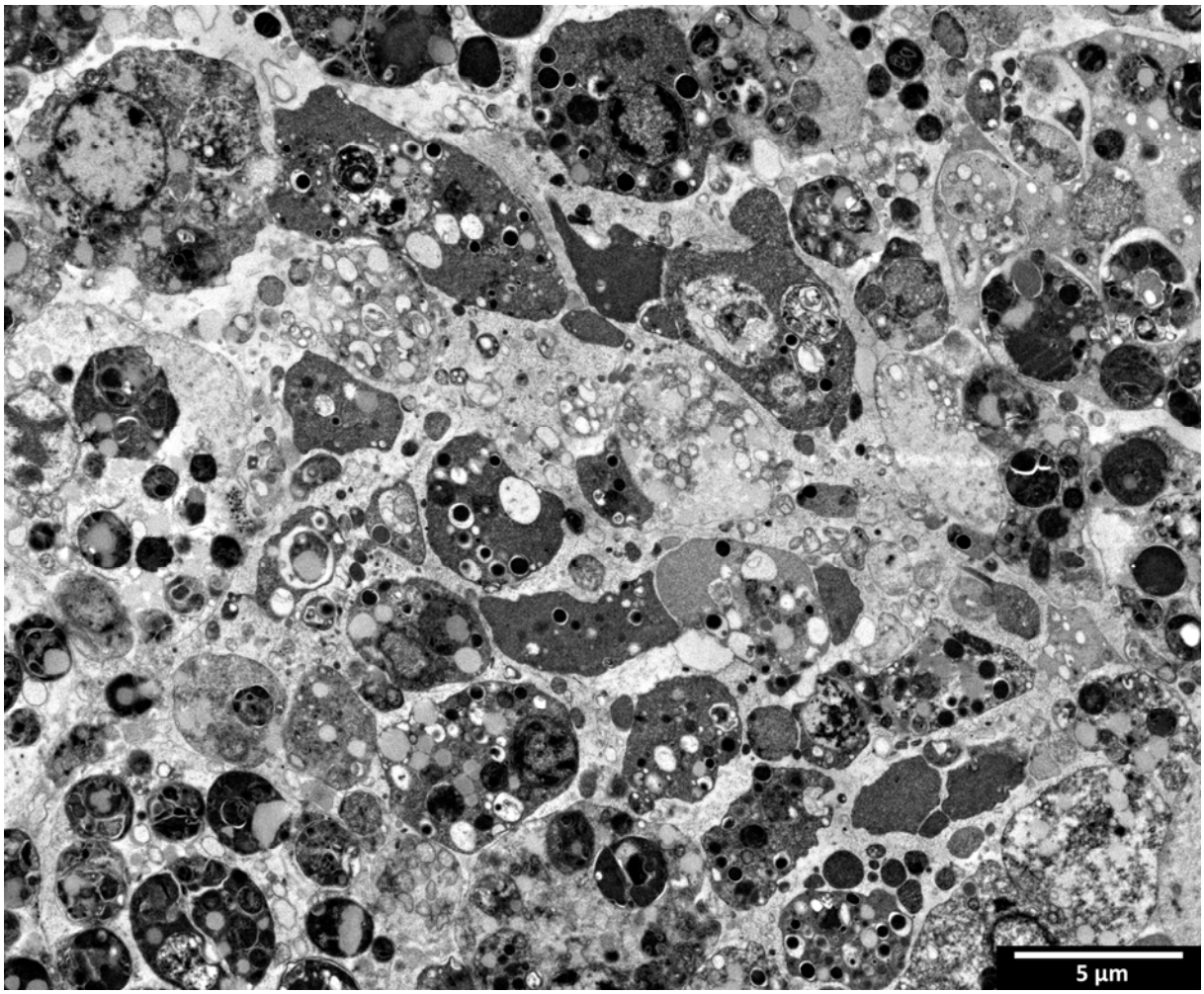

Fig. 27 Transmission electron micrograph of cross-sectioned primmorph tissue. Embedded 3 days after primmorph formation. Note that many cells show a spherical shape and are densely packed. They are filled with electron dense granules of varying density, small vesicles and large vacuoles.

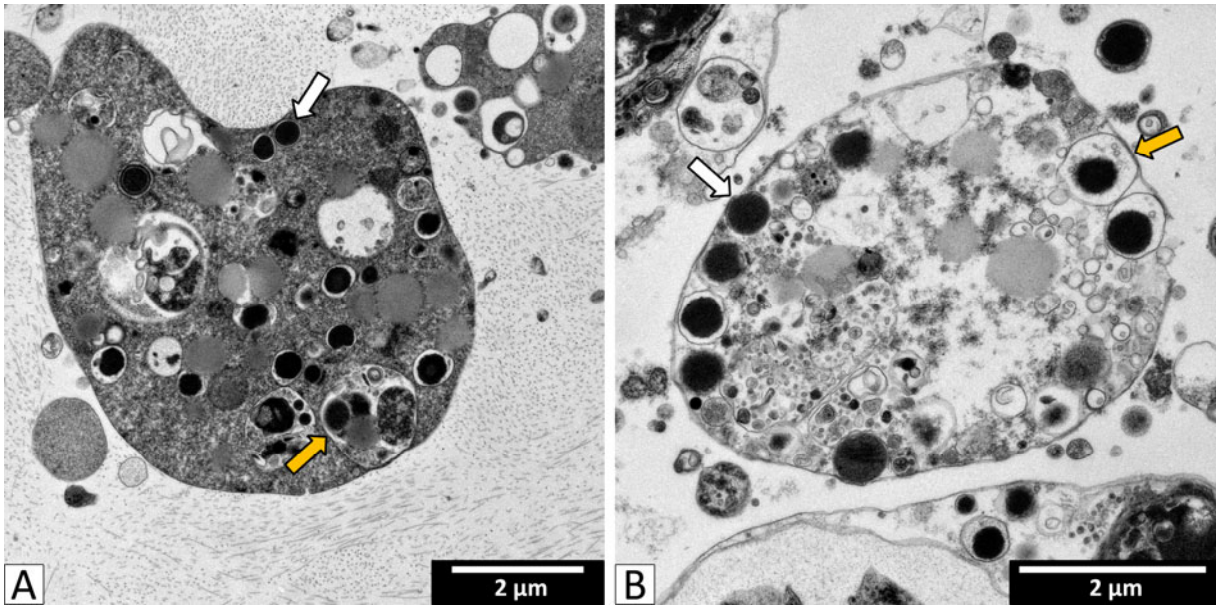

Fig. 28 Transmission electron micrographs of cross-sectioned primmorph cells. (A, B) Cells of untreated primmorphs embedded 3 days after formation. The electron dense granules are found directly in the cytoplasm (white arrows) or in vacuoles (orange arrows). Similar structures were observed in most examined primmorph cells, indicating that all these cell types live from phagocytosis of organic particles and bacteria.

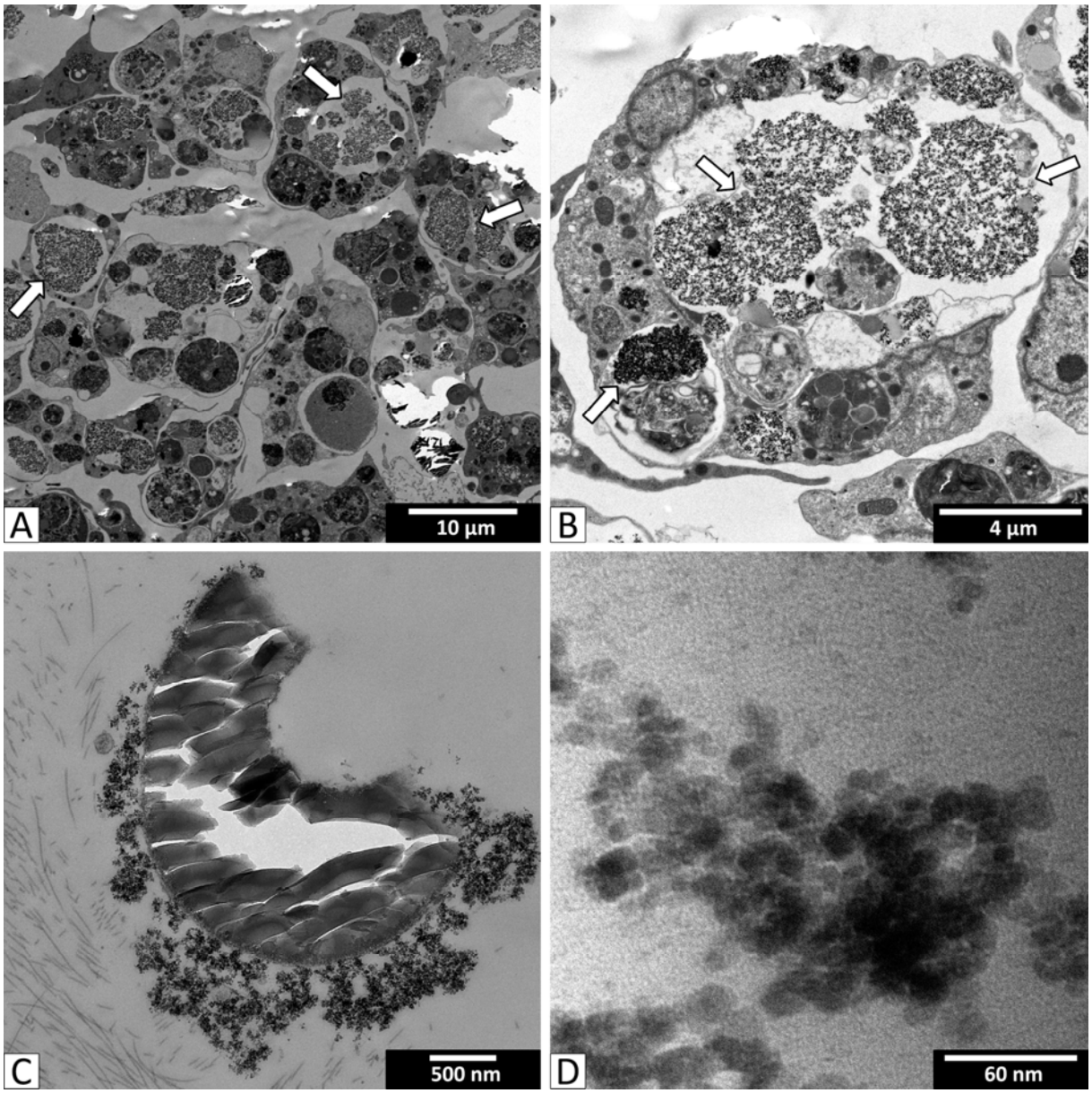

Fig. 29 Transmission electron micrographs of tissue sections of a primmorph formed from cells incubated with nano-screenMAG-CMX nanoparticles. Nanoparticle concentration 1 mg/ml, embedded 3 days after primmorph formation (A-C). **(A)** Overview of the primmorph tissue. Cells are densely aggregated and full of granules, vesicles or vacuoles. Note the flocculate material located in the cells (arrows). From its absence in the controls (see Fig. 28), the flocculate material is interpreted as aggregations of nanoparticles. **(B)** Enlargement of a single primmorph cell. Note that the flocculate material is not evenly distributed but forms clusters within the cytoplasm and also within vesicles or vacuoles (indicated by arrows). **(C)** Broken sponge spicule with typical scattered appearance, due to its biosilica compounds. In some cases, sponge spicules located in the extracellular matrix are coated or surrounded by the flocculate material. Around the spicule, collagen fibers are also visible. **(D)** Embedded pure nanoparticles, chemically fixed in the same way as the primmorph tissue. Note that the individual spherical objects, interpreted as single nanoparticles, are only ca. 10 nm in diameter.

Untreated and nanoparticle-treated primmorphs (in concentrations of 0.5 mg/ml and 1 mg/ml particles per culture medium) were embedded for electron microscopy 3, 9 and 19 days after treatment. Presumed nanoparticles ca. 10 nm in diameter were found in large numbers clustered inside the sponge cells, mostly kept in vesicles or vacuoles, and after 9 and 19 days also bound to the surface of the mature sponge spicules (see Fig. 29).

Individual nanoparticles could not be discerned, due to their accumulation (Fig. 29 B, C). However, TEM of pure nanoparticles under the same fixation conditions revealed that they were only ca. 10 nm in size (Fig. 29 D), in contrast to the 100 nm expected from the manufacturer´s specification. It is possible that dissociation of its hydrated polysaccharide shell (see Fig. 13) through the fixation procedure caused shrinking in the TEM specimen.

To identify the flocculate material observed in TEM images as nano-screenMAG-CMX nanoparticles, and to show their exact location, energy dispersive X-ray spectroscopy (EDX) in combination with transmission electron microscopy (TEM) was performed on primmorph tissue sections (Fig. 30). The TEM-EDX analysis showed the presence of iron particles inside the sponge cells, as well as iron accumulations at the outer edges of the spicules (Fig. 31).

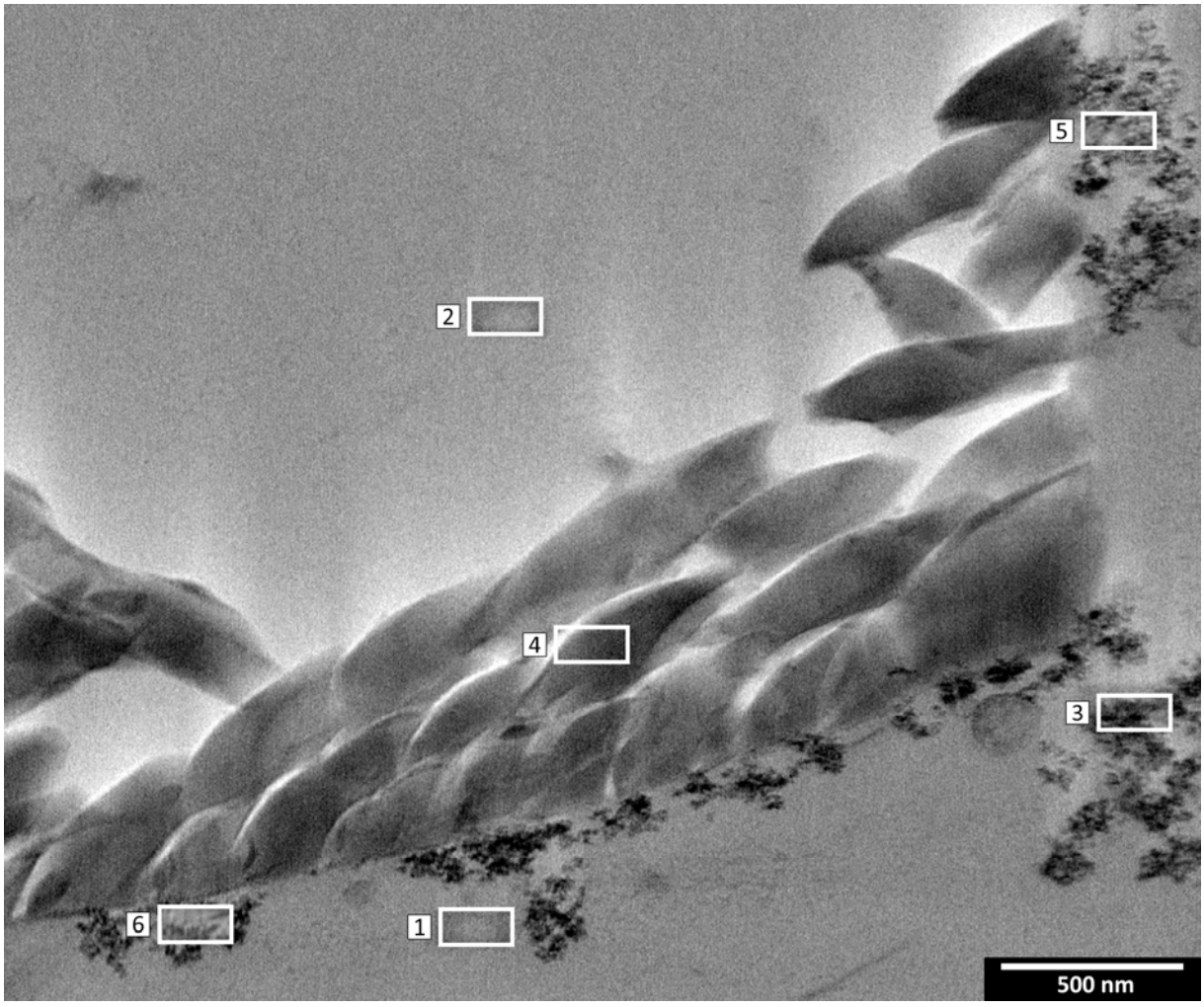

Fig. 30 Electron micrograph of a tissue section of a primmorph, showing a spicule. The primmorph formed from cells incubated with nano-screenMAG-CMX nanoparticles was embedded 9 days after primmorph formation. From the areas indicated by white boxes, EDX-scans were recorded (see Fig. 31). In field 3, 5 and 6, iron was detected, thereby identifying the flocculate material as the nanoparticles.

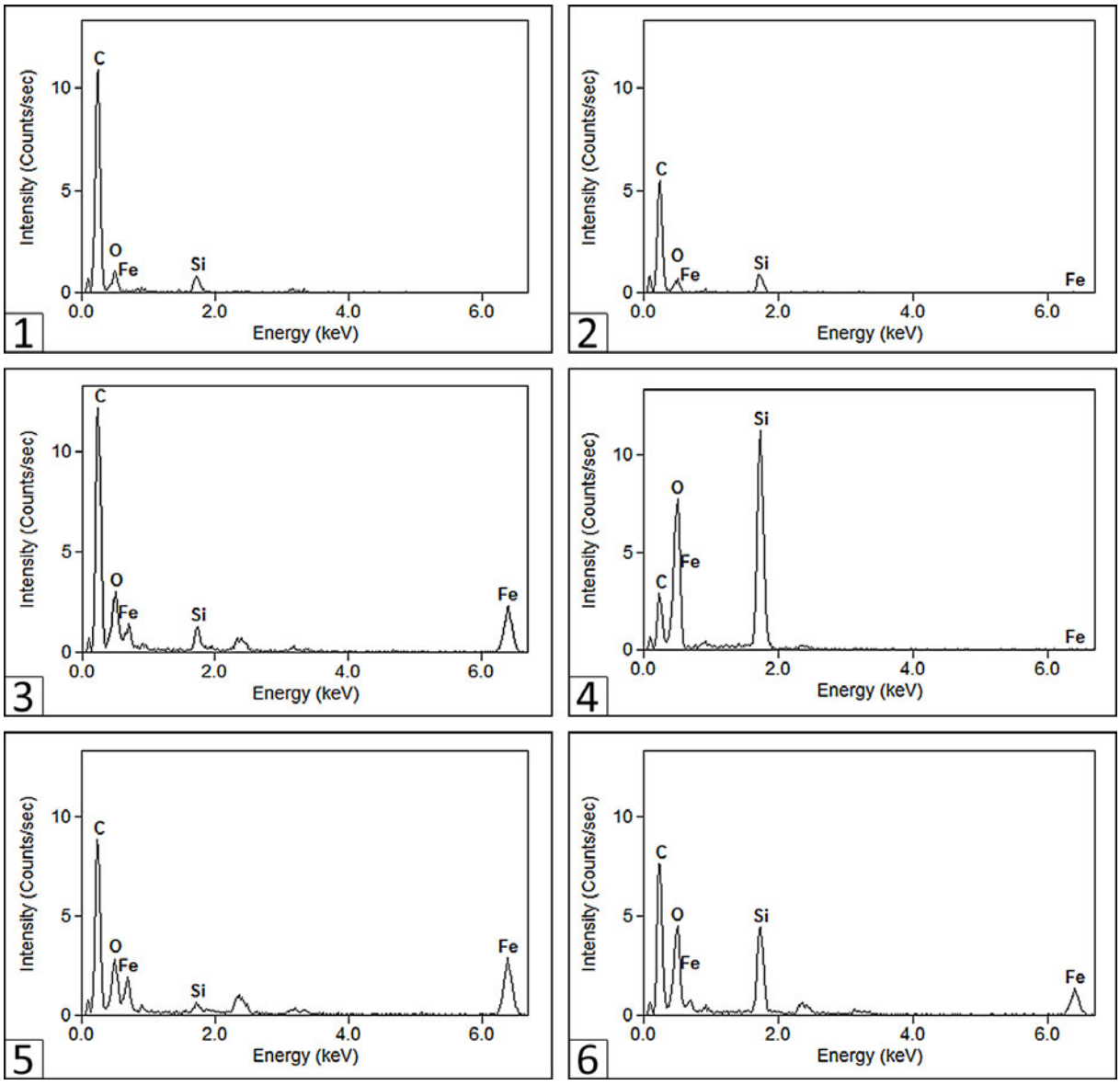

Fig. 31 EDX-spectra from the boxed areas shown in Fig. 30. Areas 1 and 2 are scans of the background, area 4 is from a part of the fractured sponge spicule, areas 3, 5 and 6 are from the dark flocculate material suspected to be the nano-screenMAG-CMX nanoparticles. The silica peak in spectrum 4 is highest as expected for spicule material. Only the spectra 3, 5 and 6 show iron peaks (one around 0.7 keV and one around 6.5 keV). Since the core of the nano-screenMAG-CMX nanoparticles consists of iron (see Fig. 13), the dark flocculate material is identified here as these nanoparticles.

To further substantiate the presence of nanoparticles within primmorph cells, scanning electron microscopy (SEM) and mapping of elements with energy dispersive X-ray spectroscopy (EDX) of the respective surfaces was performed. For the transmission electron microscopy described above, primmorphs were embedded in resin blocks, and slices were cut off at 80 nm thickness. For SEM-EDX, we scanned primmorph surfaces inside these blocks, without sputtering (Fig. 32 A, B). The mapping function of SEM-EDX clearly showed the presence of iron associated with the cloudy material

surrounding the spicules (Fig. 32 C, D). SEM-EDX analysis detected iron only in treated primmorphs, while it was only marginally found in the negative controls.

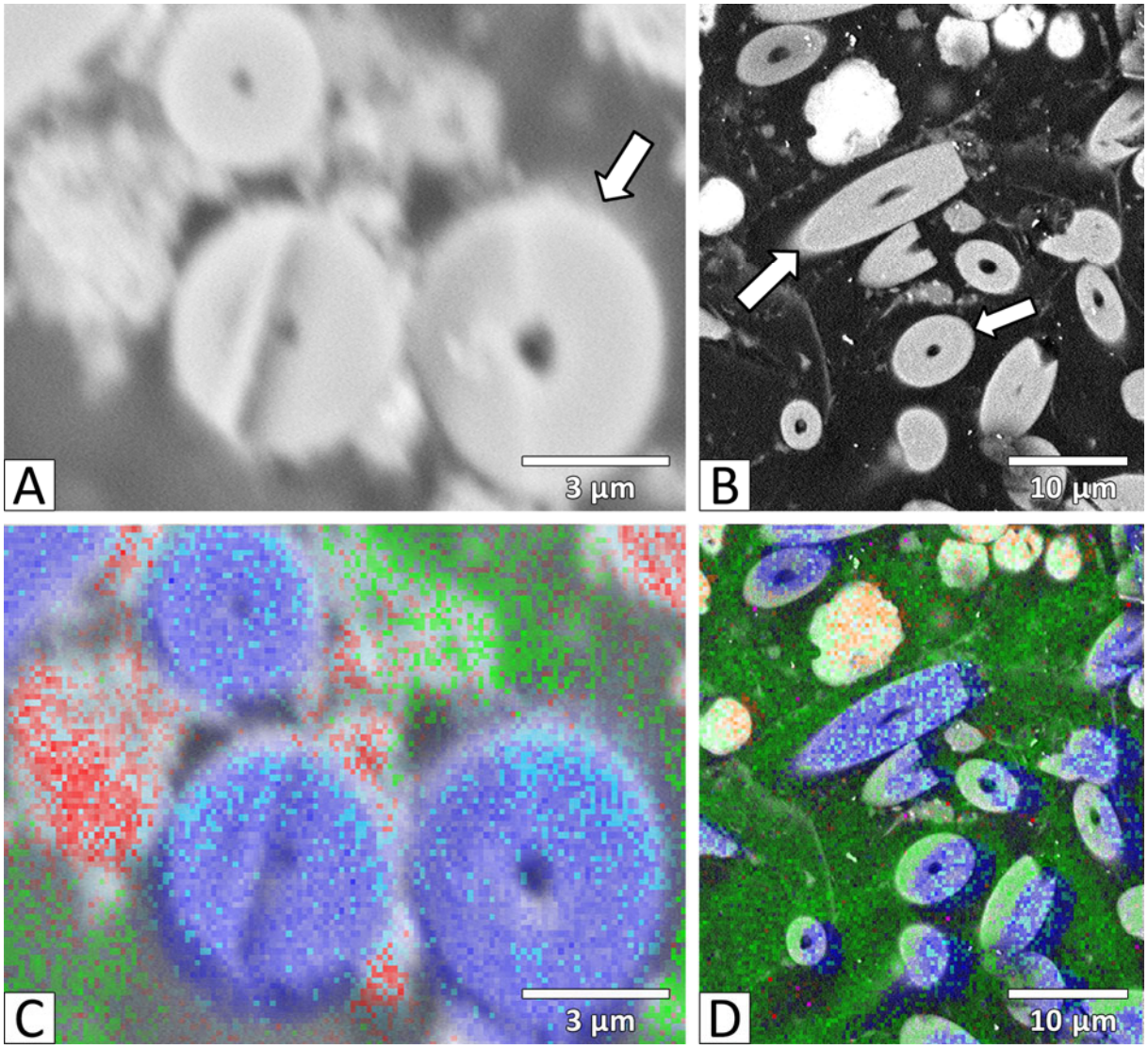

Fig. 32 Scanning electron micrographs and EDX analysis of cut primmorphs containing nano-screenMAG-CMX nanoparticles. (A, C) Nanoparticle concentration 1 mg/ml, embedded 9 days after primmorph formation. **(B, D)** Control without nanoparticles. **(C)** and **(D)** represent the mapping of elements with energy dispersive X-ray spectroscopy (EDX) of the respective surfaces shown in A and B. Each pixel represents a single measurement. Sponge spicules (indicated by arrows in (A) and (B)) are mostly cross-sectioned as deduced from the axial channel visible in their center. Note that only the treated sample shows the presence of iron (red), which is a component of the nanoparticles. It accumulates here around the spicules as a cloudy substance. Osmium (orange), in the control (D) detected, is most likely an artifact of the embedding procedure (see 4.5.3). Analyzed elements are silicon (dark blue), oxygen (cyan), carbon (green), iron (red) and osmium (orange). This experiment confirmed that nano-screenMAG-CMX nanoparticles are taken up by primmorphs and are also bound to spicule surfaces.

Table 11 Respective relative concentration (in %) of the elements as calculated from the SEM surface scan (see Fig. 32). The concentration of osmium was only measured in control primmorphs.

Element	Incubated with nano-screenMAG-CMX		Control	
	Concentration (in %)	SD	Concentration (in %)	SD
silicon	13.4	0.2	11.8	0.3
oxygen	65.3	0.0	62.9	0.1
carbon	11.1	1.3	23.0	1.4
iron	1.5	0.2	0.0	1.1
osmium	-	-	0.7	0.3

5.3.4 Quantitative PCR (qPCR) of spiculogenesis-specific RNAs after nanoparticle uptake

As shown above, the nano-screenMAG-CMX nanoparticles were often detected close to, and apparently associated with, the biosilica spicules. Therefore we analyzed, by quantitative PCR, the expression level of genes involved in spiculogenesis (Wang et al., 2012c). We focused on four different genes encoding the following proteins: silicatein-α, silicatein-β, silintaphin-1 and slowpoke-binding protein. RNA was isolated and combined from five different mature sponge individuals ("mature tissue"). From their cells, three days old primmorphs were prepared in the presence and absence of nanoparticles, and the respective RNA was isolated ("prim CMX NP" and "prim ctrl."). Quantitative PCR revealed that nanoparticle uptake by primmorphs did not change significantly the expression level of silicatein-α and silintaphin-1, and only slightly (1.2 times) up-regulated silicatein-β (Fig. 33). However, slowpoke-binding protein was significantly down-regulated (1.4 times).

In comparison to tissue from a mature sponge, the expression level of silicatein-α, silintaphin-1 and slowpoke-binding protein was more than doubled in primmorphs, while it was only slightly higher in case of silicatein-β (see Fig. 33).

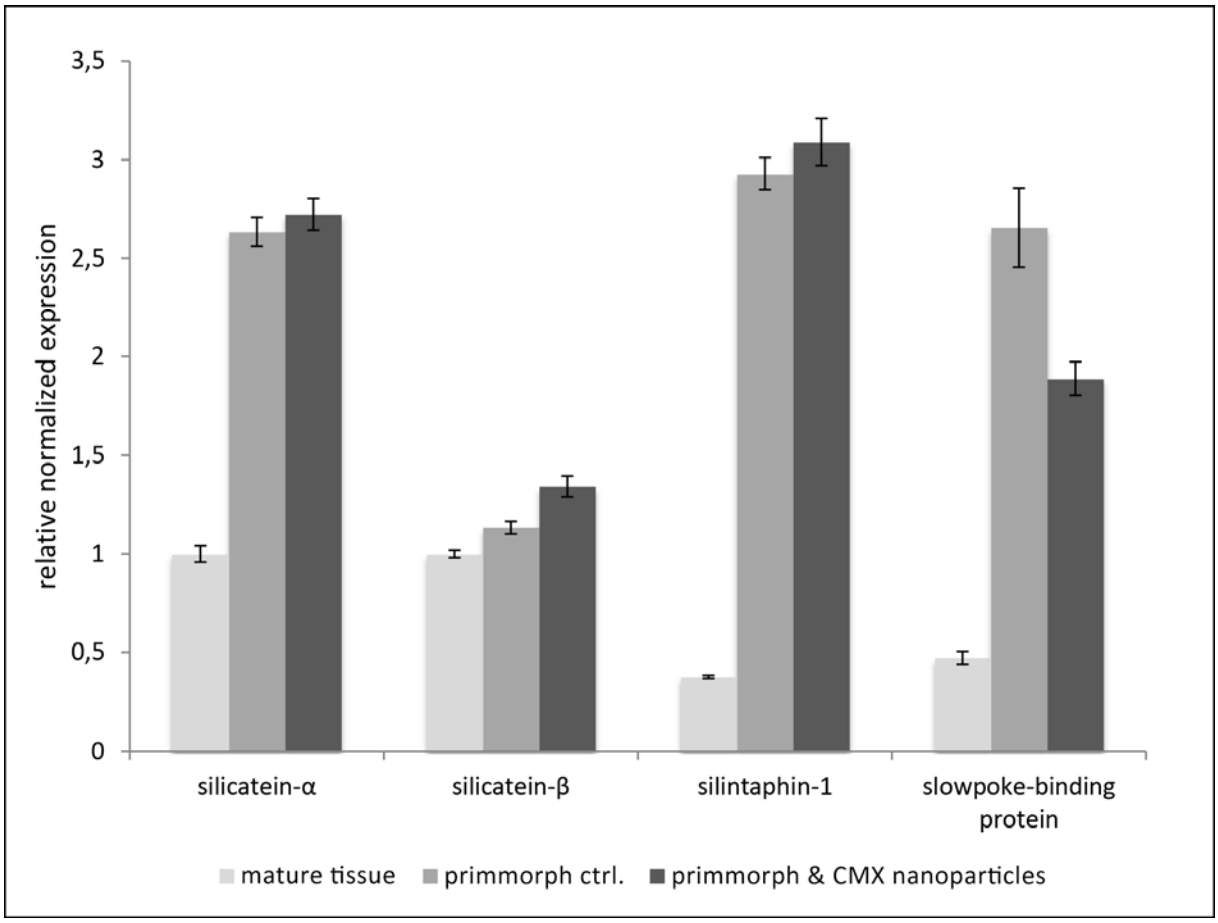

Fig. 33 Expression level analysis by qPCR of genes involved in spiculogenesis, after uptake of nano-screenMAG-CMX nanoparticles by cells forming primmorphs. Exposure of sponge cells to 1 mg/ml nano-screenMAG-CMX nanoparticles, qPCR analysis 3 days after primmorph formation. Measurements were performed in triplets with a pool of n=5 sponge individuals, columns indicate mean ± SD. The expression levels of silicatein-α and silintaphin-1 were not affected by the nanoparticle uptake, while the expression level of silicatein-β showed a slight upward trend. In contrast, slowpoke-binding protein was significantly down-regulated. Note the much lower expression levels (except for silicatein-β) in tissues from a mature sponge.

5.4 Layer-by-layer assembly of nanoscale building blocks to biosilica spicules

Spicules from siliceous sponges, like *S. domuncula*, consist of polycondensed silicic acid enclosing a central axial filament (see Fig. 6 – 9). Spicules isolated by chemical or mechanical extraction from *S. domuncula* always show, in the light microscope, a smooth and clean surface. The data collected above suggest a binding of the nano-screenMAG-CMX nanoparticles to the spicules. As a proof of concept, we studied whether it is possible to coat these spicules with such nanoparticles to create layer-by-layer biosilica spicules with new properties. We used acid-isolated spicules of a *S. domuncula* individual as templates (see 4.3.3) and successfully coated their surface with nano-screenMAG-CMX nanoparticles. (For silicon related nomenclature, see Table 1)

Fig. 34 shows a scheme of the intended and then prepared layer-by-layer structure of a coated biosilica spicule. The isolated sponge spicule forms the core of this structure, and its complete surface is silanized. Silanization of the spicule surface turned out to be crucial for a successful subsequent coating with nano-screenMAG-CMX nanoparticles. Silanization was performed with (3-aminopropyl)-trimethoxysilane, and quality controlled by FT-IR and ninhydrin (not shown). The silanized surface was then coated with nano-screenMAG-CMX nanoparticles. For this, we used 1-ethyl-3-(3-dimethylaminopropyl)carbodiimide (EDC) to activate the nanoparticles and thereby enhance their binding ability. EDC reacts with the carboxylic groups of the carboxymethyl-dextran matrix of the nano-screenMAG-CMX nanoparticles to an intermediate that can be displaced easily by the amino group of (3-aminopropyl)trimethoxysilane and thereby couple the nanoparticles to the silanized spicule surface.

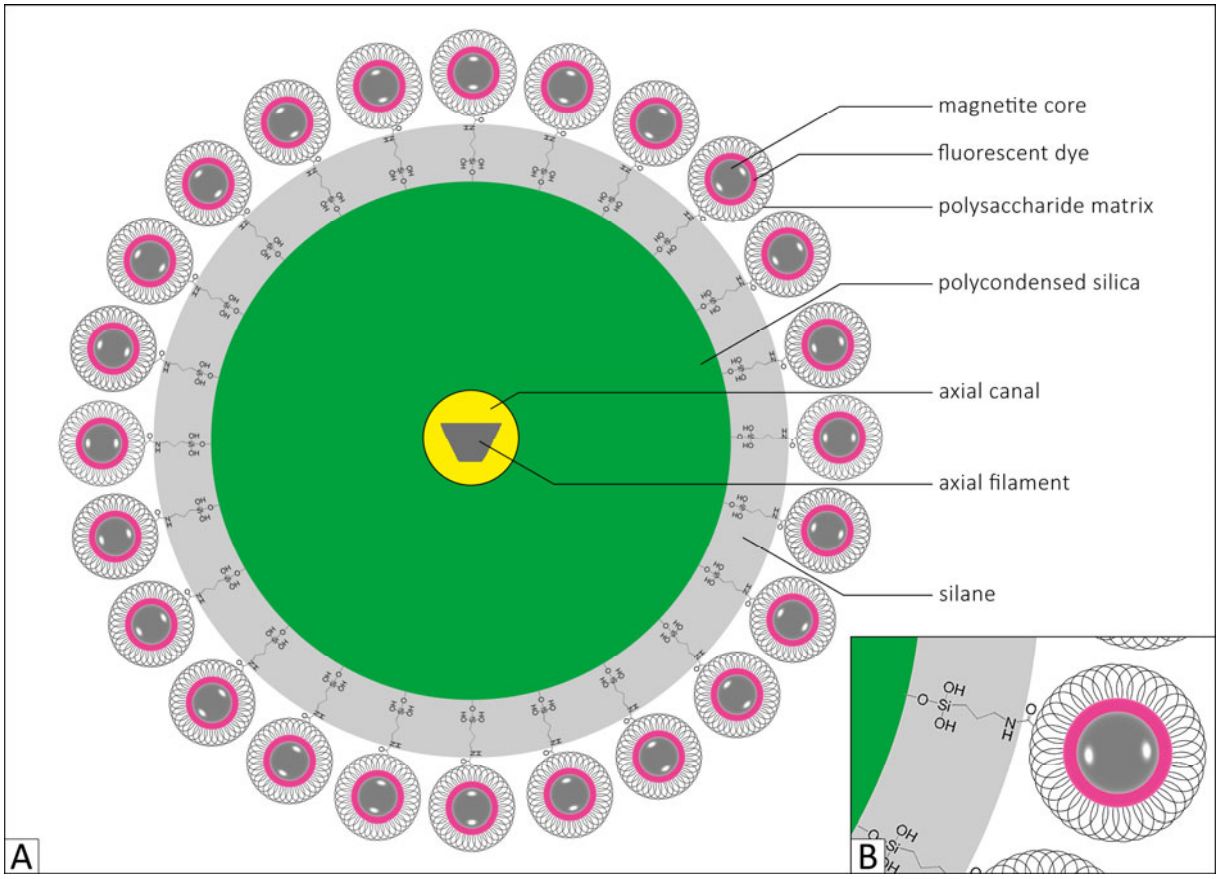

Fig. 34 Scheme of desired layer-by-layer assembly. (A) Cross-section of a silanized sponge biosilica spicule coated with carbodiimide (EDC)-activated nano-screenMAG-CMX nanoparticles. EDC-activation enhanced the binding of these nanoparticles to the silanized surface. **(B)** Magnified crosslinking between carbodiimide-activated nano-screenMAG-CMX nanoparticle and the silanized spicule surface. The resulting layer-by-layer structure possesses the combined properties of biosilica spicules and nano-screenMAG-CMX nanoparticles. (Scheme designed in ChemDraw and Adobe Photoshop)

In contrast to unsilanized control spicules incubated with nanoparticles, we found that silanized spicules efficiently bound EDC-activated nanoparticles (Fig. 35). Spicules of *S. domuncula* are about 250 - 350 µm in length, with an average diameter of 6.5 µm (Fig. 35 A). Often, activated nano-screenMAG-CMX nanoparticles formed clumps of 30 - 90 µm in diameter, bound to the silanized surface of spicules (Fig. 35 B). On the other hand, some spicules were evenly coated with a layer of nanoparticles. In most cases we found the spicules to be densely but not completely covered with nanoparticles (Fig. 35 C, D).

Apart from the typical sponge biosilica spicule properties, the resulting layer-by-layer structure additionally shows the fluorescence and magnetic properties of the nanoparticles.

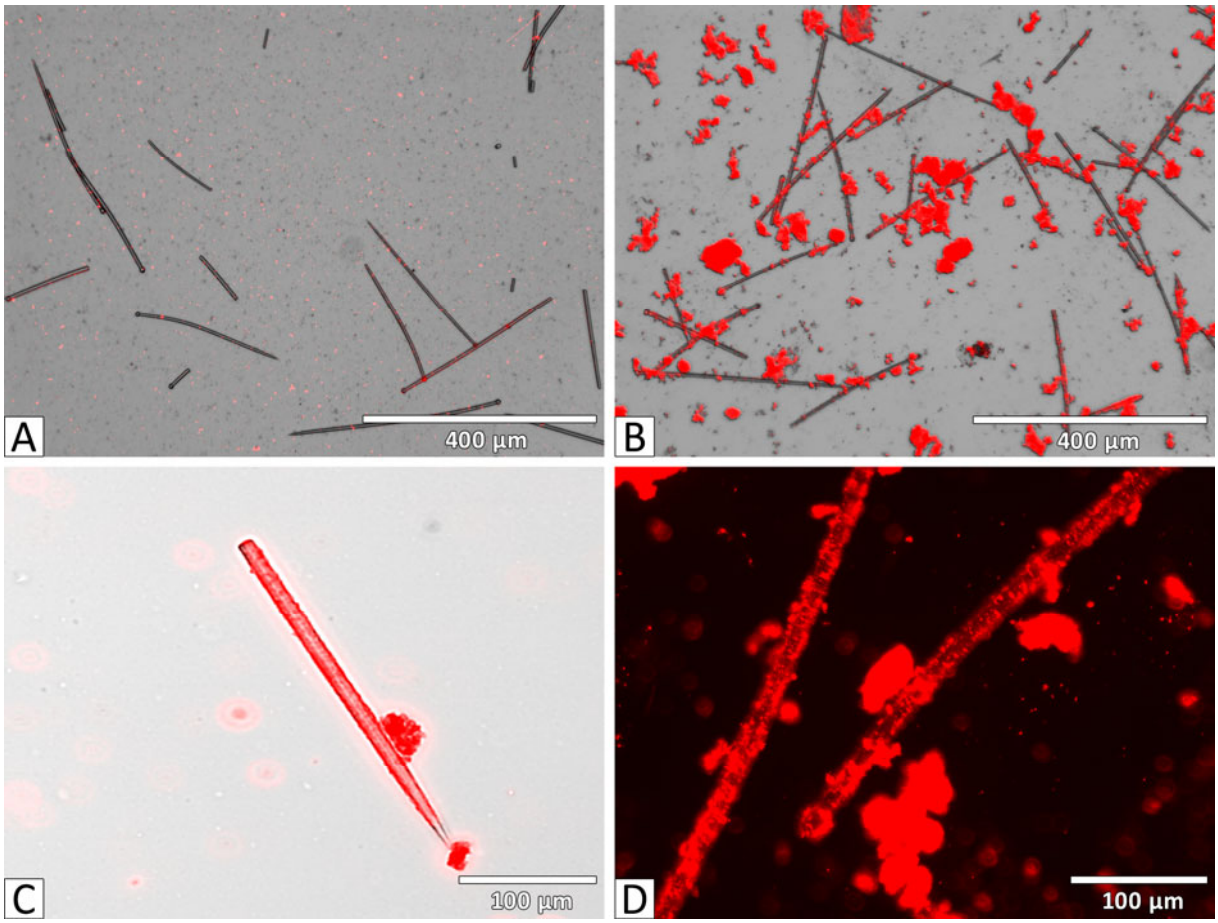

Fig. 35 Fluorescence micrographs of isolated *S. domuncula* biosilica spicules. (A) Unsilanized control spicules. **(B-D)** Silanized spicules, washed after incubation with EDC-activated nano-screenMAG-CMX nanoparticles (red fluorescence). Silanization in combination with the EDC-activation made it possible to efficiently coat sponge spicules *in vitro* with fluorescent, magnetic nanoparticles, and thereby add the nanoparticle properties to the normal spicule properties.

5.5 Uptake of fluorescent silica core-shell microparticles

Beside nano-screenMAG-CMX nanoparticles, a second type of particle was used for experiments: silica core-shell microparticles with a diameter of 800 nm. Uptake by primmorphs, as described before for nano-screenMAG-CMX nanoparticles, was also analyzed for silica core-shell microparticles with fluorescence microscopy and TEM. Also in this case, particles were found in large numbers inside the sponge cells. After one day incubation in culture medium supplemented with 0.5 mg/ml silica core-shell microparticles, cells of a freshly formed primmorph were dissociated, and then analyzed by fluorescence microscopy (Fig. 36). The microparticles with green fluorescence could be detected easily inside single sponge cells, while the negative control showed no fluorescence.

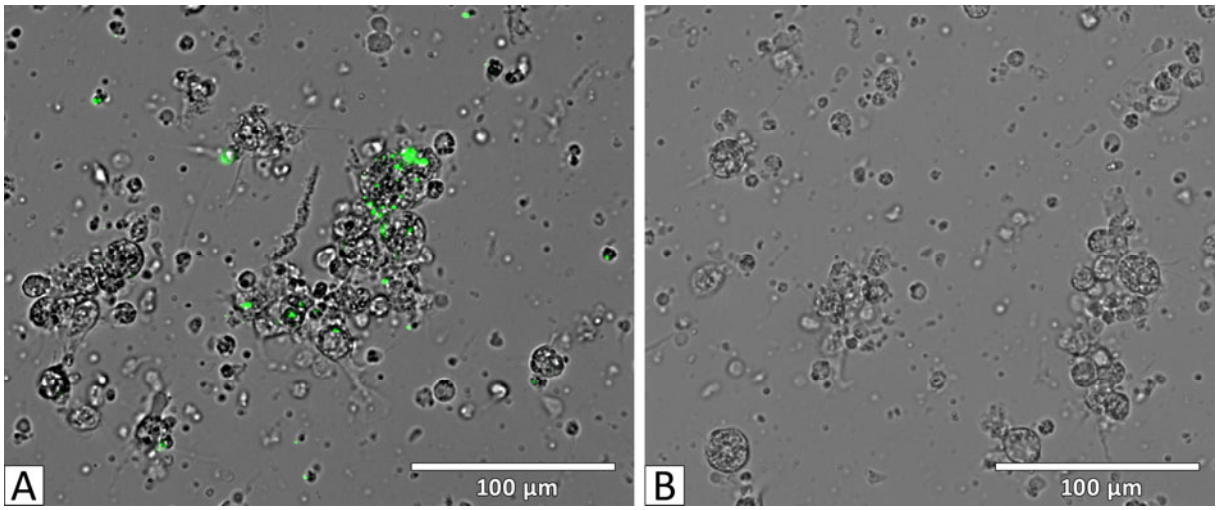

Fig. 36 Fluorescence micrographs of dissociated primmorph cells with engulfed silica core-shell microparticles. (A) One day after incubation of a cell suspension with 0.5 mg/ml silica core-shell microparticles (excitation 492 nm, emission 520 nm), and primmorph formation. **(B)** Cells from control primmorph. Microparticles are only visible inside the treated cells; their distribution within the cells seems to be heterogeneous.

Frozen tissue sections of a primmorph formed from cells incubated with silica core-shell microparticles were prepared and studied in the fluorescence microscope. The cells were found to be densely packed with round fluorescent microparticles showing a very homogeneous diameter of ca. 800 nm (Fig. 37).

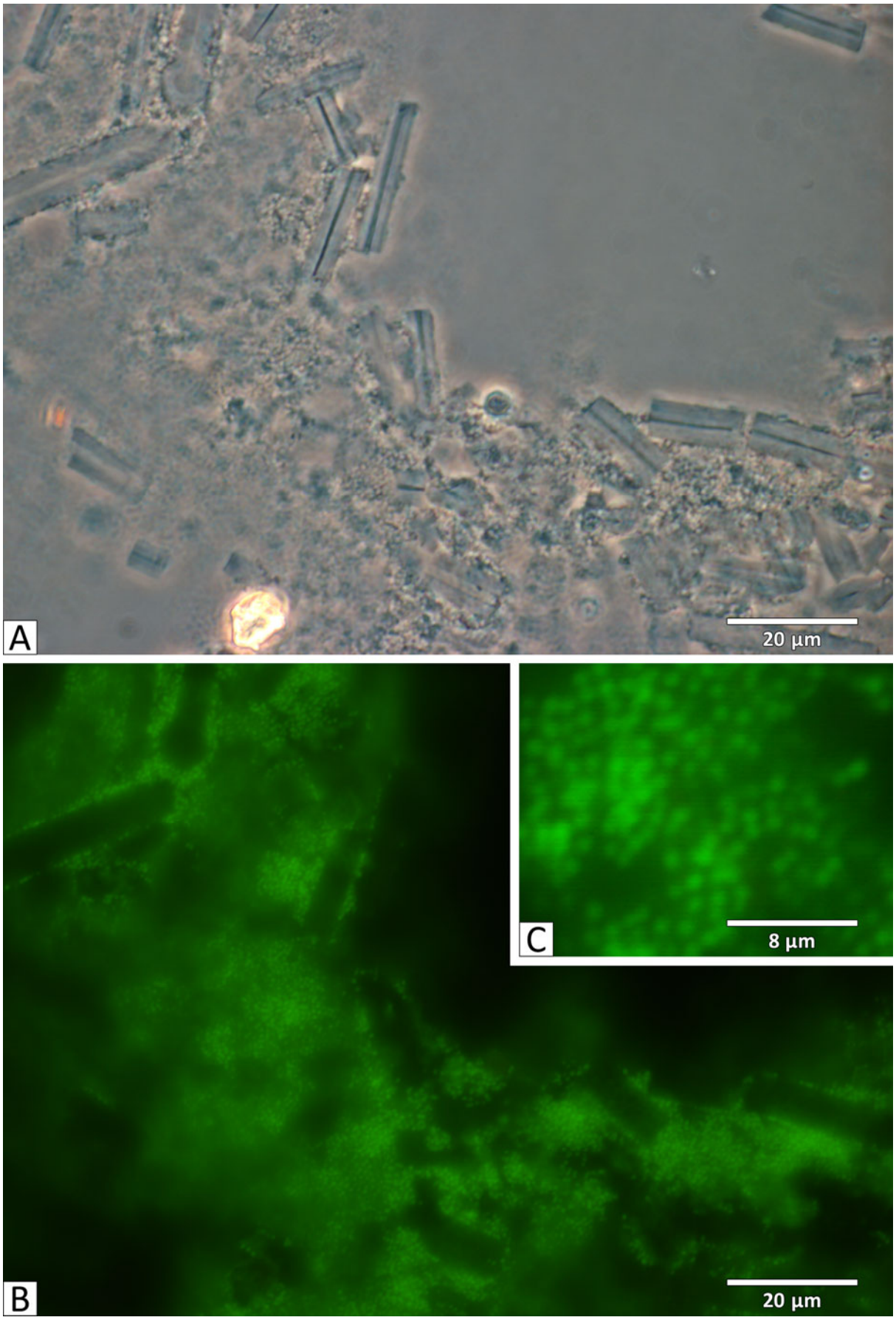

Fig. 37 Micrographs of a frozen tissue section of a primmorph formed from cells incubated with silica core-shell microparticles. (A) Phase contrast optics. **(B)** Epifluorescence optics. **(C)** Enlargement of a similar section as in (B). Note many round particles 800 nm in diameter that are absent in control tissues (not shown).

TEM images showed that regardless of their comparatively large size of 800 nm, the microparticles were taken up in vesicles or vacuoles and in the cytoplasm of all primmorph cell types (Fig. 38). Since these microparticles were made of silica, they could be identified easily in TEM images, as they show the same fractured structure like sponge spicules, except that the microparticles lack the axial filament. Interestingly, they were not evenly distributed throughout the whole cells, but often found in clusters. In contrast to the nano-screenMAG-CMX nanoparticles we did not observe silica core-shell microparticles in significant amounts directly associated with spicules.

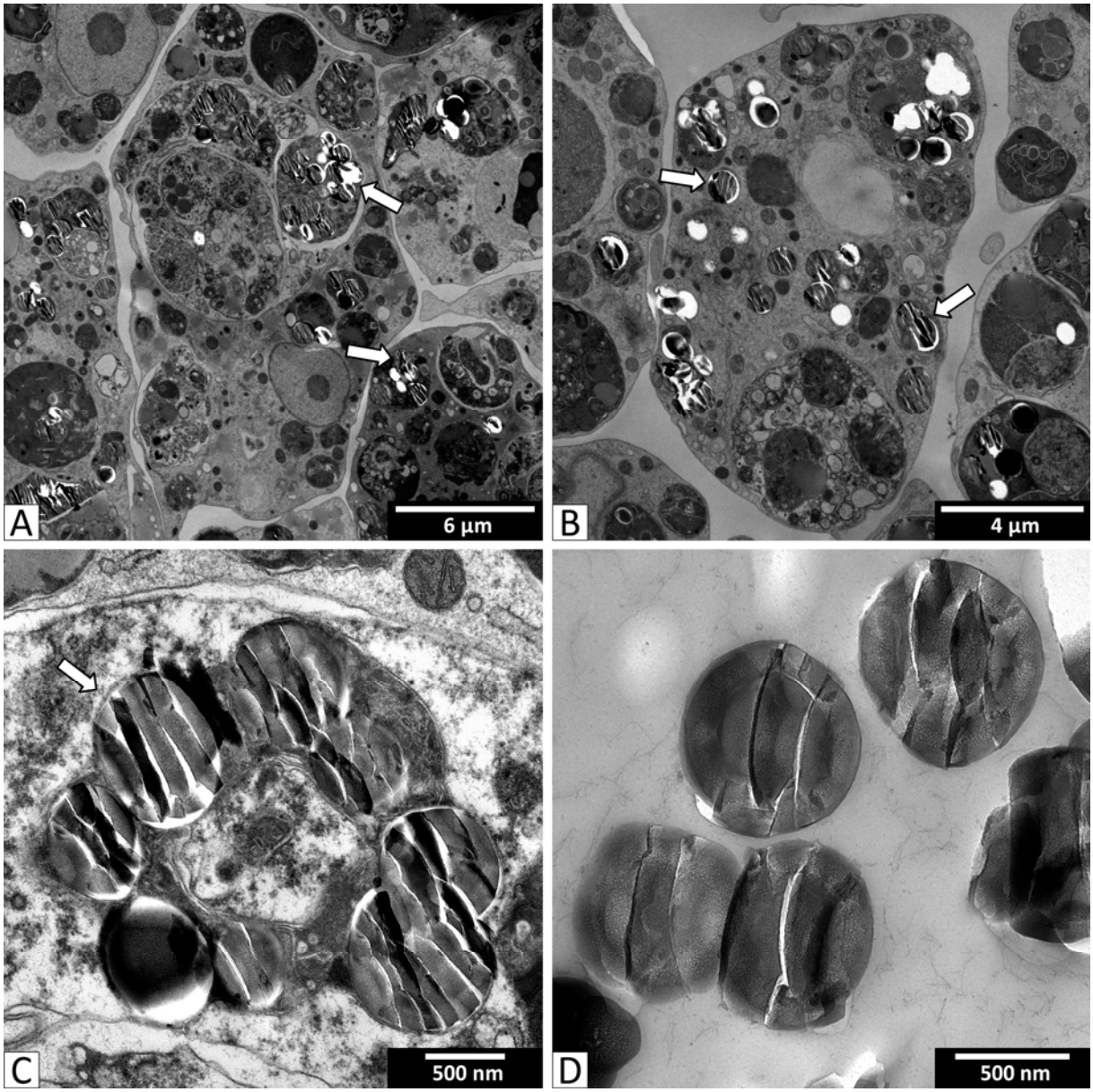

Fig. 38 Transmission electron micrographs of cross-sectioned primmorphs containing silica core-shell microparticles. Embedded 3 days after primmorph formation (A-C). **(A)** Overview of the primmorph tissue, with the microparticles (arrows) only located within the cells **(B)**. Note that the microparticles are not evenly distributed, but form clusters in vacuoles **(C**, arrow**)**. **(D)** Pure silica core-shell microparticles embedded and sectioned as done with the primmorphs. The results show that even microparticles of 800 nm in diameter are efficiently taken up and stored by cells forming primmorphs.

Due to the building material of the microparticles, silica, the expression levels of the four proteins known to be involved in spiculogenesis were again analyzed by quantitative PCR (see also Fig. 33). The expression level of silintaphin-1 was not influenced by the presence of the silica microparticles. In contrast, the expression of silicatein-α, silicatein-β and slowpoke-binding protein was significantly up-regulated in primmorphs that took up silica microparticles during cell aggregation (Fig. 39). In primmorphs with engulfed silica core-shell microparticles, slowpoke-binding protein showed an up-regulation of 1.8 times; the expression level of silicatein-β was 5.5 times higher, the expression level of silicatein-α was even 7.6 times higher. Again in comparison to mature sponge tissue, the expression level of silintaphin-1 and slowpoke-binding protein was more than doubled in normal primmorphs, while it was only 1.5 times higher in case of silicatein-α but unchanged for silicatein-β.

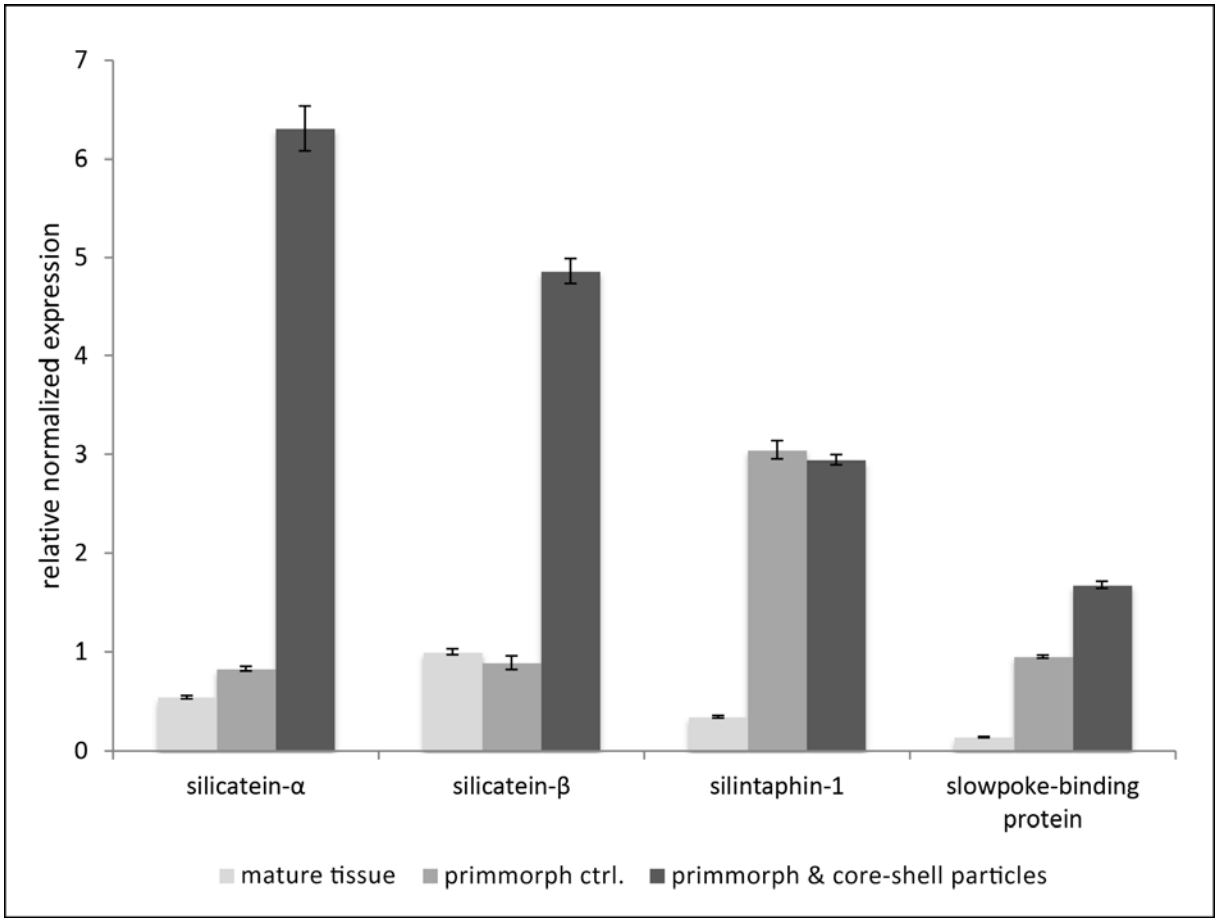

Fig. 39 Expression level analysis by qPCR of genes involved in spiculogenesis after uptake of silica core-shell microparticles by cells forming primmorphs. Exposure of sponge cells to 0.5 mg/ml silica core-shell microparticles, qPCR analysis 3 days after primmorph formation. Measurements were performed in triplets with a pool of n=5 sponge individuals, columns indicate mean ± SD. The expression level of silintaphin-1 was not affected by the microparticle uptake. In contrast, the expression levels of silicatein-α, silicatein-β and slowpoke-binding protein were significantly higher in treated compared to untreated primmorphs (7.6 times in case of silicatein-α and 5.5 times in case of silicatein-β).

5.6 Influence of silicatein-α expression on apatite formation by SaOS-2 cells

It is well known that silicatein-α is involved in the growth of biosilica spicules by sponge cells (Wang et al., 2012a). The results described above show that the expression level of silicatein-α is increased in primmorph cells, and even more increased upon supplementation of silica core-shell microparticles (see Fig. 39). Interestingly, silicatein-α is also able to enhance hydroxyapatite mineralization in SaOS-2 cells: It has been shown that growing of SaOS-2 cells on silicatein-coated surfaces yields this effect (Wiens et al., 2013). SaOS-2 cells are a human osteoblast-like cell line derived from osteosarcoma. They have the ability to mineralize after their incubation in activation medium (4.6.3.2). Thereby, they precipitate nodules in the extracellular matrix that are composed of inorganic hydroxyapatite and organic compounds. This stimulated us to attempt a direct stable transfection of SaOS-2 cells with the gene coding for *S. domuncula* silicatein-α, in order to investigate the influence of silicatein-α expression on the mineralization capacity of these cells. For this, we successfully used the mammalian TC-tag Gateway Expression vector system from Life Technologies (Darmstadt) to create an expression construct from pcDNA6.2/cTC-Tag-DEST and the gene encoding *S. domuncula* silicatein-α. This construct was termed pcDNAcTC-sili. In addition to the amino acid sequence of silicatein-α, the expressed protein had a V5 epitope for detection e.g. in Western blots, as well as a tetracysteine tag for detection of the protein in living cells. The sequence of the expressed protein is shown in Fig. 40.

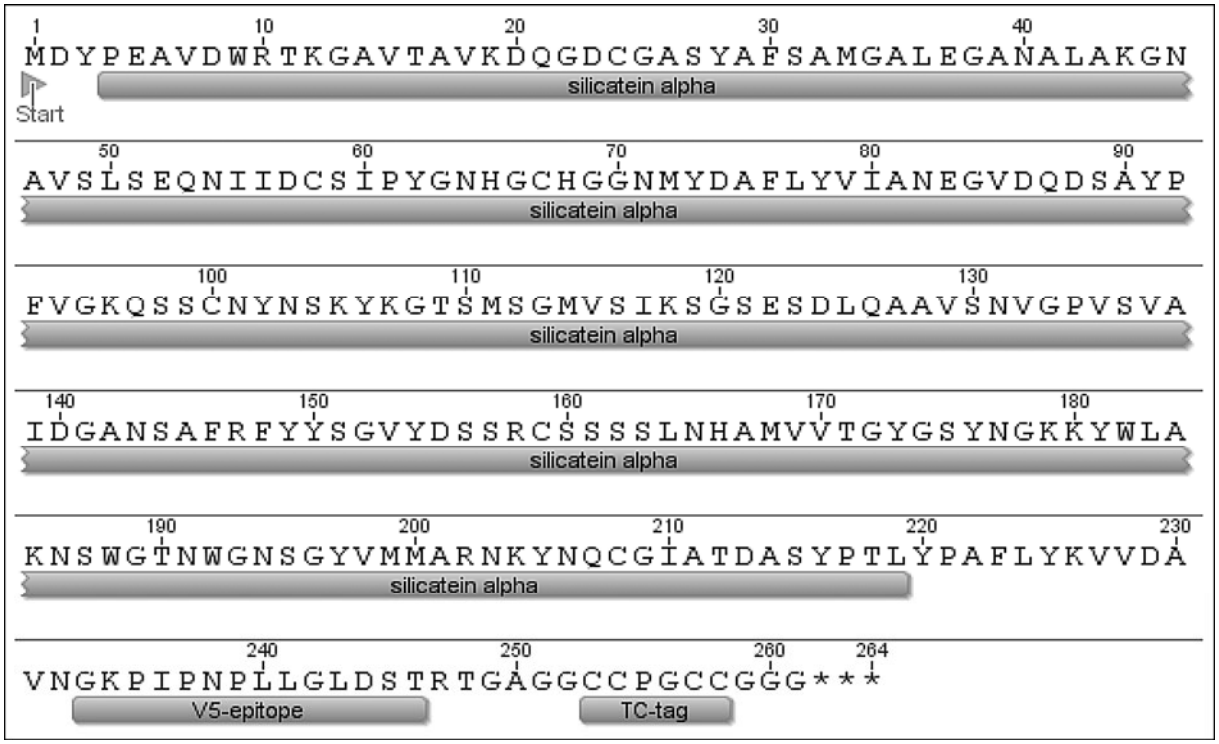

Fig. 40 Sequence of the *S. domuncula* silicatein-α construct encoded by the vector used for transfection of SaOS-2 cells.

Together with a biarsenical labeling reagent (FlAsH-EDT_2), the tetracysteine tag forms a fluorescent complex and can thereby be detected in the fluorescence microscope. Fig. 41 shows the transfected SaOS-2 cells after labeling with FlAsH-EDT_2, and the reaction mechanism. The green fluorescence of transfected SaOS-2 cells shows that they indeed express the sponge protein silicatein-α.

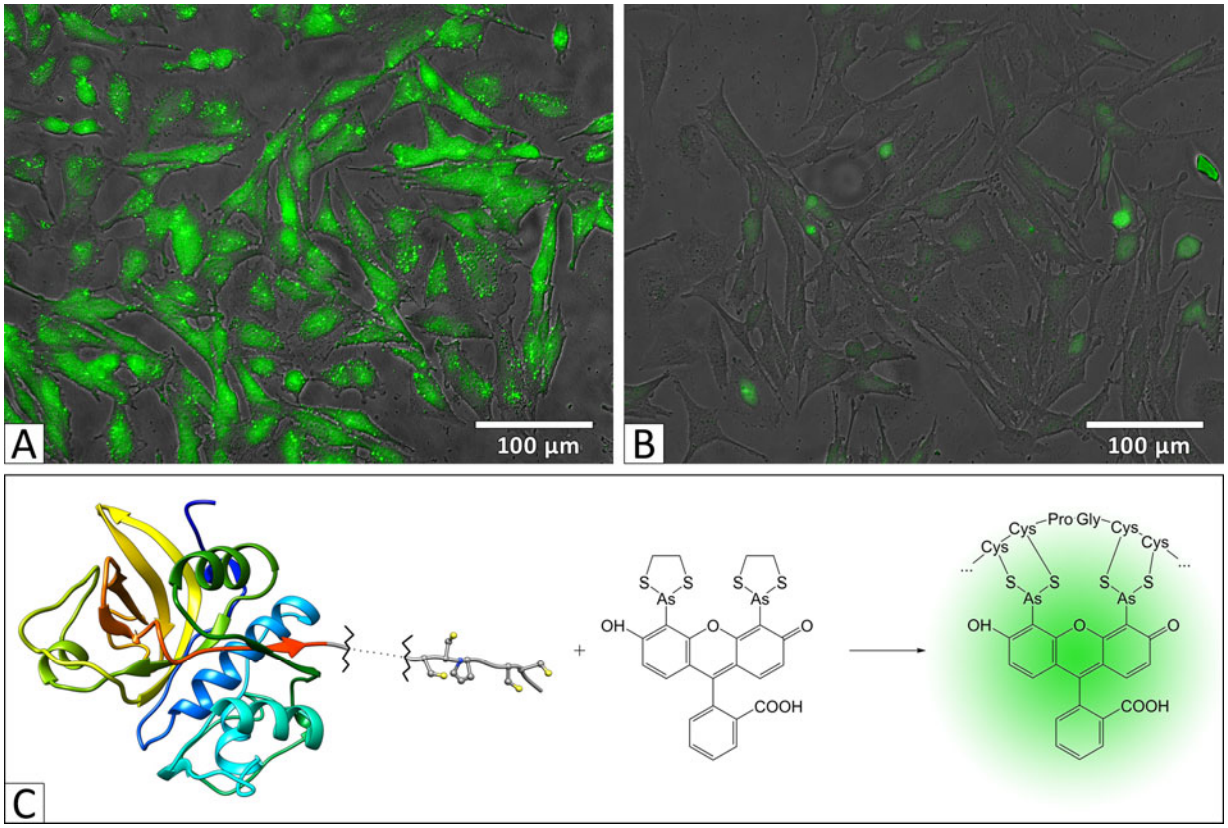

Fig. 41 Fluorescence micrographs of SaOS-2 cells. (A) Transfected cells that stably express tetracysteine(TC)-tagged *S. domuncula* silicatein-α, showing successful expression of this protein. **(B)** Mock-transfected control cells. Green fluorescence is only emitted if the recombinant protein is expressed. **(C)** Reaction mechanism of the TC-tagged recombinant silicatein-α with the biarsenical labeling reagent FlAsH-EDT_2. This results in a fluorescent complex (excitation 492 nm, emission 520 nm), which indicates the presence and location of recombinant silicatein-α in living SaOS-2 cells.

The used transfection vector (pcDNA6.2/cTC) also carried a gene for antibiotic resistance (blasticidin) by which it was possible to select stably transfected cells. In case of a stable transfection, the vector DNA is integrated in the cell nucleus, becomes part of the genome and is thereby passed to all descendants of this cell. For further experiments, this selection was done and only stably transfected cells were used.

Stably transfected cells and control cells were seeded in equal amounts. After one day, 50 % were kept in activation medium for the following ten days. The other 50 % were kept in standard growth medium,

and then the analyses were performed. All treatments were done in quadruplicates. Possible cytotoxicity of expressing silicatein-α was tested with the alamarBlue assay (Bio-Rad AbD Serotec, Puchheim), a quantitative test in which resazurin enters the living cells and is then reduced by the cell to resorufin. The resulting amount of resorufin can be measured photometrically and is proportional to the number of living cells. We could show that the viability of SaOS-2 cells is not affected by expressing silicatein-α (Fig. 42).

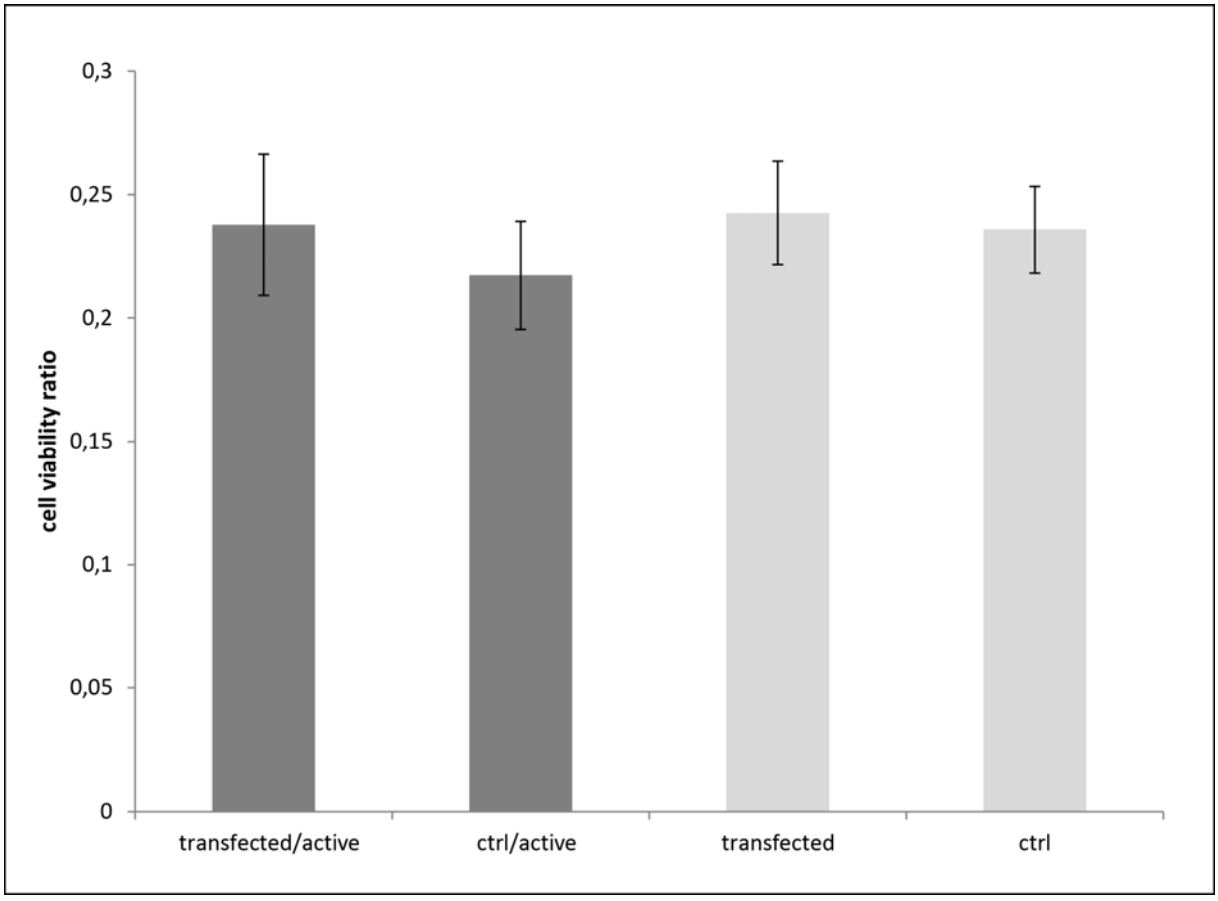

Fig. 42 Quantitative analysis for cytotoxicity of silicatein-α expression on SaOS-2 cells. The columns show the viability of stably transfected and non-transfected control SaOS-2 cells determined by alamarBlue assay. Treatments were performed in four independent replicates, columns indicate mean ± SD. SaOS-2 cells were seeded on a 48-well plate 11 days prior to quantification. After one day, cells were kept in activation medium (dark grey columns) or standard growth medium (light grey columns). The analysis of variance (ANOVA) yielded no significant difference. This means that cells expressing the protein silicatein-α from *S. domuncula* showed no reduction in viability.

In mineralizing cells, expression of the enzyme alkaline phosphatase is increased in comparison to non-mineralizing cells (Golub and Boesze-Battaglia, 2007), even before hydroxyapatite is deposited. Therefore alkaline phosphatase activity can be used as early stage marker of mineralization in SaOS-2 cells. To determine the alkaline phosphatase activity, a substrate (*p*-nitrophenyl phosphate) of the

enzyme was added to the cell extract. By hydrolyzing the substrate, a yellow color develops, which can be quantified photometrically. The same cell extracts were used to determine protein concentration to normalize the alkaline phosphatase activity. SaOS-2 cells that express silicatein-α show a ca. 20 % higher alkaline phosphatase activity than control cells. This suggests higher mineralization rates in the presence of silicatein-α (Fig. 43).

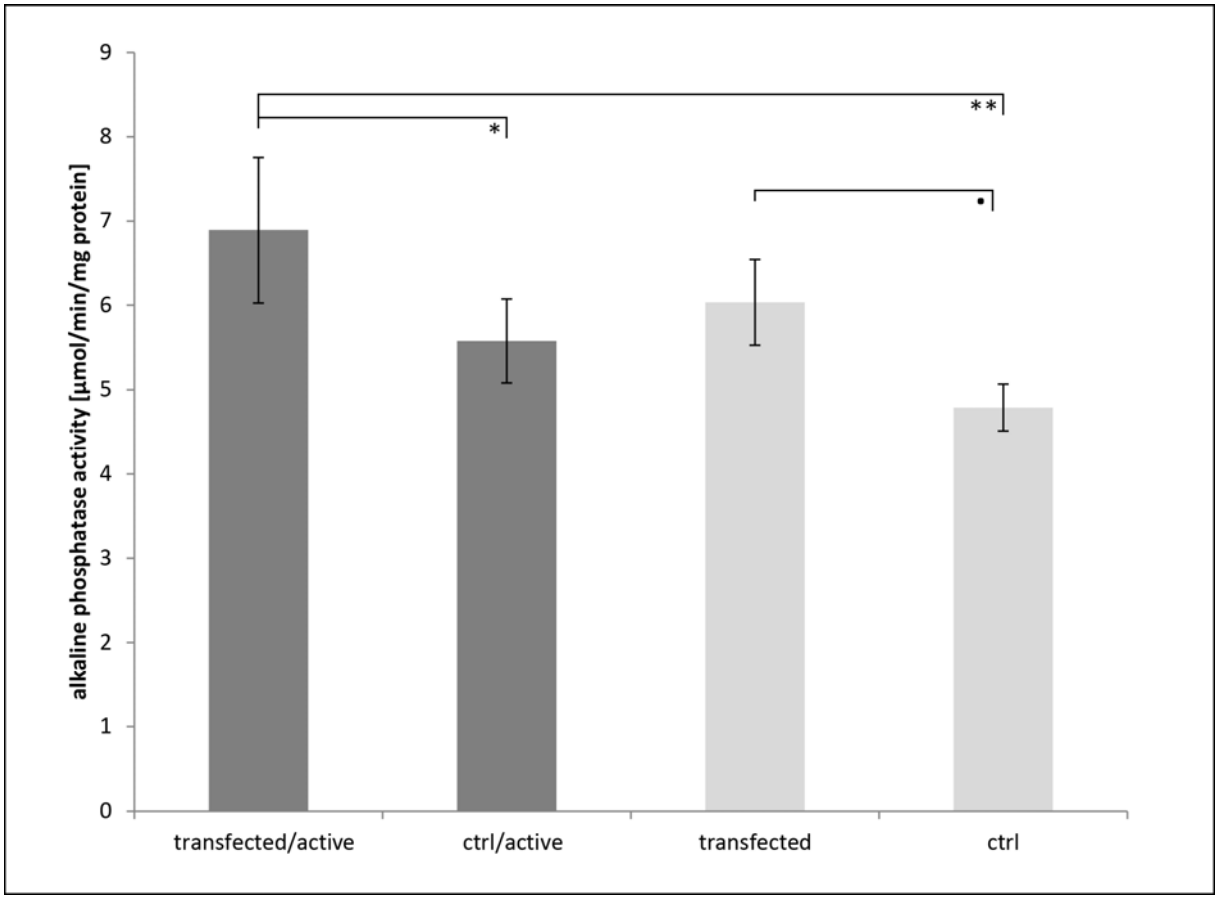

Fig. 43 Effects of silicatein-α expression on biomineralization of SaOS-2 cells. The columns represent the alkaline phosphatase (ALP) activity of the cell lysate of stably transfected and non-transfected control SaOS 2 cells. Results of the ALP activity were normalized by total cellular protein. Treatments were performed in four independent replicates, columns indicate mean ± SD. Cells were seeded on a 48-well plate 11 days prior to quantification. After one day, cells were kept in activation medium (dark grey columns) or standard growth medium (light grey columns). Tukey's honest significance test codes are *** $p < 0.001$, ** $p < 0.01$, * $p < 0.05$, • $p < 0.1$. These results show that expression of silicatein-α enhanced biomineralization.

Biomineralization of SaOS -2 cells expressing silicatein-α was analyzed qualitatively and quantitative by staining the cells with alizarin red S. This compound binds to Ca^{2+}, which is part of the hydroxyapatite nodules. For qualitative analysis, images were taken after the cell-layer was stained with alizarin red S. For quantitative analysis, stained complexes were hydrolyzed and analyzed photometrically. The greater the mineralization, the higher is the measured absorbance. We found that if transfected

SaOS -2 cells were kept in activation medium, mineralization was significantly increased (ca. 24 %), compared to control cells in the same medium. In standard growth medium the difference was even larger, meaning that mineralization in transfected SaOS-2 cells was significantly higher (ca. 84 %) than mineralization in non-transfected cells (Fig. 44).

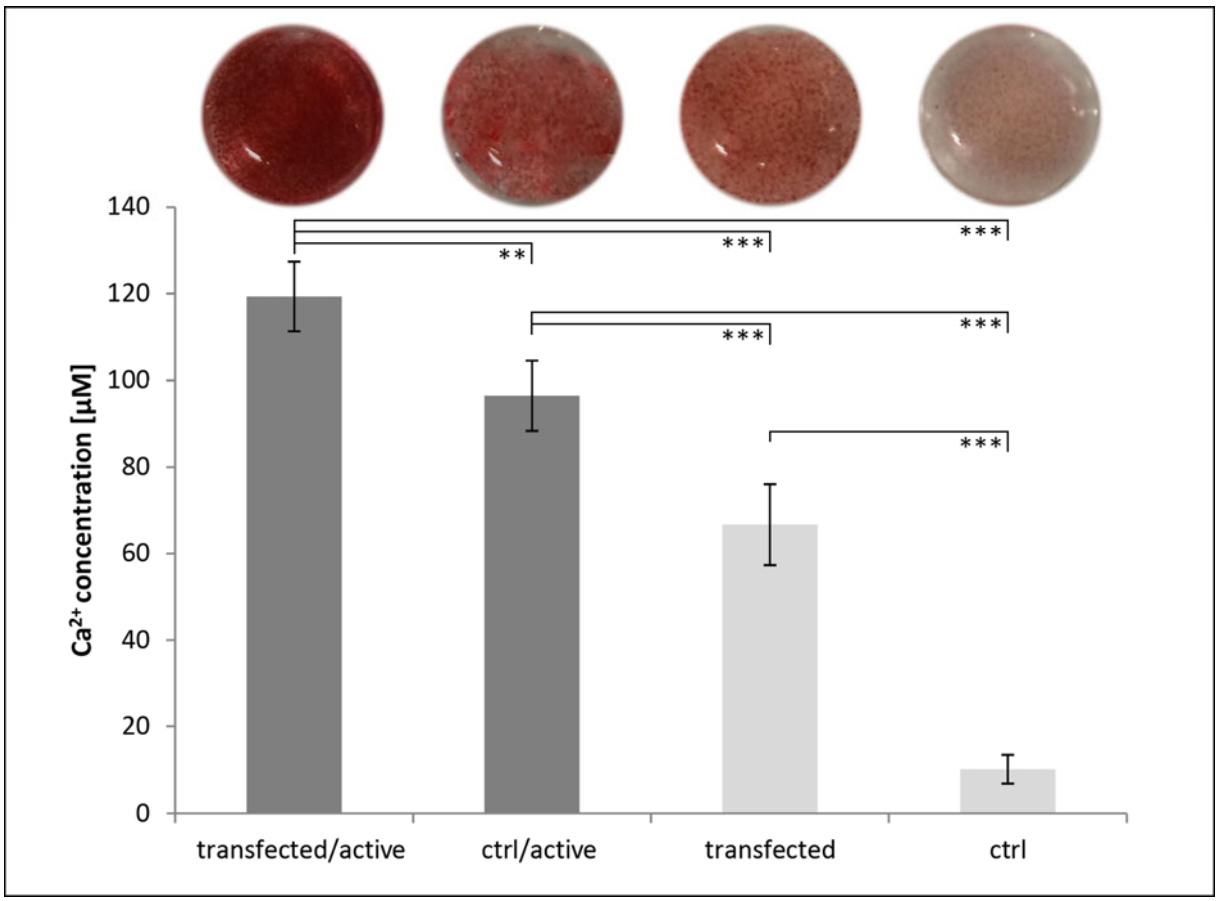

Fig. 44 Effects of silicatein-α expression on biomineralization of SaOS-2 cells. The columns show the quantification of Ca^{2+} deposition following alizarin red S staining. The insets above show respective staining intensity. Treatments were performed in four independent replicates, columns indicate mean ± SD. Stably transfected and non-transfected control SaOS-2 cells were seeded on a 48-well plate 11 days prior to quantification. After one day, cells were kept in activation medium (dark grey columns) or standard growth medium (light grey columns). Tukey's honest significance test codes are *** $p < 0.001$, ** $p < 0.01$, * $p < 0.05$, • $p < 0.1$. These results show that expression of silicatein-α enhanced hydroxyapatite deposition.

To visualize biomineralization in SaOS-2 cells, they were stained with OsteoImage (Lonza, Cologne). OsteoImage specifically binds to hydroxyapatite and has thereby the advantage to be a direct marker for mineralization in SaOS-2 cells. Transfected and non-transfected cells were seeded on coverslips and incubated in standard growth medium or activation medium for five days. After fixation with paraformaldehyde, the actin cytoskeleton, the nuclei and hydroxyapatite deposits were stained with fluorescent dyes, using rhodamine phalloidin (red), DRAQ5 (blue) and OsteoImage (green),

respectively (Fig. 45). In the sample with control cells grown in standard growth medium, no hydroxyapatite could be detected, while hydroxyapatite was present in the other three samples. Even in samples of transfected cells in standard growth medium, hydroxyapatite was detected. It was significantly less than in samples with activation medium, but the labeling was clearly visible. The staining results with OsteoImage corresponded to the results of the alizarin red S and the alkaline phosphatase assays. They all suggest a significant increase of the mineralization activity by SaOS-2 cells transfected with sponge silicatein-α.

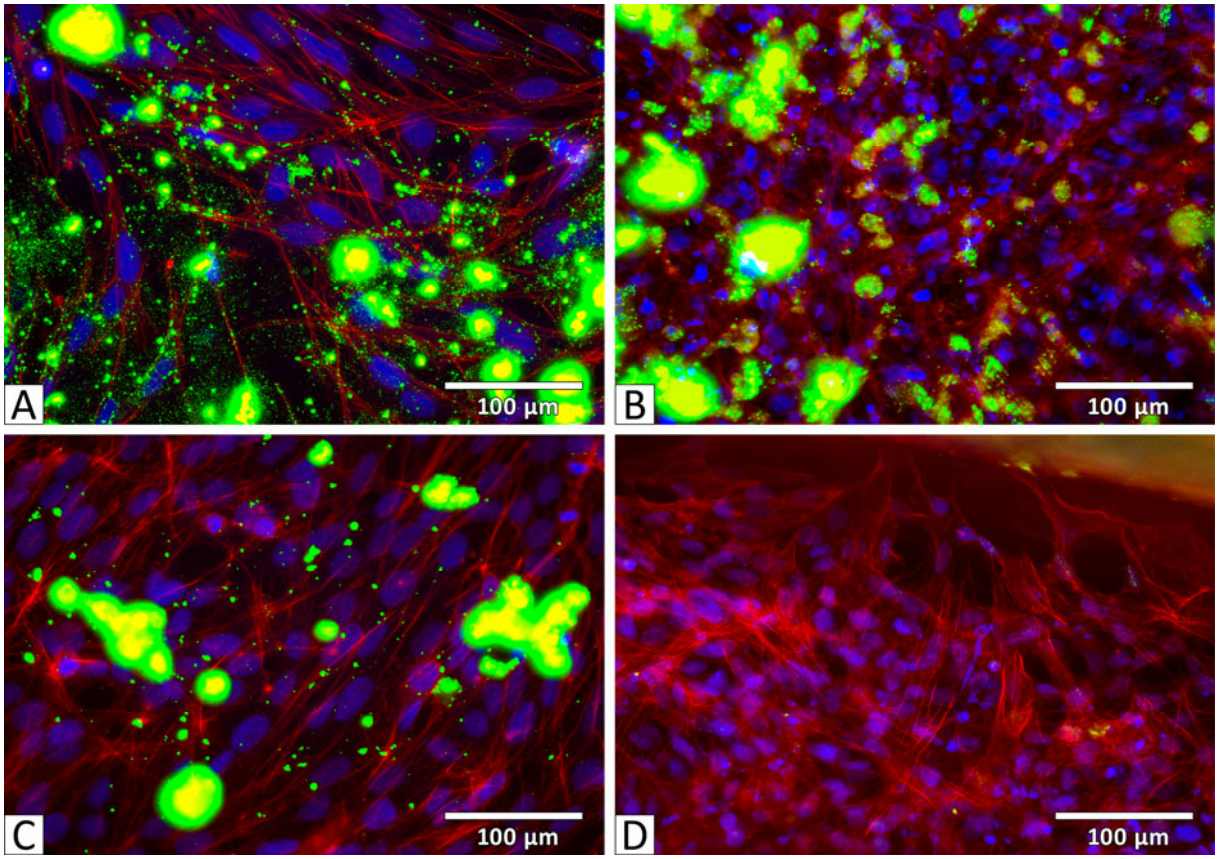

Fig. 45 Fluorescence micrographs of SaOS-2 cells to investigate the effects of transfection with silicatein-α on hydroxyapatite deposition. (A) Transfected cells and **(B)** control cells kept in activation medium. **(C)** Transfected cells and **(D)** control cells in standard growth medium. Note mineral deposits in samples grown in activation medium as well as in samples of transfected cells in standard growth medium (C). These findings support the results of the quantitative analyses shown in Fig. 43 and Fig. 44. Fluorescent staining of the actin cytoskeleton, the nuclei and mineral deposits was done with rhodamine phalloidin (red), DRAQ5 (blue) and OsteoImage (green), respectively.

6 DISCUSSION

6.1 Transcriptome and qPCR analyses of sponge tissues

Quantitative PCR is a very convenient and powerful method to analyze gene expression levels in different physiological states (Murphy et al., 1990; Bustin, 2000). However, it is very important to use replicates, since gene expression levels can differ widely even between individuals kept under the same controlled conditions (Willems et al., 2008). I found that this was also the case with our samples, stemming from identically treated individuals. That is why I decided to pool the RNA from several individuals when preparing cDNA. It was heeded that each individual contributed the same amount of RNA to such RNA pools. In accordance with other studies (Tricarico et al., 2002; Dheda et al., 2005) I used not only a single but two different reference genes (β-tubulin and GAPDH). I found that in *S. domuncula*, the expression rates of these particular genes were more stable than those determined for other standard reference genes (for example HPRT).

Transcriptome analysis is another powerful tool for analyzing protein expression levels (Cloonan et al., 2008; Mortazavi et al., 2008; Nagalakshmi et al., 2008). For the present thesis, I applied transcriptome data primarily for the analysis of protein expression levels of the same sponge individual under different physiological conditions. As a proof of principle that this approach works in the sponge *S. domuncula*, I used a physiological change that has already been studied in our lab, namely adaption of sponge individuals to light and darkness (Müller et al., 2010; Müller et al., 2013b). The results were compared to those obtained in this thesis from quantitative PCR (see above). It turned out that in case of *S. domuncula*, the results obtained from both methods were comparable (see Table 9).

From our *S. domuncula* data it can be concluded that transcriptome analysis is the method of choice if the relative expression levels of many different proteins, but only a few different tissue samples should be compared. Quantitative PCR, on the other hand, is more efficient in cases in which only a few proteins, but numerous different tissue samples should be analyzed. Consequently, in the present thesis the subsequent analyses of this kind were done by quantitative PCR, rather than by transcriptome analysis. Application of both methods provides much flexibility in answering such analytical questions, and should produce more reliable results than restriction to a single experimental approach. It should be mentioned however that both methods analyze protein expression levels indirectly *via* the mRNA concentration and thereby neglect RNA interference processes and post-translational modifications.

Transcriptome analysis is also efficient in unravelling protein sequences. Therefore, as a “by-product” of the present protein expression studies, the transcriptome dataset from *S. domuncula* provided here

already revealed various unpublished protein sequences, and has the potential to yield many more. Using the software package Geneious, I could easily assemble complete protein sequences from fragments, if the fragments were already assembled with the "*de novo* assembly" function.

However, it was difficult to detect new protein sequences using known sequences from other species. In order to find specific proteins of interest that were detected by the *de novo* assembly approach, I used an available expressed sequence tag (EST) database of our research group. EST's are unedited, short (200 - 800 bp), randomly selected single-pass sequence reads derived from cDNA libraries (Nagaraj et al., 2007). Our research group disposes of an internal EST database (called "Spongebase") with annotated *S. domuncula* sequences. Previously, ESTs were completed in a time-consuming approach *via* standard procedures (*i.e.* PCR, cloning and sequencing). The two transcriptome datasets of *S. domuncula* now provide the possibility to complete sequence fragments in very short time, although obviously prior to publication their final confirmation *via* standard procedures is required.

By combining all these approaches I could identify and sequence various novel proteins that were not detected by *de novo* assembly. Nevertheless, persecuting these new data was out of the scope of the present thesis, and had to be postponed to later research.

6.2 Improvement of sponge cell culture by a newly designed bioreactor

In nature, *S. domuncula* individuals usually grow on gastropod shells and live in symbiosis with a hermit crab (see Fig. 10). This makes it impossible to keep such a sponge under controlled conditions. Sponges removed from their support and deposited in a culture dish do not perform well and are likely to rapidly die. Thus, for sponge experiments that require strictly controlled conditions, a sponge cell culture is the only choice. Cell suspensions of *S. domuncula* and all other sponge species tested so far are unable to form cell monolayers in culture, but they readily form three-dimensional aggregates called primmorphs. *S. domuncula* primmorphs are robust and have the capacity to survive for months in seawater supplied with nutrients (Custodio et al., 1998; Müller et al., 1999). Dissociated *S. domuncula* cells loose telomerase activity, but after aggregation to primmorphs change to a telomerase-positive state (Custodio et al., 1998). *S. domuncula* primmorph cells undergo DNA synthesis even when deprived of food (Müller et al., 1999), and they produce secondary metabolites (Andrade et al., 1999; Müller et al., 2000).

It has also been demonstrated for *S. domuncula* that sponge cells need cell-cell or cell-matrix contact to survive (Müller et al., 1999). This means that a sponge cell fraction that is not incorporated into a

primmorph but remains in the single-cell state is very transient and therefore lost for future experiments. Moreover, sponge cells can recognize cells from the same donor animal and undergo allograft rejection (Gaino et al., 1999; Wiens et al., 2004). Cells from different *S. domuncula* individuals spontaneously aggregate, but then again dissociate due to the allograft rejection, which might lead to changed protein expressions independent of the actual experimental treatment (Wiens et al., 2004). Therefore, it is not helpful to mix cells from several individuals for primmorph culture, and consequently, the starting material for primmorph formation is rather limited. This makes it necessary to perform primmorph culture as efficient as possible. Prior to this work, primmorphs have been produced and kept in culture dishes or well plates at 16 °C under gentle shaking (Müller et al., 1999). The increasing experimental need for sponge cell cultures in our and other labs has stimulated us to improve and up-scale this traditional primmorph production method by introducing bioreactors.

In this thesis the first successful application of a bioreactor to sponge cell culture is described (see Fig. 22). This bioreactor was specifically designed and tested to fit the needs of *S. domuncula* primmorphs. The term “bioreactor” is here referred to as a cell culture device with continuous medium exchange that allows cells to grow in masses and to survive prolonged periods. Bioreactors are widely used to up-scale cell culture amounts and thereby the production of secondary metabolites. Such devices were invented in the middle of the last century, primarily for culturing bacteria (Bartholomew et al., 1950) and later also plant cells (Nickell and Routien, 1956). There is constant research on their improvement for specific applications (Humphrey, 1998; Sajc et al., 2000; Au et al., 2011).

Marine species produce many interesting bioactive compounds, and it is clear that the majority of such substances is still unknown (Frenz et al., 2004; Gerwick and Moore, 2012). For their detection and study, efficient cell culture methods are required. Consequently, bioreactors have been used to cultivate marine micro- and macroalgae (Rorrer et al., 1996; Chen and Chang, 2016), marine diatoms (Rossignol et al., 2000; Goksan et al., 2003) or marine bacteria (Lee et al., 2010). Also symbiotic bacteria from marine sponges have been cultured in bioreactors (Xu et al., 2012).

The achievements in sponge cultivation and sponge cell culture were reviewed by Schippers et al. (2012). Sponge explants (Osinga et al., 2003) and whole sponge individuals (Poirrier et al., 1981) were cultured in enclosed containments. However, although the application of bioreactors to sponge cell culture was proposed already 17 years ago (Osinga et al., 1999), prior to this thesis no successful bioreactor procedure for sponge cell culture was published.

Following the aims of the present thesis (see chapter 3.9), two different bioreactor applications could be established: (i) Production of exceptionally large-sized primmorphs (*i.e.* up to 2 cm) which is unprecedented, and (ii) production of large amounts of normal sized primmorphs (*i.e.* up to 2 mm in

diameter), both from a single sponge individual. As shown here, a single bioreactor allows transforming a whole, normal-sized *S. domuncula* individual into many small or single large primmorphs. In contrast, for preparing the same amount of small primmorphs traditionally, a dozen culture dishes would be needed. Moreover, preparation of large primmorphs in culture dishes was unsuccessful.

It has been demonstrated that higher initial concentrations of cells lead to larger primmorphs (Sipkema et al., 2003). Nevertheless, the previously available methods only produced primmorphs of about 2 mm maximum length, in contrast to 2 cm as achieved here. This means that compared to previous primmorphs, the volume and cell number of these "macro-primmorphs" is increased by the factor 400 - 500, depending on their individual flatness. Electron microscopy of *S. domuncula* primmorphs (see Fig. 27) showed that the cells are rather round, have an average diameter of 10 nm and are densely packed. From such TEM images it can be estimated that a globular, 2 cm primmorph contains about 8 billion (10^9) cells. This large size and high cell number should greatly facilitate future experiments on individual primmorphs. Alternatively, our novel bioreactor allows the simple production of many small primmorphs from the same donor sponge. This is achieved by hollows in the bottom of the bioreactor, enabling and promoting cell-cell contacts. This increased efficiency in primmorph production should allow many experiments that were not possible before.

It is an important result of the present study that the crucial effect in primmorph culture is not necessarily the initial cell concentration as proposed by Sipkema et al. (2003), but rather the opportunity for cells to come in contact to each other. In our bioreactors we obstruct their free crawling by barriers, together with hollows, at which they accumulate. For future improvement, I recommend attempts to control the size of the primmorphs even better by varying the depth and shape of these hollows and barriers.

6.3 Sponge primmorph cells and phagocytosis

Primmorphs have a potential as model organisms to investigate biological processes in sponges, for example biomineralization (Valisano et al., 2007; Valisano et al., 2012), or as natural sources to produce novel bioactive compounds (Schröder et al., 2003b). A variety of cell types has been identified in sponges in general and in *S. domuncula* in particular (see Fig. 2). However, it is very difficult to distinguish different cell types in *S. domuncula* primmorphs, since most of the cells show an unremarkable surface and are filled with granules, vesicles and vacuoles (see Fig. 27 and Fig. 28), and because they might all take up particles from the surrounding matrix. In normal sponge tissues the cell types are distinguished not only by their phenotype but also by their location and functionality. In primmorphs they are not in their typical local environment, and their phenotype has changed due to

dedifferentiation, redifferentiation and transdifferentiation during primmorph formation (Lavrov and Kosevich, 2014). Therefore, in the present study a discrimination of cell types within the primmorphs was not attempted, and might be possible only by using molecular markers still to be defined (see, however, Fig. 49).

Sponge cells are specialized on rapid phagocytosis of bacteria (usually 0.6 - 1 µm in diameter) and smaller particulate organic matter. It has been estimated that natural food of sponges is composed, on the average, of 20 % bacteria and 80 % detritus. They have been considered to be unselective feeders (Pile et al., 1996), with their actual uptake depending more on availability and particle size than on composition (Witte et al., 1997; Duckworth and Pomponi, 2005; Perea-Blazquez et al., 2013). Their phagocytic capacity fits our experimental observation that cells forming *S. domuncula* primmorphs took up nano- and also microparticles very fast (see Fig. 29 and Fig. 38). Within minutes after exposure, the cells were attracted by magnets, and also showed intracellular fluorescence. This proves that they incorporated considerable numbers of particles within this short period. Fast uptake of 1.0 and 0.5 µm latex beads was observed in the sponge *Sycon coactum* (Leys and Eerkes-Medrano, 2006). In this case the particles were engulfed at the cell surface by lamellipoda. Mukherjee et al. (2015) examined the phagocytic potential of different cell types of the freshwater demosponge *Eunapius carteri*. Thereby archaeocytes, granular cells and large amoebocytes were identified as the major phagocytically active cells. This fits my results that most, if not all *S. domuncula* primmorph cells were capable of particle uptake. After dedifferentiation, the cells might be in an archaeocytic state, in which they show high phagocytic activity. On the other hand, neither the phagocytic potential of mature *S. domuncula* cells, nor the time course of when dedifferentiation happens are known. Moreover, the mentioned studies on sponge particle uptake were performed on mature sponges or sponge explants, while all my studies were performed on primmorphs.

The size of nano-screenMAG-CMX nanoparticles is specified by the producer (Chemicell, Berlin) with a hydrodynamic diameter of 100 nm. However in the electron microscope, I could not detect particles of this size in any of the treated specimen; instead, nanoparticles with a maximum size of 10 nm were found (see Fig. 29). Since embedded pure nanoparticles also showed only this smaller size (see Fig. 29 D), there are two possibilities: (i) The size given by the manufacturer is wrong, or (ii) the nanoparticle drastically shrinks by dehydration when processed for the electron microscope.

It has been considered that sponges take up particles from their environment primarily by the microvillar collar of their choanocytes. The sponge choanocyte seems to be functionally identical and most probably evolved from an ancient choanoflagellate cell (Riisgard and Larsen, 2000). Leys and Eerkes-Medrano (2006) demonstrated that particles are indeed bound to the microvillar collar, but

that their phagocytosis occurs in other surface regions of these cells as well. Moreover, amoebocytes and all other sponge cell types are capable of phagocytosis because they are nourished by particles collected and then exocytosed by the choanocytes, and subsequently distributed within the sponge by amoebocytes (Simpson, 1984).

In our experiments on *S. domuncula*, we found that the vast majority of primmorph cells have the ability to take up particles, because after incubation with nano-screenMAG-CMX nanoparticles they were attracted by magnets and showed fluorescence. Only a small cell fraction was not attracted and probably dead (see Fig. 26). We have evidence from the experiments with the silica core-shell microparticles that phagocytosis occurs *via* the formation of pseudopodia (Fig. 46).

The nanoparticles are then stored in large amounts in individual vacuoles (see Fig. 29). This shows the impressive uptake capacity of sponge cells. Even if the sponge cells were incubated with rather low concentrations of nanoparticles (80 µg/ml), the latter densely accumulated in vacuoles. In an experimental series I checked the primmorphs after 9 and 19 days in nanoparticle-free medium, and still found the vacuoles filled with nanoparticles. It was proved by fluorescence microscopy that photo bleaching did not occur in this period. Apparently, the nanoparticles cannot be digested, and they are not ejected from the cells, but simply stored. Nanoparticles were not only found inside the primmorph cells, but also extracellularly bound to spicules (see below).

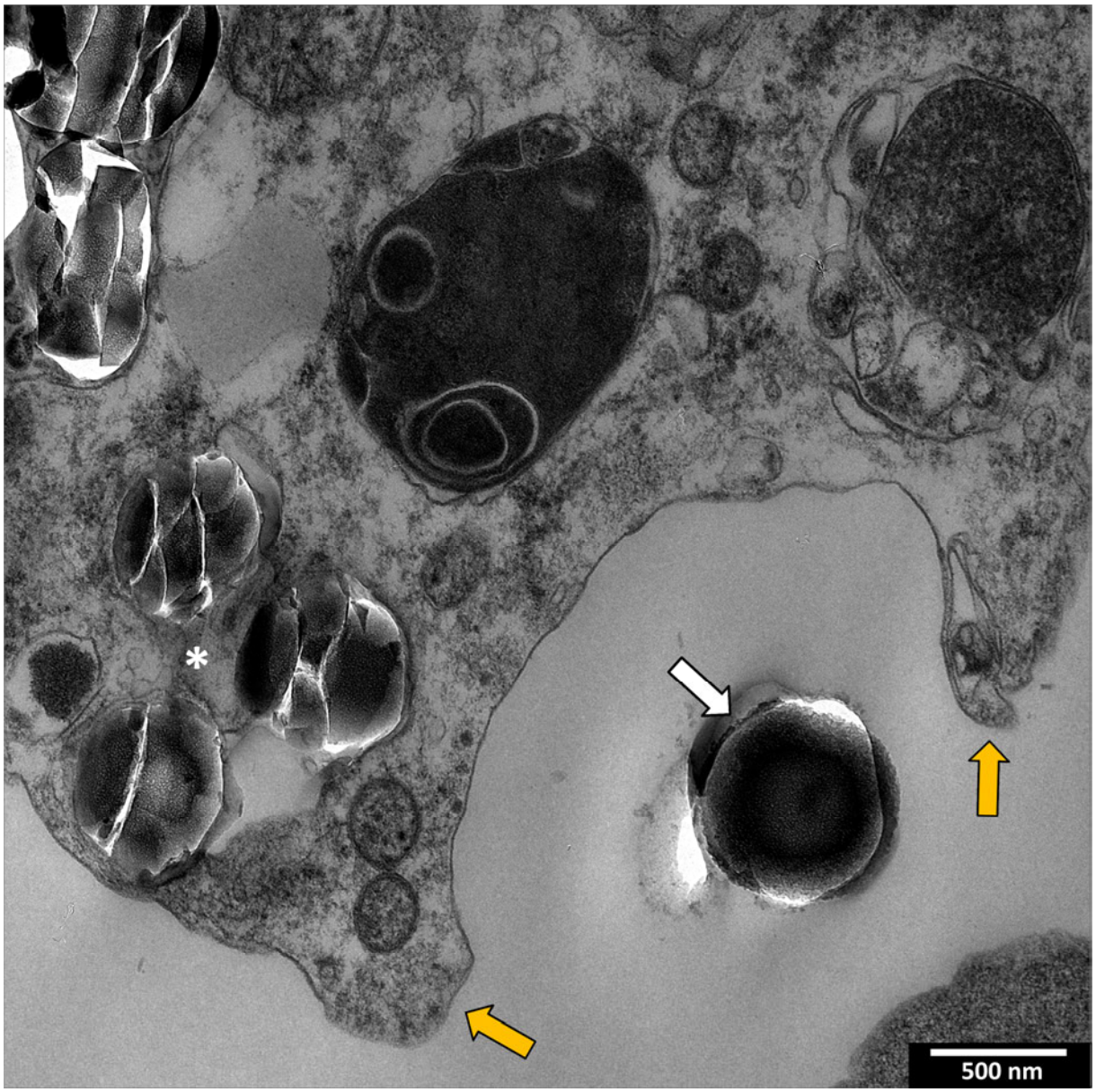

Fig. 46 Transmission electron micrograph of a cross-sectioned primmorph cell with ingested and free silica core-shell microparticles. Embedded 3 days after primmorph formation. This cell seems to form pseudopodia (orange arrows), apparently for phagocytosis of this silica core-shell microparticle (white arrow). Already ingested silica core-shell microparticles are also seen (asterisk).

6.4 New property combinations: cultured magnetic primmorph cells

We used nanoparticles with magnetic properties initially for the reason that they allowed an easy proof of successful uptake: Cells with engulfed nanoparticles were attracted by magnets. As the nanoparticles could not be digested and were permanently stored in vacuoles instead of being extruded, these sponge cells remained magnetic, without any sign of reduced vitality. We therefore considered that “cultured magnetic sponge cells” might have an applied aspect. Primmorphs are usually round or kidney-shaped (Müller et al., 1999). By using a magnet in combination with magnetic

nanoparticles, we have the possibility to influence and pre-determine the site of primmorph growth, as well as its final shape. Alternatively, we might also influence both parameters by allowing sponge cells to aggregate in molds, such as a small glass tube. However, a mold has to rest in the culture medium, whereas a magnet can be attached at the outer surface of the culture vessel. This principle of primmorph growth control might be used to attach sponge cells to specific surfaces that cannot be directly accessed for pre-coating treatments. Hypothetically, by using this approach a complex tube system could be coated at its inner surface by sponge cells if its outer surface is accessible for magnets. This might be used to establish and periodically renew a biological water filter system. In a preliminary test, we successfully coated a gastropod shell as an example of a rough surface (Fig. 47). Only if magnets and nanoparticles were used in combination coating of the shell surface occurred. The coating with primmorph cells remained unchanged during more than 3 weeks, even after removing the magnet.

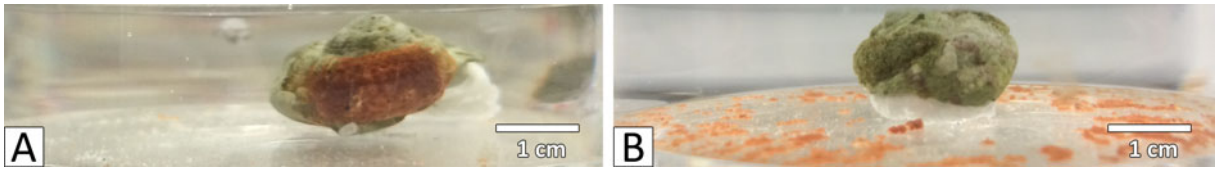

Fig. 47 Coating of a biogenic surface with sponge cells after nanoparticle uptake. Sponge cells were first incubated with 1 mg/ml nano-screenMAG-CMX nanoparticles and then combined with a marine gastropod shell (*Gibbula* spec.). **(A)** *Gibbula* shell with magnet inside. **(B)** Empty *Gibbula* shell. In both cases, the aperture was closed with sealing foil. After three weeks, the surface of the shell in (A) was covered with sponge cells, whereas the shell in (B) remained clean. This was clearly due to magnetic attraction in (A), and lack of this attraction in (B). The cells in (A) remained attached to the surface even after removing the magnet. Thus, coating of surfaces with sponge cells is now possible, due to new property combinations.

6.5 *In vivo* coating of biosilica spicules by magnetic and fluorescent nanoparticles

Nanoparticles are widely used in biology, medical research and clinics, for example in drug delivery (Yilmaz et al., 2015), cell labeling (Kacenka et al., 2015), reaction catalysis (Eshghi et al., 2015) and many more applications. Therefore, nanoparticles are objects of choice to introduce new properties to biological structures, in this case to the biosilica spicules present in primmorphs. These biosilica spicules have an average diameter of 6.5 µm and a length of 250 - 350 µm. They have an application potential as nanoscale optical fibers (Müller et al., 2010). Thus, studying new property combinations of sponge biosilica spicules is of interest, specifically properties that can be introduced *in vivo* by the primmorph cells themselves, instead of a cumbersome and probably expensive technical treatment of isolated spicules. In the present thesis I obtained possibilities to stably coat spicules *in vivo* by

nanoparticles with combined magnetic and fluorescent properties. The magnetic properties would subsequently allow convenient arrangement procedures of these spicules, and the fluorescent properties would facilitate the control of this formation.

In this context, the structure and development of the spicules is of interest. Spicule formation by sclerocytes is described in detail in the Introduction (see Fig. 6 and Fig. 7). It starts with the formation of an axial filament (Schröder et al., 2007) composed of the proteins silicatein-α, silicatein-β and silintaphin-1 (Wiens et al., 2009; Wang et al., 2012c). In electron micrographs of cross-sections of spicules, this filament is perfectly visible (Fig. 48). In the extracellular space, the spicule is embedded in collagen fibers (Müller et al., 2006b).

Spicule growth happens in two directions: axially, *via* elongation of the axial canal where the axial filament is located, and radially by apposition of silica layers to the periphery of the growing spicule (Müller et al., 2005; Schröder et al., 2006a). Subsequent release of reaction water (syneresis) by specialized cells through their aquaporin channels hardens and ages the initially soft silica (Müller et al., 2011a; Wang et al., 2011a). Thus, the spicules show an early soft state and a late hard state (see Fig. 7). This turned out to be relevant for interpretations of our coating results to be discussed below.

The silica core-shell microparticles showed, in the fluorescence microscope and the electron microscope, the expected size of ca. 800 nm, and they were very similar in shape (see Fig. 37 and Fig. 38). In TEM images they showed a fractured, shattered internal structure caused by the diamond knife used for sectioning. Thereby, and due to their similar size, they resemble the cross-sections of biosilica spicules. However, in contrast to the spicules, the silica core-shell microparticles have no axial filament. They consist of two layers, namely a core from condensed silica with fluorophore and a shell from condensed silica only. The demarcation between core and shell was clearly visible in TEM images which allowed distinguishing them unambiguously from laterally cut spicules (see Fig. 46 and Fig. 48). Embedding and cutting of pure silica core-shell microparticles ultimately made sure, in the electron microscope, that the observed structures were indeed the core-shell microparticles and not immature biosilica spicules (see Fig. 38 D). Interestingly, although the silica core-shell microparticles were taken up by the primmorph cells in large numbers, we could not detect any of them bound to the surface of spicules. This might be caused by their comparatively larger diameter/surface area that negatively affects efficient association with growing spicules.

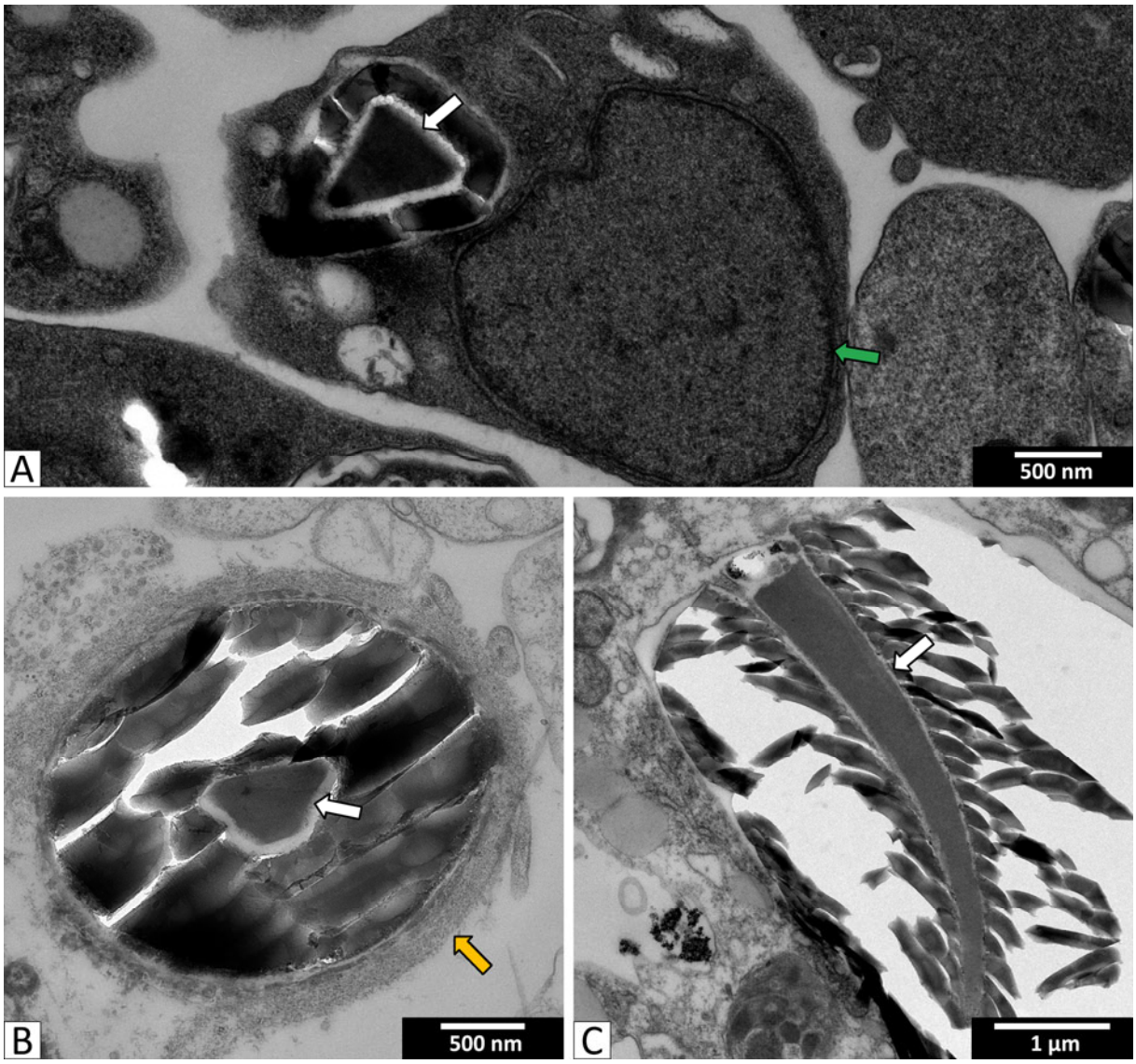

Fig. 48 Transmission electron micrographs of primmorph spicules. Tissue embedded 3 days after primmorph formation. **(A)**, **(B)** Cross-sections and **(C)** longitudinal section of a spicule. Axial filaments are clearly visible (white arrows). Cross-sectioned axial filaments were always trapezoid or triangular in shape. Longitudinally sectioned axial filaments are rarely seen, because they are usually excerpted by the diamond knife used for sectioning. Also, the fractured structure of the biosilica material visible in (A), (B) and (C) is a typical artifact caused by the diamond knife. Note that the juvenile spicule in (A) is still intracellular, within a sclerocyte, and shows a rather thin biosilica layer around its axial filament. Note the prominent cell nucleus (green arrow). In (B) the spicule is extracellular and enveloped by collagen (orange arrow); it has a rather thick biosilica layer.

In contrast to primmorph cells containing nano-screenMAG-CMX nanoparticles (see below), primmorph cells incubated with silica core-shell microparticles up-regulate their expression of silicatein-α, silicatein-β and slowpoke-binding protein (see Fig. 39). It was already known that the addition of silicate (as Na_2SiF_6 or tetraethyl orthosilicate) to primmorph culture medium induces expression of the gene encoding silicatein-α (Krasko et al., 2000). Probably the presence of silica is sufficient to start the up-regulation, without free silica being really available for spicule production. On the other hand, it is possible that the silica core-shell microparticles provide some free silica to the

primmorph culture medium. It is very likely that primmorph cells have the ability to digest silica core-shell microparticles, since they are able to degrade and recycle their own spicules (Schröder et al., 2003a). A result from our TEM studies supports this idea: Fig. 49 shows a primmorph cell associated with a spicule and with a silica core-shell microparticle. The edges of the microparticle are not sharply defined as incorporated microparticles normally do, but appear as if just dissolving.

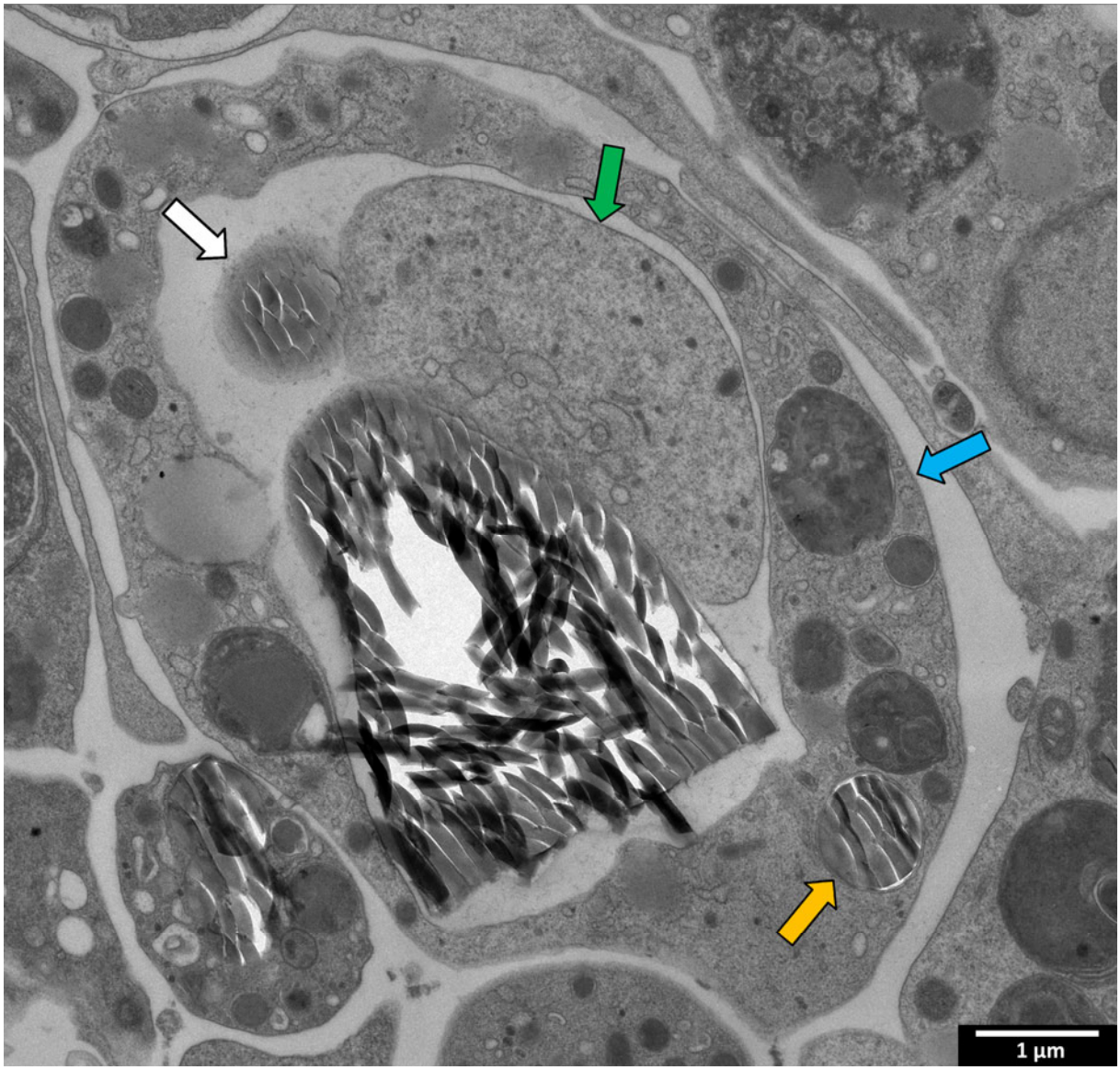

Fig. 49 Transmission electron micrograph of cross-sectioned primmorph incubated with silica core-shell microparticles. Embedded 3 days after primmorph formation. The image shows a primmorph cell (green arrow) that looks unusually pale, due to the lack of large electron-dense granules. It connects simultaneously to a spicule and a silica core-shell microparticle (white arrow). The edges of this microparticle are not sharply defined, indicating that it is just about to be dissolved. The surrounding cell (blue arrow) contains a silica core-shell microparticle in the cytosol (orange arrow). This image suggests that specific cells are dissolving silica pieces, probably by expressing silicase (Schröder et al., 2003a).

The nano-screenMAG-CMX nanoparticles proved to be promising for preparing sponge cells with new physical properties (see above). Moreover, a new hybrid material from spicules was prepared *in vivo*, as deduced from our fluorescence and electron microscopic analyses (see Fig. 30). After prolonged incubation of primmorph cells, increased numbers of spicules with bound nanoparticles were observed (see Fig. 30). This phenomenon is puzzling: During the first days of the experiment, in which the concentration of nanoparticles in the medium was still high, very few of them were bound to the extracellular spicules. Although the concentration of free nanoparticles in the medium then dropped significantly over time, due to the massive phagocytic activity of the cells, the coating of the biosilica spicules increased over time, as documented by TEM images (see Fig. 30 and Fig. 31). Although it should be pointed out that the electron microscopic approach described here is not a quantitative method, from the study of many micrographs I am convinced that the increase over time is considerable. If nanoparticles bind just randomly to spicules, one would expect them there already after a short incubation time (when the nanoparticle concentration is still high), and not in increasing amounts when the nanoparticle concentration in the medium drops to very low levels. A passive adsorption process can also be excluded as deduced from the results of our coating experiments with isolated spicules: they are incapable to stably bind these nanoparticles without silanization (see Fig. 35 and chapter 6.6). This suggests that in primmorph cells, nanoparticles are specifically bound to the surface of growing immature spicules by a natural chemical process that modifies their surface.

Incubating isolated sponge spicules for 24 hours with nanoparticles yielded a very heterogeneous pattern. Most of the spicules were completely uncoated, but some spicules were densely coated with strongly bound nanoparticles. My following hypothesis might explain this phenomenon: The nano-screenMAG-CMX nanoparticles can only bind to spicules while the silica is still soft, which means prior to the syneresis described by Müller et al. (2011b). Later, when the spicule surface is hardened, the nanoparticles cannot interact with the surface anymore. Correspondingly, if spicules were mechanically obtained from a primmorph, avoiding harsh chemical conditions like concentrated sulfuric acid, only very few of them were coated with the nano-screenMAG-CMX nanoparticles. However, in rare cases the coating was very dense and resistant. Probably these specific spicules had just been exported and were not yet hardened. Efficient artificial coating of spicules with nanoparticles requires rather harsh chemical conditions, in that the spicules are silanized beforehand (see below). In contrast, as shown here, primmorphs and possibly also mature sponges are capable to provide a coating environment under physiological conditions (chapter 5.3). It might be very interesting for materials scientists to unravel and mimic this coating mechanism.

It seems that nano-screenMAG-CMX nanoparticles lack a strong influence on the expression of genes involved in spiculogenesis. The expression levels of silicatein-α, silicatein-β and silintaphin-1 appeared

to be slightly up-regulated, but only the observed difference of silicatein-β expression was significant. This leads to the assumption that nano-screenMAG-CMX nanoparticles do not induce spicule growth. On the other hand, they were definitely bound to the spicule surface. It was even possible to isolate, from 19 days old primmorphs, single spicules with bound nanoparticles, which underlines how tight these chemical bonds might be (Fig. 50).

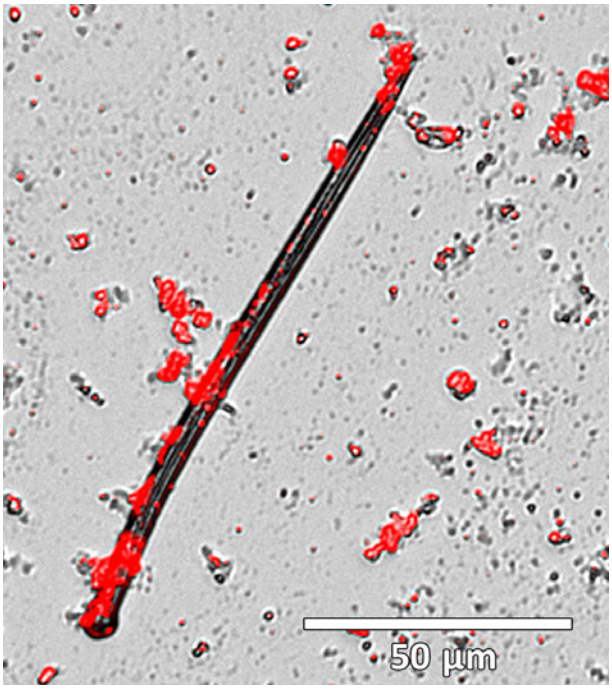

Fig. 50 Fluorescence micrograph of biosilica spicule isolated from a primmorph containing nano-screenMAG-CMX nanoparticles. Nanoparticle concentration during exposure was 1 mg/ml, spicule was extracted 19 days after primmorph formation. This shows that primmorph cells are able to bind nanoparticles (red fluorescence) tightly to spicules *in vivo*, a process that *in vitro* requires chemical silanization of the spicule surface.

6.6 Layer-by-layer assembly of nanoscale building blocks to biosilica spicules

Biosilica spicules can function similar to industrial glass fibers as light wave guide (CattaneoVietti et al., 1996; Müller et al., 2006c). In addition, due to their lamellar composite structure with protein components, their mechanical properties are remarkable as they can resist fractures much better than the relatively stiff industrial glass fibers (Sundar et al., 2003; Aizenberg et al., 2004; Mayer, 2005). These properties make spicules attractive for biomimetic and biotechnological approaches (Müller et al., 2009a).

For creating a layer-by-layer assembly of building blocks, I used natural isolated sponge spicules from *S. domuncula* as a template. This template was functionalized with alkoxysilane molecules by self-

assembly, a procedure which is known as silanization. The silanized spicule was then enveloped by a layer of carbodiimide-activated nano-screenMAG-CMX nanoparticles (see Fig. 34). This chemical modification was performed to enhance their binding capacity to amino groups of the silanized spicule surface. We found that silanization was a crucial step, since isolated untreated spicules did not significantly bind nanoparticles. After silanization, the binding of activated nanoparticles was strong and dense. This pattern could be observed by fluorescence microscopy due to the fluorescence of the used nanoparticles (see Fig. 35). This confirmed that the artificial coating of spicules was successful.

Such layer-by-layer assemblies offer the opportunity to control thickness and ordering of hybrid materials (Davis et al., 2001). Layer-by-layer structures, photoactive metal nanoparticles and organic-inorganic hybrid composite materials have drawn the attention in many fields (Kamat, 2002; Baron et al., 2007; Zhu et al., 2010). The outer envelope of the present hybrid spicules is fluorescent and attractable by magnets, while the core has the typical mechanical and light guiding properties. Attracting those novel spicules by magnets makes it possible, for example, to orient them in a magnetic field. There are many approaches to biofunctionalize nanoparticles (Murcia and Naumann, 2007). Due to their carbodiimide activation, there is also the opportunity to add a second layer to our hybrid spicules, for example by docking proteins such as silicatein-α. One of many applicable substrates of silicatein-α is titanium dioxide (Sumerel et al., 2003), which has a photocatalytic activity, and is thereby applied in solid-state technology and solar cells (Roy et al., 2015).

6.7 Enhanced apatite formation of SaOS-2 cells transfected with silicatein-α

It is currently agreed that although vertebrate bones largely consist of hydroxyapatite, which is a crystalline form of calcium phosphate, traces of silicon are also required for bone formation (Carlisle, 1986; Beattie and Avenell, 1992). Although the exact molecular mechanism of this silicon effect on bone growth and regeneration is still unknown (Han et al., 2013; Rodella et al., 2014), it has been shown that a grafted biosilica scaffold has the potential to enhance bone formation in that its presence up-regulates bone growth factors (Wiens et al., 2010b; Wiens et al., 2010a; Wang et al., 2014a). It is therefore reasonable to assume that in man an as yet unknown process is capable to synthesize biosilica (Exley, 2009). As pointed out many times in this thesis, the capability to produce such biosilica under physiological conditions is a vital process in *S. domuncula* and many other sponges.

In this process, silicatein-α plays a central role. It is not only a structural protein forming a central rod within the spicule (see Fig. 48), but also an enzyme catalyzing the polycondensation of silicic acid (Weaver and Morse, 2003). Therefore, the basic idea of our present approach was to support biosilica

formation in bone-forming SaOS-2 cells by the superior enzymatic properties of silicatein-α which in turn should enhance bone formation by these cells. I transfected SaOS-2 cells with the gene encoding *S. domuncula* silicatein-α, achieved a stable expression of the protein, and analyzed the effect of this expression on hydroxyapatite formation of the transfected cells.

Human osteosarcoma SaOS-2 cells have osteoblastic properties (Mitsui et al., 2006) and can be considered as "osteoblast-like" cells (Degasne et al., 1999), as they can differentiate and produce hydroxyapatite (Hausser and Brenner, 2005). SaOS-2 cells have been used for experiments in the context of bone formation and the development of surgical implants (Saldana et al., 2007). Such implants are often made from Si-doped calcium phosphate (Vallet-Regi and Arcos, 2005) or bioactive glass (Hench, 1991). Normally only silicon in the form of orthosilicic acid (respectively orthosilicate) is considered as a bioavailable substance (Jurkic et al., 2013), because when taking up silicon it needs to be soluble to be transported in the organism, which is only the case with orthosilicate (Jugdaohsingh et al., 2002; Reffitt et al., 2003). Shanklin and Smalley (1998) showed that silica in crystalline form can cause autoimmune responses and was found to be toxic at least in liver macrophages (Kolbbachofen, 1992). In contrast, amorphous biosilica as well as extracellular silicatein-α are nontoxic for SaOS-2 cells (Schröder et al., 2005; Schröder et al., 2006a; Wiens et al., 2013). In the present thesis it is shown that intracellular silicatein-α also has no effect on the viability of SaOS-2 cells (see Fig. 42).

For transfection I used a vector of the Gateway cloning system from Life Technologies (Darmstadt), where no His-tag was provided. Therefore, purifying the expressed protein would have been very difficult and was not attempted. Instead, we used the very convenient method of proving the presence of silicatein-α by fluorescence. The advantage of this method is that the protein can be detected in live cells which subsequently can be used for further analysis, instead of losing them through lysis for the test. In contrast to other authors (Stroffekova et al., 2001) we observed a very specific binding of the tetracysteine tag coupled with the fluorophore. This tag exclusively reacted to transfected cells, while control cells did not show a strong fluorescence (see Fig. 41).

We used two different methods to measure mineralization rates of SaOS-2 cells: (i) alkaline phosphatase activity as early marker for hydroxyapatite formation (DeLaurier et al., 2002; Golub and Boesze-Battaglia, 2007), and (ii) alizarin red S staining as late marker for hydroxyapatite formation (McGeerussell, 1958; Satomura and Nagayama, 1991; Stanford et al., 1995). In case of alizarin red S staining, the effect was much clearer. This might be due to the fact that alkaline phosphatase takes part in the biomineralization process leading to hydroxyapatite. The chemical mechanism is not completely understood as yet, but it is known that alkaline phosphatase expression is enhanced during hydroxyapatite formation (Müller et al., 2011b). In contrast, alizarin red S stains available Ca^{2+} ions,

independent of their deposition date. Thus, it indicates the synthesized hydroxyapatite in total and not only the amount that is currently synthesized. On the other hand, not only Ca^{2+} derived from hydroxyapatite is stained by alizarin red S, but all the available Ca^{2+} in the sample (Hale et al., 2000). Therefore it is necessary to use both methods in parallel, as I did. Since both tests showed the same trend for the effect, we are convinced that the intracellular presence of silicatein-α stimulates and enhances biomineralization by SaOS-2 cells.

As mentioned before, silicatein-α mediates the polycondensation of silicic acid to biosilica. Silicatein-α was therefore used earlier to coat surfaces with biosilica, which induces, together with an applied "activation cocktail", higher rates of mineralization in SaOS-2 cells growing on such surfaces (Schröder et al., 2005; Wiens et al., 2010b; Wiens et al., 2013). In the present study, expression of silicatein-α alone (with the specific surface coat and activation cocktail omitted) led to significantly higher hydroxyapatite mineralization rates in SaOS-2 cells. This is interesting, because it is highly unlikely that silicatein-α directly partakes, as a structural component, in the mineralization process in SaOS-2 cells. Rather, it should partake through its enzyme activity. However, silicatein-α activated the cells strongly, although its substrate silicic acid was not added to the culture medium. Probably, SaOS-2 cells are able to provide a substrate to silicatein-α. It is also possible that the culture medium or the well plates contain silicate which is taken up by the cells and is thereby available for the enzyme.

Also, as mentioned previously, SaOS-2 cells mineralize better on biosilica-coated surfaces (Wiens et al., 2014). The exact mechanism remains unclear, but the uptake of biosilica particles leads to a measurable up-regulation of collagen type I (Hong et al., 2010), bone morphogenic protein 2 (Wiens et al., 2010b), and osteoprotegerin (Wiens et al., 2010a), while NF-κB activation is suppressed (Beck et al., 2012). All these proteins are associated with bone formation and regeneration (Nickel et al., 2001). It is proposed that accordingly, osteoblast differentiation is induced and osteoclasts differentiation reduced, which leads to enhanced bone formation (Wiens et al., 2010a; Beck et al., 2012). Presumably, in these cultured cells, silicatein-α catalyzes the formation of biosilica from an as yet unidentified silicon source. This activates the expression of one or several of the genes involved in bone formation, yielding the observed higher mineralization rate.

It has been proposed that silicatein-α catalyzes the reaction of orthosilicic acid (respectively orthosilicate) to cyclic trisiloxane (Schröder et al., 2012), as shown in Fig. 9. Probably, in our experiments silicon is taken up by the cells as orthosilicic acid (Jurkic et al., 2013) and then, instead of directly taking part in its normal reaction, which is still to be investigated (Rodella et al., 2014), it is transformed to cyclic trisiloxane by silicatein-α and thereby forms a highly reactive core (Schröder et al., 2012).

As deduced from the results of alizarin red S staining, mineralization of transfected SaOS-2 cells in the absence of the activation cocktail was seven times higher than in control cells. Compared to SaOS-2 cells grown on extracellular silicatein-α (Wiens et al., 2014), the hydroxyapatite growth rate was significantly enhanced in SaOS-2 cells expressing silicatein-α (three times enhanced when silicatein-α was extracellular, compared to seven times in case of intracellular silicatein-α).

Concerning alkaline phosphatase activity, the absolute values obtained here can be compared to those from other authors, because the measured data are given as concentrations normalized to protein content. We found that in our hands the alkaline phosphatase activity was in the same range (5 - 10 µmol/min/mg protein) as reported previously (Wiens et al., 2013). It seems that contact to extracellular amorphous silica has a stronger osteoinductive effect than other silica forms. This assumption is supported by previous findings where SaOS-2 cells growing on biosilica showed higher mineralization rates than cells growing on non-biosilica supports (Schröder et al., 2005; Wang et al., 2014a). I have now shown that intracellular amorphous silica is even better for SaOS-2 cell differentiation and mineralization.

On this basis it can be deduced that silicatein-α expression in SaOS-2 cells is indeed superior in its capability to stimulate hydroxyapatite formation, compared to extracellular coating with recombinant silicatein-α. It has the additional advantage that silicatein-α expression in bacteria with subsequent purification, refolding and immobilization is not necessary if stably transfected SaOS-2 cells are applied instead of normal SaOS-2 cells. Of course, the problems related to clinical applications of transfected human cells remain, and also immune reactions against the expressed sponge protein are possible. On the other hand, provided such possible side effects are eliminated, in those cases in which enhanced hydroxyapatite formation is planned, just seeding SaOS-2 cells expressing silicatein-α instead of engrafting silicatein-α-coated new material, might be a major advantage. It might also allow an application of a suspension of such SaOS-2 cells to regions in the body were it is difficult or impossible to implant new materials. Thus, SaOS-2 cells stably expressing silicatein-α as designed and studied in this thesis open a new pathway for future research and clinics in the important field of bone regeneration.

7 CONCLUSION

The newly developed bioreactor for *S. domuncula* cell culture yields a significant improvement and upscaling of primmorph production from the cell suspension of a single *S. domuncula* individual. Per choice, it allows producing either a single primmorph of previously unmatched size, or many small primmorphs in previously unmatched numbers. This new device will greatly facilitate sponge cell research, the study of sponge cell substances and the production of new property materials from sponge cells.

According to the present data, most if not all primmorph cells are capable of extensive endocytosis in that they engulfed large numbers of nano-screenMAG-CMX nanoparticles and silica core-shell microparticles, respectively. The nanoparticles are permanently stored within the cells. Uptake of silica core-shell microparticles enhanced the expression of proteins known to be involved in spiculogenesis, notably silicatein-α and silicatein-β, while uptake of nano-screenMAG-CMX nanoparticles did not change the expression patterns of these proteins. This suggests that the production of biosilica spicules can be specifically influenced by feeding the sponge cells with certain particles.

The biosilica spicules were specifically coated by nanoparticles *in vivo*, whereas such coating of extracted spicules *in vitro* required prior chemical silanization of their surface. By using nanoparticles, I introduced magnetic and fluorescent properties to *S. domuncula* primmorph individuals, their cells, and their biosilica spicules. This provides convenient tools for producing new property combinations based on biosilica spicules.

Stably transfection of SaOS-2 cells with the gene encoding *S. domuncula* silicatein-α significantly enhanced their osteogenic capacity also in the absence of activation by β-glycerophosphate, ascorbic acid and dexamethasone. This is a novel approach to enhance the biomineralization activity of human bone-forming SaOS-2 cells, with the potential of future clinical applications.

The present experiments with sponge cells and human SaOS-2 cells open new possibilities in biology, material science and biomedicine in the context of research, production, modification and application of biosilica and the proteins involved in spiculogenesis.

8 LITERATURE

Adams, S. R., R. E. Campbell, L. A. Gross, B. R. Martin, G. K. Walkup, Y. Yao, J. Llopis and R. Y. Tsien (2002). "New biarsenical ligands and tetracysteine motifs for protein labeling *in vitro* and *in vivo*: Synthesis and biological applications." *Journal of the American Chemical Society* **124**(21), pp. 6063-6076.

Adl, S. M., A. G. B. Simpson, C. E. Lane, J. Lukes, D. Bass, S. S. Bowser, M. W. Brown, F. Burki, M. Dunthorn, V. Hampl, A. Heiss, M. Hoppenrath, E. Lara, L. le Gall, D. H. Lynn, H. McManus, E. A. D. Mitchell, S. E. Mozley-Stanridge, L. W. Parfrey, J. Pawlowski, S. Rueckert, L. Shadwick, C. L. Schoch, A. Smirnov and F. W. Spiegel (2012). "The revised classification of eukaryotes." *Journal of Eukaryotic Microbiology* **59**(5), pp. 429-493.

Aizenberg, J., V. C. Sundar, A. D. Yablon, J. C. Weaver and G. Chen (2004). "Biological glass fibers: Correlation between optical and structural properties." *Proceedings of the National Academy of Sciences of the United States of America* **101**(10), pp. 3358-3363.

Alric, C., J. Taleb, G. Le Duc, C. Mandon, C. Billotey, A. Le Meur-Herland, T. Brochard, F. Vocanson, M. Janier, P. Perriat, S. Roux and O. Tillement (2008). "Gadolinium chelate coated gold nanoparticles as contrast agents for both X-ray computed tomography and magnetic resonance imaging." *Journal of the American Chemical Society* **130**(18), pp. 5908-5915.

Amano, S. (1990). "Self and non-self recognition in a calcareous sponge, *Leucandra abratsbo*." *The Biological Bulletin* **179**(3), pp. 272-278.

Andrade, P., R. Willoughby, S. A. Pomponi and R. G. Kerr (1999). "Biosynthetic studies of the alkaloid, stevensine, in a cell culture of the marine sponge *Teichaxinella morchella*." *Tetrahedron Letters* **40**(26), pp. 4775-4778.

Andre, R., M. N. Tahir, H. C. Schröder, W. E. G. Müller and W. Tremel (2011). "Enzymatic synthesis and surface deposition of tin dioxide using silicatein-alpha." *Chemistry of Materials* **23**(24), pp. 5358-5365.

Andre, R., M. N. Tahir, F. Natalio and W. Tremel (2012). "Bioinspired synthesis of multifunctional inorganic and bio-organic hybrid materials." *FEBS Journal* **279**(10), pp. 1737-1749.

Arakaki, A., K. Shimizu, M. Oda, T. Sakamoto, T. Nishimura and T. Kato (2015). "Biomineralization-inspired synthesis of functional organic/inorganic hybrid materials: organic molecular control of self-organization of hybrids." *Organic & Biomolecular Chemistry* **13**(4), pp. 974-989.

Asefa, T., M. J. MacLachlan, N. Coombs and G. A. Ozin (1999). "Periodic mesoporous organosilicas with organic groups inside the channel walls." *Nature* **402**(6764), pp. 867-871.

Au, S. H., S. C. Shih and A. R. Wheeler (2011). "Integrated microbioreactor for culture and analysis of bacteria, algae and yeast." *Biomedical Microdevices* **13**(1), pp. 41-50.

Auffan, M., J. Rose, J.-Y. Bottero, G. V. Lowry, J.-P. Jolivet and M. R. Wiesner (2009). "Towards a definition of inorganic nanoparticles from an environmental, health and safety perspective." *Nature Nanotechnology* **4**(10), pp. 634-641.

Baron, R., B. Willner and I. Willner (2007). "Biomolecule-nanoparticle hybrids as functional units for nanobiotechnology." *Chemical Communications* (4), pp. 323-332.

Bartholomew, W. H., E. O. Karow, M. R. Sfat and R. H. Wilhelm (1950). "Oxygen transfer and agitation in submerged fermentations. Mass transfer of oxygen in submerged fermentation of *Streptomyces griseus*." *Industrial & Engineering Chemistry* **42**(9), pp. 1801-1809.

Beattie, J. H. and A. Avenell (1992). "Trace element nutrition and bone metabolism." *Nutrition Research Reviews* **5**(1), pp. 167-188.

Beck, G. R., Jr., S.-W. Ha, C. E. Camalier, M. Yamaguchi, Y. Li, J.-K. Lee and M. N. Weitzmann (2012). "Bioactive silica-based nanoparticles stimulate bone-forming osteoblasts, suppress bone-resorbing osteoclasts, and enhance bone mineral density *in vivo*." *Nanomedicine-Nanotechnology Biology and Medicine* **8**(6), pp. 793-803.

Bergquist, P. R. (2001). "Porifera (Sponges)." *Wiley*, United Kingdom.

Bokhari, M. A., G. Akay, S. G. Zhang and M. A. Birch (2005). "Enhancement of osteoblast growth and differentiation *in vitro* on a peptide hydrogel - polyHIPE polymer hybrid material." *Biomaterials* **26**(25), pp. 5198-5208.

Borchiellini, C., M. Manuel, E. Alivon, N. Boury-Esnault, J. Vacelet and Y. Le Parco (2001). "Sponge paraphyly and the origin of Metazoa." *Journal of Evolutionary Biology* **14**(1), pp. 171-179.

Boxshall, G. A., J. Mees, M. J. Costello, F. Hernandez, N. Bailly, N. Boury-Esnault, S. Gofas, T. Horton, M. Klautau, A. Kroh, G. Paulay, G. Poore, S. Stöhr, W. Decock, S. Dekeyzer, L. Vandepitte, B. Vanhoorne, M. J. Adams, R. Adlard, P. Adriaens et al., (2015). "World Register of Marine Species (WoRMS)." http://www.marinespecies.org, 2015-12-08.

Breter, H. J., V. A. Grebenjuk, A. Skorokhod and W. E. G. Müller (2003). "Approaches for a sustainable use of the bioactive potential in sponges: analysis of gene clusters, differential display of mRNA and DNA chips." *Progress in Molecular and Subcellular Biology* **37**, pp. 199-230.

Brutchey, R. L. and D. E. Morse (2008). "Silicatein and the translation of its molecular mechanism of biosilicification into low temperature nanomaterial synthesis." *Chemical Reviews* **108**(11), pp. 4915-4934.

Buric, P., Z. Jaksic, L. Stajner, M. D. Sikiric, D. Jurasin, C. Cascio, L. Calzolai and D. M. Lyons (2015). "Effect of silver nanoparticles on Mediterranean sea urchin embryonal development is species specific and depends on moment of first exposure." *Marine Environmental Research* **111**, pp. 50-59.

Bustin, S. A. (2000). "Absolute quantification of mRNA using real-time reverse transcription polymerase chain reaction assays." *Journal of Molecular Endocrinology* **25**(2), pp. 169-193.

Carlisle, E. M. (1972). "Silicon - An essential element for the chick." *Science* **178**(4061), pp. 619-621.

Carlisle, E. M. (1986). "Silicon as an essential trace-element in animal nutrition." *Ciba Foundation Symposia* **121**, pp. 123-139.

Caruso, T., L. Falciai and N. Zupo (2005). "Do hermit crabs like living in sponges? *Paguristes eremita* and *Suberites domuncula*: Biometric data from the southern Mediterranean Sea." *Journal of the Marine Biological Association of the United Kingdom* **85**(6), pp. 1353-1357.

CattaneoVietti, R., G. Bavestrello, C. Cerrano, M. Sara, U. Benatti, M. Giovine and E. Gaino (1996). "Optical fibres in an Antarctic sponge." *Nature* **383**(6599), pp. 397-398.

Cavalier-Smith, T., M. T. E. P. Allsopp, E. E. Chao, N. Boury-Esnault and J. Vacelet (1996). "Sponge phylogeny, animal monophyly, and the origin of the nervous system: 18S rRNA evidence." *Canadian Journal of Zoology* **74**(11), pp. 2031-2045.

Chaudhari, A., A. Braem, J. Vleugels, J. A. Martens, I. Naert, M. V. Cardoso and J. Duyck (2011). "Bone tissue response to porous and functionalized titanium and silica based coatings." *Plos One* **6**(9), e24186.

Chen, C.-Y. and H.-Y. Chang (2016). "Lipid production of microalga *Chlorella sorokiniana* CY1 is improved by light source arrangement, bioreactor operation mode and deep-sea water supplements." *Biotechnology Journal* **11**(3), pp. 356-362.

Chomczynski, P. and N. Sacchi (1987). "Single-step method of RNA isolation by acid guanidinium thiocyanate phenol chloroform extraction." *Analytical Biochemistry* **162**(1), pp. 156-159.

Cicco, S. R., D. Vona, E. De Giglio, S. Cometa, M. Mattioli-Belmonte, F. Palumbo, R. Ragni and G. M. Farinola (2015). "Chemically modified diatoms biosilica for bone cell growth with combined drug-delivery and antioxidant properties." *Chempluschem* **80**(7), pp. 1104-1112.

Cloonan, N., A. R. R. Forrest, G. Kolle, B. B. A. Gardiner, G. J. Faulkner, M. K. Brown, D. F. Taylor, A. L. Steptoe, S. Wani, G. Bethel, A. J. Robertson, A. C. Perkins, S. J. Bruce, C. C. Lee, S. S. Ranade, H. E. Peckham, J. M. Manning, K. J. McKernan and S. M. Grimmond (2008). "Stem cell transcriptome profiling *via* massive-scale mRNA sequencing." *Nature Methods* **5**(7), pp. 613-619.

Custodio, M. R., I. Prokic, R. Steffen, C. Koziol, R. Borojevic, F. Brümmer, M. Nickel and W. E. G. Müller (1998). "Primmorphs generated from dissociated cells of the sponge *Suberites domuncula*: A model system for studies of cell proliferation and cell death." *Mechanisms of Ageing and Development* **105**(1-2), pp. 45-59.

Davis, S. A., M. Breulmann, K. H. Rhodes, B. Zhang and S. Mann (2001). "Template-directed assembly using nanoparticle building blocks: A nanotectonic approach to organized materials." *Chemistry of Materials* **13**(10), pp. 3218-3226.

Degasne, I., M. F. Basle, V. Demais, G. Hure, M. Lesourd, B. Grolleau, L. Mercier and D. Chappard (1999). "Effects of roughness, fibronectin and vitronectin on attachment, spreading, and proliferation of human osteoblast-like cells (SaOS-2) on titanium surfaces." *Calcified Tissue International* **64**(6), pp. 499-507.

DeLaurier, A., B. Jackson, K. Ingham, D. Pfeiffer, M. A. Horton and J. S. Price (2002). "Biochemical markers of bone turnover in the domestic cat: Relationships with age and feline osteoclastic resorptive lesions." *Journal of Nutrition* **132**(6), pp. 1742S-1744S.

Dheda, K., J. F. Huggett, J. S. Chang, L. U. Kim, S. A. Bustin, M. A. Johnson, G. A. W. Rook and A. Zumla (2005). "The implications of using an inappropriate reference gene for real-time reverse transcription PCR data normalization." *Analytical Biochemistry* **344**(1), pp. 141-143.

Drumm, P. J., W. F. Oconnor and L. P. Renouf (1945). "The lipid pigments of the sponge *Hymeniacidon sanguineum* (Grant)." *Biochemical Journal* **39**(2), pp. 208-210.

Duckworth, A. R. and S. A. Pomponi (2005). "Relative importance of bacteria, microalgae and yeast for growth of the sponge *Halichondria melanadocia* (De Laubenfels, 1936): A laboratory study." *Journal of Experimental Marine Biology and Ecology* **323**(2), pp. 151-159.

Eshghi, H., A. Khojastehnezhad, F. Moeinpour, S. Rezaeian, M. Bakavoli, M. Teymouri, A. Rostami and K. Haghbeen (2015). "Nanomagnetic organic-inorganic hybrid (Fe@Si-Gu-Prs): A novel magnetically green catalyst for the synthesis of tetrahydropyridine derivatives at room temperature under solvent-free conditions." *Tetrahedron* **71**(3), pp. 436-444.

Estes, J. E., L. A. Selden and L. C. Gershman (1981). "Mechanism of action of phalloidin on the polymerization of muscle actin." *Biochemistry* **20**(4), pp. 708-712.

Exley, C. (2009). "Silicon in life: Whither biological silicification?" *Progress in Molecular and Subcellular Biology* **47**, pp. 173-184.

Fogh, J. and G. Trempe (1975). "New human tumor cell lines." in *Human Tumor Cells in Vitro*, J. Fogh (Ed.), Springer-Verlag, New York, USA.

Fogh, J., J. M. Fogh and T. Orfeo (1977). "127 cultured human tumor-cell lines producing tumors in nude mice." *Journal of the National Cancer Institute* **59**(1), pp. 221-226.

Frenz, J. L., A. C. Kohl and R. G. Kerr (2004). "Marine natural products as therapeutic agents: Part 2." *Expert Opinion on Therapeutic Patents* **14**(1), pp. 17-33.

Gaino, E., G. Bavestrello and G. Magnino (1999). "Self/non-self recognition in sponges." *Italian Journal of Zoology* **66**(4), pp. 299-315.

Garderes, J., G. Bedoux, V. Koutsouveli, S. Crequer, F. Desriac and G. Le Pennec (2015). "Lipopolysaccharides from commensal and opportunistic bacteria: Characterization and response of the immune system of the host sponge *Suberites domuncula*." *Marine Drugs* **13**(8), pp. 4985-5006.

Gasteiger, E., A. Gattiker, C. Hoogland, I. Ivanyi, R. D. Appel and A. Bairoch (2003). "ExPASy: The proteomics server for in-depth protein knowledge and analysis." *Nucleic Acids Research* **31**(13), pp. 3784-3788.

Gazave, E., P. Lapebie, E. Renard, J. Vacelet, C. Rocher, A. V. Ereskovsky, D. V. Lavrov and C. Borchiellini (2010). "Molecular phylogeny restores the supra-generic subdivision of homoscleromorph sponges (Porifera, Homoscleromorpha)." *Plos One* **5**(12), e14290.

Geer, L. Y., A. Marchler-Bauer, R. C. Geer, L. Han, J. He, S. He, C. Liu, W. Shi and S. H. Bryant (2010). "The NCBI BioSystems database." *Nucleic Acids Research* **38**(Database issue), pp. D492-496.

Gerwick, W. H. and B. S. Moore (2012). "Lessons from the past and charting the future of marine natural products drug discovery and chemical biology." *Chemistry & Biology* **19**(1), pp. 85-98.

Giannitelli, S. M., D. Accoto, M. Trombetta and A. Rainer (2014). "Current trends in the design of scaffolds for computer-aided tissue engineering." *Acta Biomaterialia* **10**(2), pp. 580-594.

Goksan, T., Y. Durmaz and S. Gokpinar (2003). "Effects of light path lengths and initial culture density on the cultivation of *Chaetoceros muelleri* (Lemmermann, 1898)." *Aquaculture* **217**(1-4), pp. 431-436.

Golub, E. E. and K. Boesze-Battaglia (2007). "The role of alkaline phosphatase in mineralization." *Current Opinion in Orthopaedics* **18**(5), pp. 444-448.

Gomes, P. S., C. Botelho, M. A. Lopes, J. D. Santos and M. H. Fernandes (2010). "Evaluation of human osteoblastic cell response to plasma-sprayed silicon-substituted hydroxyapatite coatings over titanium substrates." *Journal of Biomedical Materials Research Part B-Applied Biomaterials* **94B**(2), pp. 337-346.

Griffin, B. A., S. R. Adams and R. Y. Tsien (1998). "Specific covalent labeling of recombinant protein molecules inside live cells." *Science* **281**(5374), pp. 269-272.

Griffin, B. A., S. R. Adams, J. Jones and R. Y. Tsien (2000). "Fluorescent labeling of recombinant proteins in living cells with FlAsH." *Applications of Chimeric Genes and Hybrid Proteins Pt B* **327**, pp. 565-578.

Griffiths, P. R. and J. A. de Haseth (2007). "Attenuated total reflection." in *Fourier Transform Infrared Spectrometry*, Wiley, Hoboken, New Jersey, USA.

Hale, L. V., Y. F. Ma and R. F. Santerre (2000). "Semi-quantitative fluorescence analysis of calcein binding as a measurement of *in vitro* mineralization." *Calcified Tissue International* **67**(1), pp. 80-84.

Han, P., C. Wu and Y. Xiao (2013). "The effect of silicate ions on proliferation, osteogenic differentiation and cell signalling pathways (WNT and SHH) of bone marrow stromal cells." *Biomaterials Science* **1**(4), pp. 379-392.

Han, Y., D. Mayer, A. Offenhaeusser and S. Ingebrandt (2006). "Surface activation of thin silicon oxides by wet cleaning and silanization." *Thin Solid Films* **510**(1-2), pp. 175-180.

Harrison, F. W. and D. A. Davis (1982). "Morphological and cytochemical patterns during early stages of reduction body formation in *Spongilla lacustris* (Porifera: Spongillidae)." *Transactions of the American Microscopical Society* **101**(4), pp. 317-324.

Hausser, H. J. and R. E. Brenner (2005). "Phenotypic instability of SaOS-2 cells in long-term culture." *Biochemical and Biophysical Research Communications* **333**(1), pp. 216-222.

Hayat, M. A. (2000). "Principles and techniques of electron microsopy: Biological applications." *Cambridge University Press*, New York, USA.

Hench, L. L., A. E. Clark and H. F. Schaake (1972). "Amorphous and liquid semiconductors effects of microstructure on the radiation stability of amorphous semiconductors." *Journal of Non-Crystalline Solids* **8**, pp. 837-843.

Hench, L. L. (1991). "Bioceramics - From concept to clinic." *Journal of the American Ceramic Society* **74**(7), pp. 1487-1510.

Hench, L. L. (2006). "The story of Bioglass®." *Journal of Materials Science-Materials in Medicine* **17**(11), pp. 967-978.

Hench, L. L. (2013). "Chronology of bioactive glass development and clinical applications." *New Journal of Glass and Ceramics* **3**(2), pp. 67-73.

Hochuli, E., W. Bannwarth, H. Dobeli, R. Gentz and D. Stuber (1988). "Genetic approach to facilitate purification of recombinant proteins with a novel metal chelate adsorbent." *Bio-Technology* **6**(11), pp. 1321-1325.

Hong, D., H.-X. Chen, H.-Q. Yu, Y. Liang, C. Wang, Q.-Q. Lian, H.-T. Deng and R.-S. Ge (2010). "Morphological and proteomic analysis of early stage of osteoblast differentiation in osteoblastic progenitor cells." *Experimental Cell Research* **316**(14), pp. 2291-2300.

Humphrey, A. (1998). "Shake flask to fermentor: What have we learned?" *Biotechnology Progress* **14**(1), pp. 3-7.

Hunter, G. K. and H. A. Goldberg (1994). "Modulation of crystal-formation by bone phosphoproteins: Role of glutamic acid-rich sequences in the nucleation of hydroxyapatite by bone sialoprotein." *Biochemical Journal* **302**, pp. 175-179.

Javalkote, V. S., A. P. Pandey, P. R. Puranik and P. K. Deshmukh (2015). "Magnetically responsive siliceous frustules for efficient chemotherapy." *Materials Science & Engineering C-Materials for Biological Applications* **50**, pp. 107-116.

Jones, J. R. (2013). "Review of bioactive glass: From Hench to hybrids." *Acta Biomaterialia* **9**(1), pp. 4457-4486.

Jugdaohsingh, R., S. H. C. Anderson, K. L. Tucker, H. Elliott, D. P. Kiel, R. P. H. Thompson and J. J. Powell (2002). "Dietary silicon intake and absorption." *American Journal of Clinical Nutrition* **75**(5), pp. 887-893.

Jurkic, L. M., I. Cepanec, S. K. Pavelic and K. Pavelic (2013). "Biological and therapeutic effects of ortho-silicic acid and some ortho-silicic acid-releasing compounds: New perspectives for therapy." *Nutrition & Metabolism* **10**, pp. 1-12.

Kacenka, M., O. Kaman, S. Kikerlova, B. Pavlu, Z. Jirak, D. Jirak, V. Herynek, J. Cerny, F. Chaput, S. Laurent and I. Lukes (2015). "Fluorescent magnetic nanoparticles for cell labeling: Flux synthesis of manganite particles and novel functionalization of silica shell." *Journal of Colloid and Interface Science* **447**, pp. 97-106.

Kaiser, E., Colescot.Rl, Bossinge.Cd and P. I. Cook (1970). "Color test for detection of free terminal amino groups in solid-phase sythesis of peptides." *Analytical Biochemistry* **34**(2), pp. 595-598.

Kalia, P., R. A. Brooks, S. D. Kinrade, D. J. Morgan, A. P. Brown, N. Rushton and R. Jugdaohsingh (2016). "Adsorption of amorphous silica nanoparticles onto hydroxyapatite surfaces differentially alters surfaces properties and adhesion of human osteoblast cells." *Plos One* **11**(2), e0144780.

Kamat, P. V. (2002). "Photophysical, photochemical and photocatalytic aspects of metal nanoparticles." *Journal of Physical Chemistry B* **106**(32), pp. 7729-7744.

Kearse, M., R. Moir, A. Wilson, S. Stones-Havas, M. Cheung, S. Sturrock, S. Buxton, A. Cooper, S. Markowitz, C. Duran, T. Thierer, B. Ashton, P. Meintjes and A. Drummond (2012). "Geneious basic: an integrated and extendable desktop software platform for the organization and analysis of sequence data." *Bioinformatics* **28**(12), pp. 1647-1649.

Kim, E.-J., S.-Y. Bu, M.-K. Sung and M.-K. Choi (2013). "Effects of silicon on osteoblast activity and bone mineralization of MC3T3-E1 cells." *Biological Trace Element Research* **152**(1), pp. 105-112.

Kim, M.-H., Y.-J. Bae, M.-K. Choi and Y.-S. Chung (2009). "Silicon supplementation improves the bone mineral density of calcium-deficient ovariectomized rats by reducing bone resorption." *Biological Trace Element Research* **128**(3), pp. 239-247.

King, N., M. J. Westbrook, S. L. Young, A. Kuo, M. Abedin, J. Chapman, S. Fairclough, U. Hellsten, Y. Isogai, I. Letunic, M. Marr, D. Pincus, N. Putnam, A. Rokas, K. J. Wright, R. Zuzow, W. Dirks, M. Good, D. Goodstein, D. Lemons, W. Li, J. B. Lyons, A. Morris, S. Nichols, D. J. Richter, A. Salamov, P. Bork, W. A. Lim, G. Manning, W. T. Miller, W. McGinnis, H. Shapiro, R. Tjian, I. V. Grigoriev, D. Rokhsar and J. G. I. Sequencing (2008). "The genome of the choanoflagellate *Monosiga brevicollis* and the origin of metazoans." *Nature* **451**(7180), pp. 783-788.

Kisailus, D., J. H. Choi, J. C. Weaver, W. J. Yang and D. E. Morse (2005). "Enzymatic synthesis and nanostructural control of gallium oxide at low temperature." *Advanced Materials* **17**(3), pp. 314-318.

Kolbbachofen, V. (1992). "Uptake of toxic silica particles by isolated rat-liver macrophages (Kupfer cells) is receptor mediated and can be blocked by competition." *Journal of Clinical Investigation* **90**(5), pp. 1819-1824.

Krasko, A., B. Lorenz, R. Batel, H. C. Schröder, I. M. Müller and W. E. G. Müller (2000). "Expression of silicatein and collagen genes in the marine sponge *Suberites domuncula* is controlled by silicate and myotrophin." *European Journal of Biochemistry* **267**(15), pp. 4878-4887.

Kulchin, Y. N., A. V. Bezverbny, O. A. Bukin, S. S. Voznesensky, A. N. Galkina, A. L. Drozdov and I. G. Nagorny (2009). "Optical and nonlinear optical properties of sea glass sponge spicules." *Progress in Molecular and Subcellular Biology* **47**, pp. 315-340.

Langenbach, F., K. Berr, C. Naujoks, A. Hassel, M. Hentschel, R. Depprich, N. R. Kubler, U. Meyer, H.-P. Wiesmann, G. Koegler and J. Handschel (2011). "Generation and differentiation of

microtissues from multipotent precursor cells for use in tissue engineering." *Nature Protocols* **6**(11), pp. 1726-1735.

Laursen, A. B., S. Kegnaes, S. Dahl and I. Chorkendorff (2012). "Molybdenum sulfides-efficient and viable materials for electro- and photoelectrocatalytic hydrogen evolution." *Energy & Environmental Science* **5**(2), pp. 5577-5591.

Lavrov, A. I. and I. A. Kosevich (2014). "Sponge cell reaggregation: Mechanisms and dynamics of the process." *Russian Journal of Developmental Biology* **45**(4), pp. 205-223.

Lee, B.-H., B.-K. Kim, Y.-J. Lee, C.-H. Chung and J.-W. Lee (2010). "Industrial scale of optimization for the production of carboxymethylcellulase from rice bran by a marine bacterium, *Bacillus subtilis* subsp *subtilis* A-53." *Enzyme and Microbial Technology* **46**(1), pp. 38-42.

Leys, S. P. and D. I. Eerkes-Medrano (2006). "Feeding in a calcareous sponge: Particle uptake by pseudopodia." *The Biological Bulletin* **211**(2), pp. 157-171.

Leys, S. P., S. A. Nichols and E. D. M. Adams (2009). "Epithelia and integration in sponges." *Integrative and Comparative Biology* **49**(2), pp. 167-177.

Liang, Y., Y. Li, H. Wang, J. Zhou, J. Wang, T. Regier and H. Dai (2011). "Co_3O_4 nanocrystals on graphene as a synergistic catalyst for oxygen reduction reaction." *Nature Materials* **10**(10), pp. 780-786.

Ma, H., J. Zhang and I. B. Levitan (2011). "Slob, a slowpoke channel-binding protein, modulates synaptic transmission." *Journal of General Physiology* **137**(2), pp. 225-238.

Macdonald, H. M., A. C. Hardcastle, R. Jugdaohsingh, W. D. Fraser, D. M. Reid and J. J. Powell (2012). "Dietary silicon interacts with oestrogen to influence bone health: Evidence from the Aberdeen Prospective Osteoporosis Screening Study." *Bone* **50**(3), pp. 681-687.

Maddison, D. R. and K.-S. Schulz (2007). "The Tree of Life Web Project." http://tolweb.org, 2015-12-08.

Maisano, M., T. Cappello, E. Catanese, V. Vitale, A. Natalotto, A. Giannetto, D. Barreca, E. Brunelli, A. Mauceri and S. Fasulo (2015). "Developmental abnormalities and neurotoxicological effects of CuO NPs on the black sea urchin *Arbacia lixula* by embryotoxicity assay." *Marine Environmental Research* **111**, pp. 121-127.

Mayer, G. (2005). "Rigid biological systems as models for synthetic composites." *Science* **310**(5751), pp. 1144-1147.

McGeerussell, S. M. (1958). "Histochemical methods for calcium." *Journal of Histochemistry & Cytochemistry* **6**(1), pp. 22-42.

Mieszawska, A. J., N. Fourligas, I. Georgakoudi, N. M. Ouhib, D. J. Belton, C. C. Perry and D. L. Kaplan (2010). "Osteoinductive silk-silica composite biomaterials for bone regeneration." *Biomaterials* **31**(34), pp. 8902-8910.

Mitsui, N., N. Suzuki, Y. Koyama, M. Yanagisawa, K. Otsuka, N. Shimizu and M. Maeno (2006). "Effect of compressive force on the expression of MMPs, PAs, and their inhibitors in osteoblastic SaOS-2 cells." *Life Sciences* **79**(6), pp. 575-583.

Morelli, E., E. Salvadori, B. Basso, D. Tognotti, P. Cioni and E. Gabellieri (2015). "The response of *Phaeodactylum tricornutum* to quantum dot exposure: Acclimation and changes in protein expression." *Marine Environmental Research* **111**, pp. 149-157.

Moroz, L. L., K. M. Kocot, M. R. Citarella, S. Dosung, T. P. Norekian, I. S. Povolotskaya, A. P. Grigorenko, C. Dailey, E. Berezikov, K. M. Buckley, A. Ptitsyn, D. Reshetov, K. Mukherjee, T. P. Moroz, Y. Bobkova, F. Yu, V. V. Kapitonov, J. Jurka, Y. V. Bobkov, J. J. Swore, D. O. Girardo, A. Fodor, F. Gusev, R. Sanford, R. Bruders, E. Kittler, C. E. Mills, J. P. Rast, R. Derelle, V. V. Solovyev, F. A. Kondrashov, B. J. Swalla, J. V. Sweedler, E. I. Rogaev, K. M. Halanych and A. B. Kohn (2014). "The ctenophore genome and the evolutionary origins of neural systems." *Nature* **510**(7503), pp. 109-114.

Mortazavi, A., B. A. Williams, K. McCue, L. Schaeffer and B. Wold (2008). "Mapping and quantifying mammalian transcriptomes by RNA-Seq." *Nature Methods* **5**(7), pp. 621-628.

Mukherjee, S., M. Ray and S. Ray (2015). "Phagocytic efficiency and cytotoxic responses of Indian freshwater sponge (*Eunapius carteri*) cells isolated by density gradient centrifugation and flow cytometry: A morphofunctional analysis." *Zoology* **118**(1), pp. 8-18.

Müller, W. E. G. (1995). "Molecular phylogeny of metazoa (animals) - Monophyletic origin." *Naturwissenschaften* **82**(7), pp. 321-329.

Müller, W. E. G., M. Wiens, R. Batel, R. Steffen, H. C. Schröder, R. Borojevic and M. R. Custodio (1999). "Establishment of a primary cell culture from a sponge: Primmorphs from *Suberites domuncula*." *Marine Ecology Progress Series* **178**, pp. 205-219.

Müller, W. E. G., M. Böhm, R. Batel, S. De Rosa, G. Tommonaro, I. M. Müller and H. C. Schröder (2000). "Application of cell culture for the production of bioactive compounds from sponges: Synthesis of avarol by primmorphs from *Dysidea avara*." *Journal of Natural Products* **63**(8), pp. 1077-1081.

Müller, W. E. G. and I. M. Müller (2003). "Analysis of the sponge (Porifera) gene repertoire: Implications for the evolution of the metazoan body plan." in *Sponges (Porifera)*, W. E. G. Müller (Ed.), Springer-Verlag, Berlin, Heidelberg, Germany.

Müller, W. E. G., A. Krasko, G. LePennec, R. Steffen, M. Wiens, M. S. A. Ammar, I. M. Müller and H. C. Schröder (2003). "Molecular mechanism of spicule formation in the demosponge *Suberites domuncula*: Silicatein - collagen - myotrophin." in *Silicon Biomineralization: Biology - Biochemistry - Molecular Biology - Biotechnology*, W. E. G. Müller (Ed.), Springer-Verlag Berlin, Heidelberg, Germany.

Müller, W. E. G., V. A. Grebenjuk, G. Le Pennec, H. C. Schröder, F. Brümmer, U. Hentschel, I. M. Müller and H. J. Breter (2004). "Sustainable production of bioactive compounds by sponges - Cell culture and gene cluster approach: A review." *Marine Biotechnology* **6**(2), pp. 105-117.

Müller, W. E. G., M. Rothenberger, A. Boreiko, W. Tremel, A. Reiber and H. C. Schröder (2005). "Formation of siliceous spicules in the marine demosponge *Suberites domuncula*." *Cell and Tissue Research* **321**(2), pp. 285-297.

Müller, W. E. G., I. M. Müller and H. C. Schröder (2006a). "Evolutionary relationship of Porifera within the eukaryotes." *Hydrobiologia* **568**, pp. 167-176.

Müller, W. E. G., S. I. Belikov, W. Tremel, C. C. Perry, W. W. Gieskes, A. Boreiko and H. C. Schröder (2006b). "Siliceous spicules in marine demosponges (example *Suberites domuncula*)." *Micron* **37**(2), pp. 107-120.

Müller, W. E. G., K. Wendt, C. Geppert, M. Wiens, A. Reiber and H. C. Schröder (2006c). "Novel photoreception system in sponges? Unique transmission properties of the stalk spicules from the hexactinellid *Hyalonema sieboldi*." *Biosensors & Bioelectronics* **21**(7), pp. 1149-1155.

Müller, W. E. G., A. Boreiko, X. Wang, A. Krasko, W. Geurtsen, M. R. Custodio, T. Winkler, L. Lukic-Bilela, T. Link and H. C. Schröder (2007a). "Morphogenetic activity of silica and bio-silica on the expression of genes controlling biomineralization using SaOS-2 cells." *Calcified Tissue International* **81**(5), pp. 382-393.

Müller, W. E. G., A. Boreiko, X. Wang, S. I. Belikov, M. Wiens, V. A. Grebenjuk, U. Schlossmacher and H. C. Schröder (2007b). "Silicateins, the major biosilica forming enzymes present in demosponges: Protein analysis and phylogenetic relationship." *Gene* **395**(1-2), pp. 62-71.

Müller, W. E. G., U. Schlossacher, X. Wang, A. Boreiko, D. Brandt, S. E. Wolf, W. Tremel and H. C. Schröder (2008). "Poly(silicate)-metabolizing silicatein in siliceous spicules and silicasomes of demosponges comprises dual enzymatic activities (silica polymerase and silica esterase)." *FEBS Journal* **275**(2), pp. 362-370.

Müller, W. E. G., X. Wang, F.-Z. Cui, K. P. Jochum, W. Tremel, J. Bill, H. C. Schröder, F. Natalio, U. Schlossmacher and M. Wiens (2009a). "Sponge spicules as blueprints for the biofabrication of inorganic-organic composites and biomaterials." *Applied Microbiology and Biotechnology* **83**(3), pp. 397-413.

Müller, W. E. G., M. Kasueske, X. Wang, H. C. Schröder, Y. Wang, D. Pisignano and M. Wiens (2009b). "Luciferase a light source for the silica-based optical waveguides (spicules) in the demosponge *Suberites domuncula*." *Cellular and Molecular Life Sciences* **66**(3), pp. 537-552.

Müller, W. E. G., X. Wang, H. C. Schröder, M. Korzhev, V. A. Grebenjuk, J. S. Markl, K. P. Jochum, D. Pisignano and M. Wiens (2010). "A cryptochrome-based photosensory system in the siliceous sponge *Suberites domuncula* (Demospongiae)." *FEBS Journal* **277**(5), pp. 1182-1201.

Müller, W. E. G., X. Wang, M. Wiens, U. Schlossmacher, K. P. Jochum and H. C. Schröder (2011a). "Hardening of bio-silica in sponge spicules involves an aging process after its enzymatic polycondensation: Evidence for an aquaporin-mediated water absorption." *Biochimica Et Biophysica Acta-General Subjects* **1810**(7), pp. 713-726.

Müller, W. E. G., X. Wang, B. Diehl-Seifert, K. Kropf, U. Schlossmacher, I. Lieberwirth, G. Glasser, M. Wiens and H. C. Schröder (2011b). "Inorganic polymeric phosphate/polyphosphate as an inducer of alkaline phosphatase and a modulator of intracellular Ca^{2+} level in osteoblasts (SaOS-2 cells) *in vitro*." *Acta Biomaterialia* **7**(6), pp. 2661-2671.

Müller, W. E. G., X. Wang, M. Binder, J. von Lintig, M. Wiens and H. C. Schröder (2012). "Differential expression of the demosponge (*Suberites domuncula*) carotenoid oxygenases in response to light: Protection mechanism against the self-produced toxic protein (suberitine)." *Marine Drugs* **10**(1), pp. 177-199.

Müller, W. E. G., X. Wang, K. P. Jochum and H. C. Schröder (2013a). "Self-healing, an intrinsic property of biomineralization processes." *IUBMB Life* **65**(5), pp. 382-396.

Müller, W. E. G., H. C. Schröder, D. Pisignano, J. S. Markl and X. Wang (2013b). "Metazoan circadian rhythm: Toward an understanding of a light-based zeitgeber in sponges." *Integrative and Comparative Biology* **53**(1), pp. 103-117.

Müller, W. E. G., H. C. Schröder, J. S. Markl, V. A. Grebenjuk, M. Korzhev, R. Steffen and X. Wang (2013c). "Cryptochrome in sponges: A key molecule linking photoreception with phototransduction." *Journal of Histochemistry & Cytochemistry* **61**(11), pp. 814-832.

Müller, W. E. G., H. C. Schröder, Q. Feng, U. Schlossmacher, T. Link and X. Wang (2015). "Development of a morphogenetically active scaffold for three-dimensional growth of bone cells: biosilica-alginate hydrogel for SaOS-2 cell cultivation." *Journal of Tissue Engineering and Regenerative Medicine* **9**(11), pp. E39-E50.

Murcia, M. J. and C. A. Naumann (2007). "Biofunctionalization of fluorescent nanoparticles." in *Biofunctionalization of nanomaterials*, C. Kumar (Ed.), Wiley, Weinheim, Germany.

Murphy, L. D., C. E. Herzog, J. B. Rudick, A. T. Fojo and S. E. Bates (1990). "Use of the polymerase chain-reaction in the quantitation of MDR-1 gene-expression." *Biochemistry* **29**(45), pp. 10351-10356.

Nagalakshmi, U., Z. Wang, K. Waern, C. Shou, D. Raha, M. Gerstein and M. Snyder (2008). "The transcriptional landscape of the yeast genome defined by RNA sequencing." *Science* **320**(5881), pp. 1344-1349.

Nagaraj, S. H., R. B. Gasser and S. Ranganathan (2007). "A hitchhiker's guide to expressed sequence tag (EST) analysis." *Briefings in Bioinformatics* **8**(1), pp. 6-21.

Natalio, F., T. Link, W. E. G. Müller, H. C. Schröder, F.-Z. Cui, X. Wang and M. Wiens (2010). "Bioengineering of the silica-polymerizing enzyme silicatein-alpha for a targeted application to hydroxyapatite." *Acta Biomaterialia* **6**(9), pp. 3720-3728.

Nickel, J., M. K. Dreyer, T. Kirsch and W. Sebald (2001). "The crystal structure of the BMP-2: BMPR-IA complex and the generation of BMP-2 antagonists." *Journal of Bone and Joint Surgery-American Volume* **83A**, pp. S7-S14.

Nickell, L. G. and J. B. Routien (1956). "Cultivation of plant tissue." United States Patent US2747334 A.

Orimo, H. and T. Shimada (2006). "Effects of phosphates on the expression of tissue-nonspecific alkaline phosphatase gene and phosphate-regulating genes in short-term cultures of human osteosarcoma cell lines." *Molecular and Cellular Biochemistry* **282**(1-2), pp. 101-108.

Orimo, H. (2010). "The mechanism of mineralization and the role of alkaline phosphatase in health and disease." *Journal of Nippon Medical School* **77**(1), pp. 4-12.

Osinga, R., J. Tramper and R. H. Wijffels (1999). "Cultivation of marine sponges." *Marine Biotechnology* **1**(6), pp. 509-532.

Osinga, R., E. H. Belarbi, E. M. Grima, J. Tramper and R. H. Wijffels (2003). "Progress towards a controlled culture of the marine sponge *Pseudosuberites andrewsi* in a bioreactor." *Journal of Biotechnology* **100**(2), pp. 141-146.

Patel, N., S. M. Best, W. Bonfield, I. R. Gibson, K. A. Hing, E. Damien and P. A. Revell (2002). "A comparative study on the *in vivo* behavior of hydroxyapatite and silicon substituted hydroxyapatite granules." *Journal of Materials Science: Materials in Medicine* **13**(12), pp. 1199-1206.

Perea-Blazquez, A., S. K. Davy, B. Magana-Rodriguez and J. J. Bell (2013). "Temporal variation in food utilisation by three species of temperate demosponge." *Marine Ecology Progress Series* **485**, pp. 91-103.

Pettersen, E., T. Goddard, C. Huang, G. Couch, D. Greenblatt, E. Meng and T. Ferrin (2004). "UCSF Chimera - A visualization system for exploratory research and analysis." *Journal of Computational Chemistry* **25**(13), pp. 1605-1612.

Philippe, H., R. Derelle, P. Lopez, K. Pick, C. Borchiellini, N. Boury-Esnault, J. Vacelet, E. Renard, E. Houliston, E. Queinnec, C. Da Silva, P. Wincker, H. Le Guyader, S. Leys, D. J. Jackson, F. Schreiber, D. Erpenbeck, B. Morgenstern, G. Woerheide and M. Manuel (2009). "Phylogenomics revives traditional views on deep animal relationships." *Current Biology* **19**(8), pp. 706-712.

Pile, A. J., M. R. Patterson and J. D. Witman (1996). "*In situ* grazing on plankton <10 µm by the boreal sponge *Mycale lingua*." *Marine Ecology Progress Series* **141**(1-3), pp. 95-102.

Poirrier, M. A., J. C. Francis and R. A. Labiche (1981). "A continuous-flow system for growing fresh-water sponges in the laboratory." *Hydrobiologia* **79**(3), pp. 255-259.

Porter, A. E., S. M. Best and W. Bonfield (2004). "Ultrastructural comparison of hydroxyapatite and silicon-substituted hydroxyapatite for biomedical applications." *Journal of Biomedical Materials Research Part A* **68A**(1), pp. 133-141.

Pozzolini, M., F. Mussino, C. Cerrano, S. Scarfi and M. Giovine (2014). "Sponge cell cultivation: Optimization of the model *Petrosia ficiformis* (Poiret 1789)." *Journal of Experimental Marine Biology and Ecology* **454**, pp. 70-77.

R-Core-Team (2014). "R: A language and environment for statistical computing" *R Foundation for Statistical Computing*, Vienna, Austria, http://www.R-project.org/.

Rai, A. and C. C. Perry (2010). "Facile fabrication of uniform silica films with tunable physical properties using silicatein protein from sponges." *Langmuir* **26**(6), pp. 4152-4159.

Reffitt, D. M., N. Ogston, R. Jugdaohsingh, H. F. J. Cheung, B. A. J. Evans, R. P. H. Thompson, J. J. Powell and G. N. Hampson (2003). "Orthosilicic acid stimulates collagen type 1 synthesis and osteoblastic differentiation in human osteoblast-like cells *in vitro*." *Bone* **32**(2), pp. 127-135.

Richter, D. J. and N. King (2013). "The genomic and cellular foundations of animal origins." *Annual Review of Genetics* **47**, pp. 509-537.

Riisgard, H. U. and P. S. Larsen (2000). "Comparative ecophysiology of active zoobenthic filter feeding, essence of current knowledge." *Journal of Sea Research* **44**(3-4), pp. 169-193.

Rodella, L. F., V. Bonazza, M. Labanca, C. Lonati and R. Rezzani (2014). "A review of the effects of dietary silicon intake on bone homeostasis and regeneration." *Journal of Nutrition Health & Aging* **18**(9), pp. 820-826.

Rorrer, G. L., C. X. Zhi and M. Polne-Fuller (1996). "Development and bioreactor cultivation of a novel semidifferentiated tissue suspension derived from the marine plant *Acrosiphonia coalita*." *Biotechnology and Bioengineering* **49**(5), pp. 559-567.

Rossignol, N., T. Lebeau, P. Jaouen and J. M. Robert (2000). "Comparison of two membrane-photobioreactors, with free or immobilized cells, for the production of pigments by a marine diatom." *Bioprocess Engineering* **23**(5), pp. 495-501.

Roy, S., G. S. Han, H. Shin, J. W. Lee, J. Mun, H. Shin and H. S. Jung (2015). "Low temperature synthesis of rutile TiO_2 nanocrystals and their photovoltaic and photocatalytic properties." *Journal of Nanoscience and Nanotechnology* **15**(6), pp. 4516-4521.

Ruppert, E. E., R. S. Fox and R. D. Barnes (2004). "Invertebrate Zoology: A functional evolutionary approach." 7th ed., *Cengage Learning,* Boston, USA.

Ryan, J. F., K. Pang, C. E. Schnitzler, A.-D. Nguyen, R. T. Moreland, D. K. Simmons, B. J. Koch, W. R. Francis, P. Havlak, S. A. Smith, N. H. Putnam, S. H. D. Haddock, C. W. Dunn, T. G. Wolfsberg, J.

C. Mullikin, M. Q. Martindale, A. D. Baxevanis and N. C. S. Program (2013). "The genome of the ctenophore *Mnemiopsis leidyi* and its implications for cell type evolution." *Science* **342**(6164), pp. 1242592-1-1242592-8.

Sajc, L., D. Grubisic and G. Vunjak-Novakovic (2000). "Bioreactors for plant engineering: An outlook for further research." *Biochemical Engineering Journal* **4**(2), pp. 89-99.

Saldana, L., A. Mendez-Vilas, L. Jiang, M. Multigner, J. L. Gonzalez-Carrasco, M. T. Perez-Prado, M. L. Gonzalez-Martin, L. Munuera and N. Vilaboa (2007). "*In vitro* biocompatibility of an ultrafine grained zirconium." *Biomaterials* **28**(30), pp. 4343-4354.

Sambrook, J. and D. W. Russell (2001). "Molecular cloning: A laboratory manual." 3rd ed., *Cold Spring Harbor Laboratory Press*, Cold Spring Harbor, New York, USA.

Saravanapavan, P., J. R. Jones, R. S. Pryce and L. L. Hench (2003). "Bioactivity of gel-glass powders in the CaO-SiO_2 system: A comparison with ternary (CaO-P_2O_5-SiO_2) and quaternary glasses (SiO_2-CaO-P_2O_5-Na_2O)." *Journal of Biomedical Materials Research Part A* **66A**(1), pp. 110-119.

Satomura, K. and M. Nagayama (1991). "Ultrastructure of mineralized nodules formed in rat bone-marrow stromal cell-culture *in vitro*." *Acta Anatomica* **142**(2), pp. 97-104.

Schippers, K. J., D. Sipkema, R. Osinga, H. Smidt, S. A. Pomponi, D. E. Martens and R. H. Wijffels (2012). "Cultivation of sponges, sponge cells and symbionts: Achievments and future prospects." in *Advances in Sponge Science: Physiology, Chemical and Microbial Diversity, Biotechnology*, M. A. Becerro, M. J. Uriz, M. Maldonado and X. Turon (Eds.), Elsevier, Oxford, United Kingdom.

Schröder, H. C., A. Krasko, G. Le Pennec, T. Adell, M. Wiens, H. Hassanein, I. M. Müller and W. E. G. Müller (2003a). "Silicase, an enzyme which degrades biogenous amorphous silica: Contribution to the metabolism of silica deposition in the demosponge *Suberites domuncula*." *Progress in Molecular and Subcellular Biology* **33**, pp. 249-268.

Schröder, H. C., F. Brümmer, E. Fattorusso, A. Aiello, M. Menna, S. de Rosa, R. Batel and W. E. G. Müller (2003b). "Sustainable production of bioactive compounds from sponges: Primmorphs as bioreactors." *Progress in Molecular and Subcellular Biology* **37**, pp. 163-197.

Schröder, H. C., O. Boreiko, A. Krasko, A. Reiber, H. Schwertner and W. E. G. Müller (2005). "Mineralization of SaOS-2 cells on enzymatically (silicatein) modified bioactive osteoblast-stimulating surfaces." *Journal of Biomedical Materials Research Part B-Applied Biomaterials* **75B**(2), pp. 387-392.

Schröder, H. C., A. Boreiko, M. Korzhev, M. N. Tahir, W. Tremel, C. Eckert, H. Ushijima, I. M. Müller and W. E. G. Müller (2006a). "Co-expression and functional interaction of silicatein with galectin - Matrix-guided formation of siliceous spicules in the marine demosponge *Suberites domuncula*." *Journal of Biological Chemistry* **281**(17), pp. 12001-12009.

Schröder, H. C., H. J. Breter, E. Fattorusso, H. Ushijima, M. Wiens, R. Steffen, R. Batel and W. E. G. Müller (2006b). "Okadaic acid, an apoptogenic toxin for symbiotic/parasitic annelids in the demosponge *Suberites domuncula*." *Applied and Environmental Microbiology* **72**(7), pp. 4907-4916.

Schröder, H. C., F. Natalio, I. Shukoor, W. Tremel, U. Schlossmacher, X. Wang and W. E. G. Müller (2007). "Apposition of silica lamellae during growth of spicules in the demosponge *Suberites domuncula*: Biological/biochemical studies and chemical/biomimetical confirmation." *Journal of Structural Biology* **159**(3), pp. 325-334.

Schröder, H. C., M. Wiens, U. Schlossmacher, D. Brandt and W. E. G. Müller (2012). "Silicatein-mediated polycondensation of orthosilicic acid: Modeling of a catalytic mechanism involving ring formation." *Silicon* **4**(1), pp. 33-38.

Seaborn, C. D. and F. H. Nielsen (2002). "Dietary silicon and arginine affect mineral element composition of rat femur and vertebra." *Biological Trace Element Research* **89**(3), pp. 239-250.

Sepulveda, P., J. R. Jones and L. L. Hench (2001). "Characterization of melt-derived 45S5 and sol-gel-derived 58S bioactive glasses." *Journal of Biomedical Materials Research* **58**(6), pp. 734-740.

Shanklin, D. R. and D. L. Smalley (1998). "The immunopathology of siliconosis - History, clinical presentation, and relation to silicosis and the chemistry of silicon and silicone." *Immunologic Research* **18**(3), pp. 125-173.

Shimizu, K., J. Cha, G. D. Stucky and D. E. Morse (1998). "Silicatein alpha: Cathepsin L-like protein in sponge biosilica." *Proceedings of the National Academy of Sciences of the United States of America* **95**(11), pp. 6234-6238.

Shioi, A., Y. Nishizawa, S. Jono, H. Koyama, M. Hosoi and H. Morii (1995). "Beta-glycerophosphate accelerates calcification in cultured bovine vascular smooth-muscle cells." *Arteriosclerosis Thrombosis and Vascular Biology* **15**(11), pp. 2003-2009.

Shukoor, M. I., F. Natalio, H. A. Therese, M. N. Tahir, V. Ksenofontov, M. Panthoefer, M. Eberhardt, P. Theato, H. C. Schröder, W. E. G. Müller and W. Tremel (2008). "Fabrication of a silica coating on magnetic gamma-Fe_2O_3 nanoparticles by an immobilized enzyme." *Chemistry of Materials* **20**(11), pp. 3567-3573.

Simpson, T. L. (1984). "The cell biology of sponges." *Springer-Verlag*, New York, USA.

Singh, S. P., M. Sharma and P. K. Gupta (2015). "Cytotoxicity of curcumin silica nanoparticle complexes conjugated with hyaluronic acid on colon cancer cells." *International Journal of Biological Macromolecules* **74**, pp. 162-170.

Sipkema, D., R. van Wielink, A. A. M. van Lammeren, J. Tramper, R. Osinga and R. H. Wijffels (2003). "Primmorphs from seven marine sponges: Formation and structure." *Journal of Biotechnology* **100**(2), pp. 127-139.

Smith, P. J., N. Blunt, M. Wiltshire, T. Hoy, P. Teesdale-Spittle, M. R. Craven, J. V. Watson, W. B. Amos, R. J. Errington and L. H. Patterson (2000). "Characteristics of a novel deep red/infrared fluorescent cell-permeant DNA probe, DRAQ5, in intact human cells analyzed by flow cytometry, confocal and multiphoton microscopy." *Cytometry* **40**(4), pp. 280-291.

Smith, P. K., R. I. Krohn, G. T. Hermanson, A. K. Mallia, F. H. Gartner, M. D. Provenzano, E. K. Fujimoto, N. M. Goeke, B. J. Olson and D. C. Klenk (1985). "Measurement of protein using bicinchoninic acid." *Analytical Biochemistry* **150**(1), pp. 76-85.

Somogyi, E., U. Petersson, R. V. Sugars, K. Hultenby and M. Wendell (2004). "Nucleobindin - A Ca^{2+}-binding protein present in the cells and mineralized tissues of the tooth." *Calcified Tissue International* **74**(4), pp. 366-376.

Srivastava, M., E. Begovic, J. Chapman, N. H. Putnam, U. Hellsten, T. Kawashima, A. Kuo, T. Mitros, A. Salamov, M. L. Carpenter, A. Y. Signorovitch, M. A. Moreno, K. Kamm, J. Grimwood, J. Schmutz, H. Shapiro, I. V. Grigoriev, L. W. Buss, B. Schierwater, S. L. Dellaporta and D. S. Rokhsar (2008). "The *Trichoplax* genome and the nature of placozoans." *Nature* **454**(7207), pp. 955-960.

Srivastava, M., O. Simakov, J. Chapman, B. Fahey, M. E. A. Gauthier, T. Mitros, G. S. Richards, C. Conaco, M. Dacre, U. Hellsten, C. Larroux, N. H. Putnam, M. Stanke, M. Adamska, A. Darling, S. M. Degnan, T. H. Oakley, D. C. Plachetzki, Y. Zhai, M. Adamski, A. Calcino, S. F. Cummins, D. M. Goodstein, C. Harris, D. J. Jackson, S. P. Leys, S. Shu, B. J. Woodcroft, M. Vervoort, K. S. Kosik, G. Manning, B. M. Degnan and D. S. Rokhsar (2010). "The *Amphimedon queenslandica* genome and the evolution of animal complexity." *Nature* **466**(7307), pp. 720-726.

Stanford, C. M., P. A. Jacobson, E. D. Eanes, L. A. Lembke and R. J. Midura (1995). "Rapidly forming apatitic mineral in an osteoblastic cell-line (UMR 106-01 BSP)." *Journal of Biological Chemistry* **270**(16), pp. 9420-9428.

Stroffekova, K., C. Proenza and K. G. Beam (2001). "The protein-labeling reagent FlAsH-EDT_2 binds not only to CCXXCC motifs but also non-specifically to endogenous cysteine-rich proteins." *Pflügers Archiv - European Journal of Physiology* **442**(6), pp. 859-866.

Sumerel, J. L., W. J. Yang, D. Kisailus, J. C. Weaver, J. H. Choi and D. E. Morse (2003). "Biocatalytically templated synthesis of titanium dioxide." *Chemistry of Materials* **15**(25), pp. 4804-4809.

Sundar, V. C., A. D. Yablon, J. L. Grazul, M. Ilan and J. Aizenberg (2003). "Fibre-optical features of a glass sponge - Some superior technological secrets have come to light from a deep-sea organism." *Nature* **424**(6951), pp. 899-900.

Tahir, M. N., P. Theato, W. E. G. Müller, H. C. Schröder, A. Borejko, S. Faiss, A. Janshoff, J. Huth and W. Tremel (2005). "Formation of layered titania and zirconia catalysed by surface-bound silicatein." *Chemical Communications* (44), pp. 5533-5535.

Tahir, M. N., M. Eberhardt, H. A. Therese, U. Kolb, P. Theato, W. E. G. Müller, H.-C. Schröder and W. Tremel (2006). "From single molecules to nanoscopically structured functional materials: Au nanocrystal growth on TiO_2 nanowires controlled by surface-bound silicatein." *Angewandte Chemie-International Edition* **45**(29), pp. 4803-4809.

Thakur, N. L., U. Hentschel, A. Krasko, C. T. Pabel, A. C. Anil and W. E. G. Müller (2003). "Antibacterial activity of the sponge *Suberites domuncula* and its primmorphs: Potential basis for epibacterial chemical defense." *Aquatic Microbial Ecology* **31**(1), pp. 77-83.

Tricarico, C., P. Pinzani, S. Bianchi, M. Paglierani, V. Distante, M. Pazzagli, S. A. Bustin and C. Orlando (2002). "Quantitative real-time reverse transcription polymerase chain reaction: Normalization to rRNA or single housekeeping genes is inappropriate for human tissue biopsies." *Analytical Biochemistry* **309**(2), pp. 293-300.

Valisano, L., G. Bavestrello, M. Giovine, A. Arillo and C. Cerrano (2007). "Effect of iron and dissolved silica on primmorphs of *Petrosia ficiformis* (Poiret, 1789)." *Chemistry and Ecology* **23**(3), pp. 233-241.

Valisano, L., M. Pozzolini, M. Giovine and C. Cerrano (2012). "Biosilica deposition in the marine sponge *Petrosia ficiformis* (Poiret, 1789): The model of primmorphs reveals time dependence of spiculogenesis." *Hydrobiologia* **687**(1), pp. 259-273.

Vallet-Regi, M. and D. Arcos (2005). "Silicon substituted hydroxyapatites. A method to upgrade calcium phosphate based implants." *Journal of Materials Chemistry* **15**(15), pp. 1509-1516.

Wang, X., H. C. Schröder and W. E. G. Müller (2009). "Giant siliceous spicules from the deep-sea glass sponge *Monorhaphis chuni*." *International Review of Cell and Molecular Biology* **273**, pp. 69-115.

Wang, X., H. C. Schröder, D. Brandt, M. Wiens, I. Lieberwirth, G. Glasser, U. Schlossmacher, S. Wang and W. E. G. Müller (2011a). "Sponge biosilica formation involves syneresis following polycondensation *in vivo*." *ChemBioChem* **12**(15), pp. 2316-2324.

Wang, X., M. Wiens, H. C. Schröder, U. Schlossmacher, D. Pisignano, K. P. Jochum and W. E. G. Müller (2011b). "Evagination of cells controls bio-silica formation and maturation during spicule formation in sponges." *Plos One* **6**(6), e20523.

Wang, X., U. Schlossmacher, M. Wiens, R. Batel, H. C. Schröder and W. E. G. Müller (2012a). "Silicateins, silicatein interactors and cellular interplay in sponge skeletogenesis: Formation of glass fiber-like spicules." *FEBS Journal* **279**(10), pp. 1721-1736.

Wang, X., X. Fan, H. C. Schröder and W. E. G. Müller (2012b). "Flashing light in sponges through their siliceous fiber network: A new strategy of "neuronal transmission" in animals." *Chinese Science Bulletin* **57**(25), pp. 3300-3311.

Wang, X., H. C. Schöeder, K. Wang, J. A. Kaandorp and W. E. G. Müller (2012c). "Genetic, biological and structural hierarchies during sponge spicule formation: From soft sol-gels to solid 3D silica composite structures." *Soft Matter* **8**(37), pp. 9501-9518.

Wang, X., H. C. Schröder, M. Wiens, U. Schlossmacher and W. E. G. Müller (2012d). "Biosilica: Molecular biology, biochemistry and function in demosponges as well as its applied aspects for tissue engineering." in *Advances in Sponge Science: Physiology, Chemical and Microbial Diversity, Biotechnology*, M. A. Becerro, M. J. Uriz, M. Maldonado and X. Turon (Eds.),

Wang, X., E. Tolba, H. C. Schröder, M. Neufurth, Q. Feng, B. Diehl-Seifert and W. E. G. Müller (2014a). "Effect of bioglass on growth and biomineralization of SaOS-2 cells in hydrogel after 3D cell bioprinting." *Plos One* **9**(11), e112497.

Wang, X., H. C. Schröder and W. E. G. Müller (2014b). "Enzyme-based biosilica and biocalcite: Biomaterials for the future in regenerative medicine." *Trends in Biotechnology* **32**(9), pp. 441-447.

Wang, Y. H., Y. Liu, P. Maye and D. W. Rowe (2006). "Examination of mineralized nodule formation in living osteoblastic cultures using fluorescent dyes." *Biotechnology Progress* **22**(6), pp. 1697-1701.

Weaver, J. C. and D. E. Morse (2003). "Molecular biology of demosponge axial filaments and their roles in biosilicification." *Microscopy Research and Technique* **62**(4), pp. 356-367.

Wiechelman, K. J., R. D. Braun and J. D. Fitzpatrick (1988). "Investigation of the bicinchoninic acid protein assay: Identification of the groups responsible for color formation." *Analytical Biochemistry* **175**(1), pp. 231-237.

Wiens, M., S. Perović-Ottstadt, I. M. Müller and W. E. G. Müller (2004). "Allograft rejection in the mixed cell reaction system of the demosponge *Suberites domuncula* is controlled by differential expression of apoptotic genes." *Immunogenetics* **56**(8), pp. 597-610.

Wiens, M. (2004). "Fundamental mechanisms of apoptosis in the most simple invertebrates, the Porifera." *Zeitschrift fuer Gerontologie und Geriatrie* **37**(3), pp. 190-199.

Wiens, M., M. Bausen, F. Natalio, T. Link, U. Schlossmacher and W. E. G. Müller (2009). "The role of the silicatein-alpha interactor silintaphin-1 in biomimetic biomineralization." *Biomaterials* **30**(8), pp. 1648-1656.

Wiens, M., X. Wang, H. C. Schröder, U. Kolb, U. Schlossmacher, H. Ushijima and W. E. G. Müller (2010a). "The role of biosilica in the osteoprotegerin/RANKL ratio in human osteoblast-like cells." *Biomaterials* **31**(30), pp. 7716-7725.

Wiens, M., X. Wang, U. Schlossmacher, I. Lieberwirth, G. Glasser, H. Ushijima, H. C. Schröder and W. E. G. Müller (2010b). "Osteogenic potential of biosilica on human osteoblast-like (SaOS-2) cells." *Calcified Tissue International* **87**(6), pp. 513-524.

Wiens, M., T. Link, T. A. Elkhooly, S. Isbert and W. E. G. Müller (2012). "Formation of a micropatterned titania photocatalyst by microcontact printed silicatein on gold surfaces." *Chemical Communications* **48**(92), pp. 11331-11333.

Wiens, M., T. Niem, T. A. Elkhooly, R. Steffen, S. Neumann, U. Schloßmacher and W. E. G. Müller (2013). "Osteogenic potential of a biosilica-coated P(UDMA-co-MPS) copolymer." *Journal of Materials Chemistry B* **1**(27), pp. 3339-3343.

Wiens, M., T. A. Elkhooly, H. C. Schröder, T. H. Mohamed and W. E. G. Müller (2014). "Characterization and osteogenic activity of a silicatein/biosilica-coated chitosan-graft-polycaprolactone." *Acta Biomaterialia* **10**(10), pp. 4456-4464.

Willems, E., L. Leyns and J. Vandesompele (2008). "Standardization of real-time PCR gene expression data from independent biological replicates." *Analytical Biochemistry* **379**(1), pp. 127-129.

Witte, U., T. Brattegard, G. Graf and B. Springer (1997). "Particle capture and deposition by deep sea sponges from the Norwegian-Greenland Sea." *Marine Ecology Progress Series* **154**, pp. 241-252.

Xu, B., Y. Yin, F. Zhang, Z. Li and L. Wang (2012). "Operating conditions optimization for (+)-terrein production in a stirred bioreactor by *Aspergillus terreus* strain PF-26 from marine sponge *Phakellia fusca*." *Bioprocess and Biosystems Engineering* **35**(9), pp. 1651-1655.

Yahel, G., D. I. Eerkes-Medrano and S. P. Leys (2006). "Size independent selective filtration of ultraplankton by hexactinellid glass sponges." *Aquatic Microbial Ecology* **45**(2), pp. 181-194.

Yilmaz, T., P. Unak, F. Z. B. Muftuler, E. I. Medine, C. Ichedef and A. Y. Kilcar (2015). "Magnetic nanoparticle-conjugated and radioiodinated-DESG: *In vitro* and *in vivo* efficiency investigation." *Journal of Radioanalytical and Nuclear Chemistry* **303**(1), pp. 63-69.

Zhu, C., S. Guo, Y. Zhai and S. Dong (2010). "Layer-by-layer self-assembly for constructing a graphene/platinum nanoparticle three-dimensional hybrid nanostructure using ionic liquid as a linker." *Langmuir* **26**(10), pp. 7614-7618.

9 APPENDICES

9.1 Abbreviations

ALP	alkaline phosphatase
ANOVA	analysis of variance
APTS	(3-aminopropyl)triethoxysilane
bp	base pairs
CCD	charge-couples device
CMFSW	calcium and magnesium free seawater
CMX	carboxymethyl dextran
co	coccospheres
ctrl	control
dATP	deoxyadenosine triphosphate
dCTP	deoxycytidine triphosphate
DEPC-H_2O	nuclease-free water
dGTP	deoxyguanosine triphosphate
dNTP	deoxynucleotide
DPBS	Dulbecco's phosphate-buffered saline
DTT	DL-dithiothreitol solution
dTTP	deoxythymidine triphosphate
EDC	1-ethyl-3-(3-dimethylaminopropyl)carbodiimide
EDT	ethane dithiol
EDTA	ethylenediaminetetraacetic acid
EDX	energy-dispersive X-ray
EM	emission maximum

EST	expressed sequence tag
EX	excitation maximum
FITC	fluorescein isothiocyanate
FlAsH	fluorescein arsenical helix binder
FT-IR	Fourier transform infrared
GAPDH	glycerol 3-phosphate dehydrogenase
HPRT	hypoxanthine-guanine phosphoribosyltransferase
LB	lysogeny broth
Oligo(dT)$_{20}$ Primer	primer with 20 deoxythymidines
om	organic macromolecules
OPG	osteoprotegerin
PCR	polymerase chain reaction
qPCR	quantitative PCR
RANKL	receptor activator of NF-kB ligand
SaOS-2	sarcoma osteogenic
SD	standard deviation
SEM	scanning electron microscopy
sil	silicatein
TBE	Tris-borate-EDTA
TC	tetracysteine
TE	Tris-EDTA
TEM	transmission electron microscopy
VE water	purified water

9.2 List of figures

9.3 List of tables

10 ACKNOWLEDGEMENTS

I wish to thank all the people who made this thesis possible. Notably, I am indebted to my *Doktorvater* Prof. Dr. Werner E. G. Müller for the opportunity to work in a splendid research environment on this challenging topic. Moreover, I thank him for his excellent supervision, constant support and countless stimulating discussions. I am also grateful to Dr. Matthias Wiens for his direct supervision in the laboratory and many advices, and for the critical reading of the manuscript. I wish to thank all my colleagues and friends from the Müller research group for the inspiring and pleasant working atmosphere and the great time, as well as their kind help whenever questions emerged. Specifically, I thank Dr. Thorben Link, Vladislav Grebenyuk, Dr. Johan Garderes and Dr. Tarek Elkhooly, all from the Müller research group, for their numerous technical advices and experimental support. My special thanks go to Dr. Maria Kokkinopoulou, who immensely helped me with the electron microscopy. Maria Sehn from the Wolfrum research group kindly offered me her TEM experience, and Prof. Dr. Uwe Wolfrum provided the resources for TEM sample preparation. Dr. Galina Matveeva from the Kolb research group and Dr. Frank Depoix from the Markl research group helped me with the TEM-EDX analysis. Wilfried Helle from LOT-QuantumDesign in Darmstadt kindly offered me to perform, under his supervision in his laboratory, the SEM-EDX analysis. Thomas Schubert from the Markl research group showed me the technique of cryosectioning and immunofluorescence microscopy. My husband Christoph supported various aspects of my computer work with his EDV expertise. I greatly benefitted from discussing my data and the manuscript with my father Prof. Dr. Jürgen Markl. The English was kindly polished by Prof. Dr. J. Robin Harris.

Last but not least I wish to thank my dear mother and father for the opportunity to achieve this level of qualification, and for letting me accompany them, from early childhood, on countless zoological field trips – terrestrial as well as subaquatic. Furthermore, I thank my sister, grandmother and family in-law for their encouragement and concern. And ultimately, I am most happy about the constant appreciation, support and love of my husband Christoph.

11 ERKLÄRUNG

Hiermit erkläre ich, die vorliegende Arbeit selbständig und nur mit Hilfe der angegebenen Personen und Mittel (Literatur, Apparaturen, Material) angefertigt zu haben. Bei den von mir durchgeführten Untersuchungen habe ich die Grundsätze guter wissenschaftlicher Praxis, wie sie in der Satzung der Johannes Gutenberg-Universität Mainz niedergelegt sind, eingehalten.

Ort, Datum

Julia Markl